# Anomalous rejection ratios in nanofiltration experiments.

Shirley, Jason Dennis

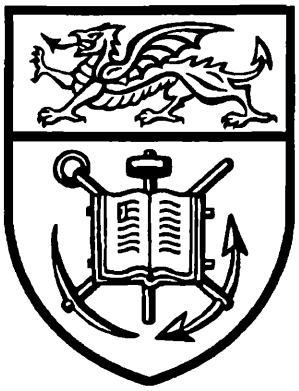

School of Engineering

University of Wales Swansea

# Anomalous Rejection Ratios in Nanofiltration Experiments

by

**Jason Dennis Shirley**

M. Eng. (Wales)

A Thesis Submitted in Fulfilment of the Requirement

for the Degree

DOCTOR OF PHILOSOPHY

Philosophiae Doctor (Ph.D.)

August 2008

## *CONTENTS*

# SUMMARY

Nanofiltration by its nature is used to concentrate material. It has been found that varying the solute feed concentration had an effect on the rejection of amino acids and polar molecules. The rejection of these organic solutes has been shown to increase with concentration during nanofitration experiments for a NTR 7450 membrane. The rejection of glycine increased from 29.4% to 72.2% for a concentration of 0.004 g/l and 4.0 g/l respectively. Similar increases in rejection with respect to concentration were observed for glutamine and glutamic acid, as well as for glucose, sucrose and raffinose over the same concentration range. The reliability of the filtration measurements was established by error analysis and the associated error for the glycine rejection was found to be ± 3%. Therefore, the observed rejection increase could not be attributed to experimental error.

This phenomenon was further investigated by particle size analysis and osmotic pressure measurement. The results from these experiments indicated that dimerisation was not occurring, thus no association between increasing molecular weight and solute concentration.

The properties of the NTR 7450 membrane were investigated by streaming potential measurements, titrations and molecular weight cut-off experiments. The molecular weight cut-off of the membrane was found to reduce for an increase in solute concentration. This result implied that the effective pore size changed as a function of concentration and was attributed to adsorption occurring on the inner pore wall. The level of adsorption was further investigated by applying the Freundlich adsorption isotherm to measured permeated flux decline for increasing solute concentration. This method was adapted to enable analysis of the effect of adsorption on rejection with concentration.

## *DECLARATION*

This work has not previously been accepted in substance for any degree and is not being concurrently submitted in candidature for any degree.

Signed: .... .....(*Candidate*: Jason Dennis Shirley)
Date: ..... 17/8/08 .....

**STATEMENT 1**

This thesis is the result of my own investigation, except where otherwise stated. Other sources are acknowledged by footnotes giving explicit references. A bibliography is appended.

Signed: .. .....(*Candidate*: Jason Dennis Shirley)
Date: ..... 17/8/08 .....

Signed: .....(*Supervisor*: Dr M. G. Jones)
Date: ..... 20/8/8 .....

**STATEMENT 2**

I hereby give consent for my thesis, if accepted, to be available for photocopying and inter-library loan, and for the title and summary to be made available to outside organisations.

Signed: ..... .....(*Candidate*: Jason Dennis Shirley)
Date: ..... 17/8/08 .....

## ACKNOWLEDGEMENTS

I wish to thank the following people who have helped me throughout this degree:

My PhD Supervisor Meirion Jones for his guidance, support and enthusiasm throughout this project.

Steve Mandale who assisted me in all aspects of research from helping setting up equipment and conducting experiments, to assisting with modelling.

Steven Moss who helped develop the data-logging program used in osmotic pressure experiments.

Paul Williams who assisted in setting up the HPPS experiments.

I would also like to give special thanks to my Mum and Dad for supporting me through my time at University.

And finally, I would like to thank my beautiful wife, Angharad, for her love and continued support throughout my career.

*Jason Shirley*

# 1 Introduction

This section provides a brief overview to microfiltration (MF), ultrafiltration (UF) and reverse osmosis (RO) processes, with a more detailed review of nanofiltration (NF). The last section discusses the overall objectives of this research and how these objectives will contribute to the overall development of NF membrane processes.

## *1.1 Overview of membrane processes*

The use of membranes in industry has become popular since 1960, when asymmetric reverse osmosis membranes were first commercially available (Loeb and Sourirajan, 1960). A membrane may be defined as 'an interphase separating two phases and selectivity controlling the transport of materials between those phases' (Strathmann, 1981). Membrane processes offer many advantages including highly selective separation, relatively low capital and operating costs, low energy usage at constant temperature without any phase change in a continuous and automatic operation using simple and modular construction units. Due to these advantages there has been constant research and development into this field, and membrane technology has been developed rapidly. In recent years, membrane technology has carved a niche in various industries as an alternative to conventional separation technologies (Bowen, 2001b), especially for certain types of materials that have been inherently difficult and expensive to separate, such as:

1 Finely dispersed solids, especially those that are compressible, have a high density close to that of the liquid phase, have high viscosity, or are gelatinous.
2 Low molecular weight, non-volatile organics or pharmaceuticals and dissolved salts.
3 Biological materials which are very sensitive to their physical and chemical environment.

The materials processed have categorised the different types of membranes. The categories of membranes currently available are microfiltration (MF), ultrafiltration (UF) and reverse Osmosis (RO), nanofiltration (NF), dialysis (D) and electrodialysis (ED); each of which have properties outlined in Table 1.1.

| Name of process | Driving force (ΔP) | Separation size range | Examples of materials separated |
|---|---|---|---|
| Microfiltration | Pressure gradient (< 0.2 MPa) | 10-0.1 μm | Small particles, large colloids, microbial cells |
| Ultrafiltration | Pressure gradient (0.1 - 0.5 MPa) | < 0.1 μm- 5 nm | Emulsions, colloids, macromolecules, proteins |
| Nanofiltration | Pressure gradient (3- 9 MPa) | ≤ 2 nm | Low molecular weight organics and charged species |
| Reverse Osmosis | Pressure gradient (1 – 10 MPa) | ≤ 1 nm | Dissolved salts, small organics |
| Dialysis | Concentration gradient | < 5 nm | Treatment renal failure |
| Electrodialysis | Electro field | < 5 nm | Dissolved salts |

**Table 1.1 Classification of Membrane Separation Processes for Liquid Systems (Bowen, 2001b)**

The membranes used for all four processes are most commonly made of polymeric materials, usually polyamide, polysulphone, polycarbonate and increasingly advanced polymers (Merry, 2001) (Bessarabov and Twardowski, 2002) (Balannec *et al.*, 2004) (Platt *et al.*, 2004). Inorganic membranes are relatively new in design and are fabricated from ceramics or metals. Generally, the fabrication of inorganic membranes for MF and UF is well established, but the fabrication of truly NF inorganic membranes is still under development (Garem *et al.*, 1997). Typical materials for these membranes are ceramics and zeolites (alumina, titania and zircona). Organic membranes are mechanically weaker than inorganic membranes but they are cheaper (Bessarabov and Twardowski, 2002) and although they are not as chemically or physically resistant, they can offer sufficient chemical stability with high resistance to microbial degradation and to solvents.

Most MF membranes have a symmetrical pore structure, with porosities as high as 80% and thickness typically in the range of 50-100 μm. UF membranes are also porous membranes with an asymmetric pore structure comprising a 1-2 μm thick top layer of very fine pore sizes supported by a ~ 100 μm thick openly porous layer. The

thin-film composite (TFC) membrane is another type of UF membrane. It consists of an extremely thin layer, typically ~ 1 μm thick, of the finest pore structure, deposited on a more openly porous matrix. In TFC membranes, the thin layer and the support are made from different materials. RO and NF membranes are generally considered to have no microscopic pore structure but to consist of a polymer network in which solutes can be dissolved (Bowen, 2001b).

## 1.2 Nanofiltration Membranes

Nanofiltration membranes (NF) have been available for 20 years, making them the newest type of membrane. NF membranes were born out of the success of high rejection reverse osmosis membranes (RO), which created interest in other applications requiring less demanding salt rejection and lower net driving pressures. Cadotte was one of the first workers to designate these membranes as Nanofiltration membranes to distinguish them from RO membranes. The name Nanofiltration corresponds to a hypothetical pore in the membrane surface of approximately 10 angstrom in diameter, which is equivalent to 1 nanometre (Cadotte *et al.*, 1988). The apparent pore size corresponds to the molecular weight cut off (MWCO), which is determined by measurement of rejection of single salt solutions (Bowen and Mukhtar, 1996). NF membranes have been referred to as 'loose' low-pressure RO membranes (Tsuru *et al.*, 1991), where high-pressure RO membranes have been referred to as 'tight membranes' (Merry, 2001).

The operating pressure used in NF ($1 < \Delta P < 3$ MPa) are lower than in RO because of the more open pore structure which allows some permeation of solutes, reducing the osmotic potential gradient.

UF membranes are often used as the porous support layer, on to which the 'active' layer (thickness approximately 1-2 nm), which is assumed to control all separation characteristics, is deposited using either a dip coating or interfacial polymerisation. Polyamide is often used as the thin film membrane layer in NF and RO membranes (Merry, 2001). The presence of the ionisable groups in the active layer provides the membrane with an ionic charge; a key characteristic of NF membranes. These charges can either be positive (formed from cationic groups such as $-NH_3^+$) or negative

(formed from anionic groups such as $-CO_2^-$, $-SO_3^-$ and $H_2PO_4$), however, most NF membranes tend to be negatively charged at neutral pH values.

Industrial scale membranes can be configured in tubular, spiral, flat sheet or hollow fibre arrangements. Spiral membranes consist of tightly packed filter material formed into a *"Swiss Roll"* arrangement with mesh spacers, and wrapped in a small tube. This configuration is often used because the packing density (approximately 300 – 1000 $m^2m^{-3}$) significantly increases the surface area compared with tubular or flat sheet membranes. However, this type of arrangement is prone to fouling and therefore requires pre-filtration (Bowen, 2001b; Merry, 2001).

## 1.3 Separation mechanisms of NF membranes

Understanding the factors that affect the separation properties of NF membranes is very important for engineering applications. The development of predictive models should take into account the following factors:

- The NF membrane itself; structural parameters such as pore radius and membrane thickness, electrical parameters such as charge density
- The feed solution: characteristics of ions or solutions, concentrations, pH and fouling potential.
- The operating unit: capacity, dimensions, flow rate, mass and heat transfer parameters.
- The process environment: temperature and pressure

The last two factors involve fundamental principles of chemical engineering and are elaborated in great detail in various chemical engineering textbooks (Coulson and Richardson, 2001). The first two factors, which are specific to the NF membrane system, are interrelated and are very important in understanding the separation behaviour in NF systems.

NF membranes have properties that lie between those of UF and RO membranes (Table 1.1). RO membranes ideally allow only solvent (usually water) molecules to

pass through, and reject almost all solutes. UF membranes are used for the concentration and separation of colloids, proteins and other relatively large macromolecules (Table 1.1). NF membranes have a molecular weight cut off (*MWCO*) below 1000 Da, and are predominantly used for the concentration and fractionation of low molecular weight (100-1000 Da) species. NF membranes have another striking difference from RO and UF membranes; most of them have a charged layer as the separating zone or 'skin', this layer gives the membranes an inherent charge. Therefore NF membranes exhibit two distinct separation mechanisms:

1. Steric exclusion – uncharged solutes are rejected through a purely steric mechanism and dependent only on the relative size of the pore.
2. Donnan effects – charged solutes are rejected through charge repulsion.

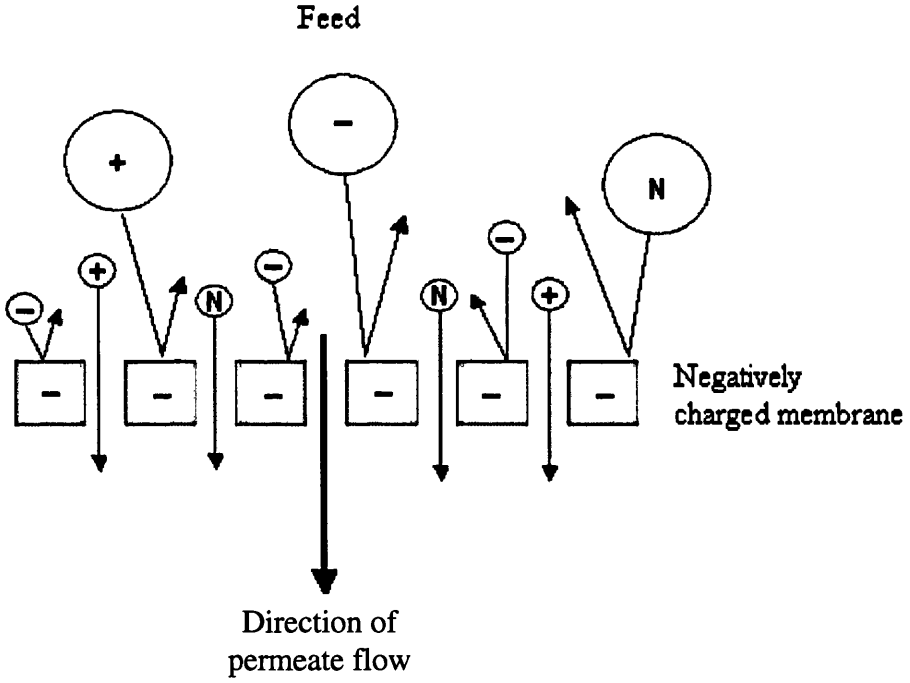


**Figure 1.1 Separation mechanisms of charged nanofiltration membranes (Tsuru *et al.*, 1994)**

Rejection of charged solutes through charge repulsion is a unique property of NF membranes. This enables NF membranes to fractionate molecules of the same size depending on their charge. The combination of small pore size and fixed surface charges make NF membranes especially suitable for the fractionation of small organic molecular weight ions of different valences.

## 1.4 Industrial applications of NF membranes

NF technology has a large and growing market place in the field of water treatment processes. Over recent years, the range of application of NF membranes has broadened, and is becoming more commonplace for specific applications. Approximately 65 % of the NF membrane market is accounted for by the water treatment industry, 25 % for the food & dairy industry, and less than 10 % for the chemical industry (Bessarabov and Twardowski, 2002). Some of the more recent applications for NF membrane technology are reported in Table 1.2

| Application | Reference |
|---|---|
| **Wastewater Treatment** | |
| Textile dying effluent | (Van der Bruggen *et al.*, 2001) |
| Coke plant effluent | (Minhalma and Norberta de Pinho, 2004) |
| Ni-P electroless plating effluent | (Mohammad *et al.*, 2004) |
| Reactive dye effluent | (Kim *et al.*, 2004) |
| Estrogenic hormone removal | (Nghiem *et al.*, 2004) |
| Biologically treated textile effluents | (Bes-Pía *et al.*, 2004) |
| Metal removal from pulp mill effluent | (Lastra *et al.*, 2004) |
| | |
| **Food and Biotechnology** | |
| Dairy by-product removal | (Nguyen *et al.*, 2003) |
| Biotransformation pharmaceutical reaction | (Bowen *et al.*, 2004) |
| Utilization of whey protein and lactose | (Atra *et al.*, 2004) |
| Pharmaceutical recovery | (Zhu *et al.*, 2003) |
| Separation of amino acids | (Gotoh *et al.*, 2004) |
| | |
| **Chemical Industry** | |
| Separation of organometallic catalysts | (Scarpello *et al.*, 2002) |
| Benzene/cyclohexane separation | (Villaluenga and Tabe-Mohammadi, 2000) |

**Table 1.2 Nanofiltration membrane technology applications**

## 1.5 Objectives of the present work

Recent work into NF membranes has been to produce reliable predictive models for scale up and optimisation of membrane separation processes (Oatley, 2004). Other work has been concerned with the prediction and characterisation of NF membrane rejection properties for high value products such as amino acids Li *et al.* (2003), Gotoh *et al.* (2004), Wang *et al.* (2002). Methods now exist for prediction of the rejection mechanisms for simple monovalent salts. However, there is currently insufficient knowledge of NF separations of amino acids, and some surprising phenomenon has been observed, where rejection increases with concentration (Li *et al.*, 2003).

The present work was intended to contribute to the understanding of nanofiltration separations for amino acids and uncharged organic molecules, particularly concentration dependent rejection. This was achieved by:

a) Experiments in which different amino acids were filtered through a nanofiltration membrane, with particular emphasis on the effect of concentration. Comparison between existing models and experimental data.
b) Experimental observation of concentration dependency for dimerisation and polymerisation of amino acids, and the associated gain in the molecular weight for the amino acid species.
c) Practical evaluation on the effect of solute concentration on molecular weight cut-off of the nanofiltration membrane.
d) A comparison between the experimental and theoretical results for the rejection of small-uncharged organic molecules, with respect to concentration.
e) Characterisation of membrane properties by streaming potential titrimetric measurements with emphasis on the membrane's surface charged groups.
f) Finally, the rejection data was compared to adsorption models and conclusions were drawn with respect to the governing rejection mechanisms occurring.

# 2 Literature Review

## 2.1 Introduction

It was beneficial to conduct a study of publications relating to membrane technology and make a qualitative assessment of the type of studies conducted and how they influenced the course of research presented in this report. This was achieved by splitting the research into categories and then addressing them individually.

The categories investigated were:

i. nanofiltration of ions;
ii. the nanofiltration of amino acids: investigation of the influence of pH, molecular charge;
iii. investigation of theoretical techniques: transport models that have been used to describe the behaviour of small organic molecules during nanofiltration;
iv. membrane properties and membrane chemistry: charge and structural properties;
v. double layer effects: solute surface interactions and dipole moment;
vi. measurement of surface forces: streaming potential, titrimetric measurements and osmotic pressure.

The published research relating to these topics is summarised below.

## 2.2 Nanofiltration of ions

Rautenbach and Gröschl analysed the separation potential of nanofiltration membranes for anions of different valences and fractionation of low molecular weight organics, including amino acids (Rautenbach and Gröschl, 1990). Practically, rejection at NF membranes is low for salts with monovalent ions and uncharged solutes with molecular weights < 150 Da, while high for salts with diavalent and multivalent ions and organics with molecular weights > 200 Da (Levenstein *et al.*, 1996).

It has been widely assumed that ions undergo partitioning at the entrance of NF membranes by means of the Donnan exclusion mechanism (Levenstein *et al.*, 1996). The Donnan exclusion principle predicts that the efficiency of ion exclusion decreases as the valence of the counter-ion increases or increases as the valence of the co-ion increases. As an example, for a negatively charged membrane, rejection of salts with divalent anions such as $Na_2SO_4$ is always high compared to a monovalent salt such as NaCl.

Bowen included steric effects in their analysis of salt rejection (Bowen and Mukhtar, 1996). Steric effects play an important part in NF rejection, because of the fact that hydrated ions can have similar size to that of an NF pore. Bowen (Bowen *et al.*, 1997b) further investigated the relative importance of the size effect by studying the order of rejection for LiCl, NaCl and KCl from the CA30 NF membrane. The order of rejection was found to be LiCl > NaCl > KCl, indicating that rejection was indeed a function of size (as well as charge density) in the apparent narrow pores of NF membranes (Bowen and Mohammad, 1998).

Peeters conducted a series of experiment for various membranes and solutes, which identified three types of salt rejection characteristics (Peeters *et al.*, 1998)

a) membranes where $R(Na_2SO_4) > R(NaCl) > R(CaCl_2)$
b) membranes where $R(CaCl_2) > R(NaCl) > R(Na_2SO_4)$, and
c) membranes where $R(Na_2SO_4) > R(CaCl_2) > R(NaCl)$

where $R$ signifies rejection, given by:

$$R = 1 - \frac{C_P}{C_R}$$

where $C_P$ is the concentration of solutes in the permeate and $C_R$ is the initial concentration of solutes in the system.

Donnan exclusion is the dominant mechanism, this is seen in a) and b) where rejection increases with co-ion valence and decrease; with increasing counter-ion valence for negatively and positively charged membranes respectively.

Yaroshchuk further discussed rejection mechanisms of NF membranes (Yaroshchuk, 1998). It was found that, along with Donnan exclusion, NF membranes may exhibit dielectric exclusion and hydration mechanism. Dielectric exclusion is caused by the interactions of ion with the polarisation charges induced by them at the pore surface. The strength of these interactions is proportional to the square of ion charge. So the rejection of divalent ions was greater than monovalent ions, irrespective of the sign of the charge. This effect would explain the behaviour of the membrane in c) above. However, the statement was made that the presence of fixed charges on the membranes surface would diminish the importance of this method of dielectric exclusion due to screening of the interactions by the counter-ions that compensate for the fixed membrane charge (indicating an extremely important coupling of Donnan and dielectric mechanisms).

Bowen assessed the performance of models of NF membranes (Bowen and Welfoot, 2002b). They found that the dielectric mechanisms could be expressed theoretically in terms of an energy barrier to solvation for ions when passing from one solvent at a particular dielectric constant, to another solvent at a different dielectric constant. The confinement of solvent molecules within pores (which are only about one order of magnitude greater than atomic dimensions) causes macroscopic descriptions of hydrodynamics and interactions to breakdown. Therefore parameters such as solvent viscosity and solvent dielectric constant are affected. Electrochemical studies of colloidal systems have shown the presence of one layer of water molecules at the colloid-solvent interface with a dielectric constant that is significantly smaller than bulk water (Israelachvili, 1991). Orientation of the solvent molecules at pore walls will similarly lead to a reduction in dielectric constant, as this realignment of the solvent into discreet yet diffuse layers causes a shift in the physical and electrical properties of the solvent. This model was originally proposed by Born (Born, 1920) and is dependent on the square of the ion valence.

The hydration mechanism was suggested to work by the loss of solvent dissolving ability which is related to the changes in its dielectric properties (Yaroshchuk, 1998). In this case multiple-charge ions should be excluded from pores more so than single-charged ones, so this mechanism is also capable of describing the behaviour of the

membranes in c). Bardot carried out work in this field to observe the effect of electrolyte mixtures on membrane performance ((Bardot *et al.*, 1995).

Therefore, at present, the separation characteristics of ion at charged membranes are thought to be by the following three mechanisms:

1. steric effects – related to the relative size of the solute pore;
2. electrostatic (Donnan) effects – can be either attractive or repulsive depending on the valence of the ions and the magnitude of the fixed membranes charge. The higher the valence of the co-ion, the higher the salt retention; the higher the valence of the counter-ion, the lower the salt retention (Peeters, 1997);
3. dielectric interactions – where multivalent ions are rejected to a higher degree than monovalent ions due to interactions between the ions, membranes and solvent at the surface and inside the NF pores.

Schaep reported experimental evidence to support the suggested three separation mechanisms (Schaep *et al.*, 2001). Four NF membranes were studied using a range of salts and the results are summarised in Table 2.1.

| Salt | CA30 | NTR7450 | NF40 | UTC20 |
|---|---|---|---|---|
| | *R* | *R* | *R* | *R* |
| NaCl | 0.08 | 0.41 | 0.41 | 0.47 |
| $MgCl_2$ | 0.20 | 0.15 | 0.97 | 0.94 |
| $Na_2SO_4$ | 0.29 | 0.88 | 0.98 | 0.98 |
| $MgSO_4$ | 0.56 | 0.53 | 1.00 | 0.97 |

**Table 2.1 Rejection characteristics of four NF membranes (Schaep *et al.*, 2001)**

From Table 2.1, it can be see that the NTR7450 membrane exhibits classical Donnan exclusion behaviour for a negatively charged membrane. The CA30 membrane indicates dielectric exclusion characteristics as $MgSO_4$ is significantly more highly rejected than either $Na_2SO_4$ or $MgCl_2$. However, the other two membranes appear to show characteristics related to a combination of all three mechanisms.

The rejection of solutes at a nanofiltration membrane decreases with increasing solute concentration. This is a typical phenomenon if electrostatic interactions are involved in the rejection mechanism, Hagmeyer and Gimbel, 1998, Garba *et al.*, 2003 Mohammad and Takiiff, 2003 and Oatley *et al.*, 2005 have been among the latest to report this observation. As concentrations increase, the membrane's fixed charge becomes increasingly neutralised (shielded) by the counter-ions in solution, resulting in lower rejection. Thus, the importance of the Donnan mechanism becomes progressively diminished with increasing feed concentration. However, some workers (Hagmeyer and Gimbel, Bowen and Welfoot, and Bandini and Vezzani) have observed the rejection of salts increasing with feed concentration (Bandini and Vezzani, 2003). Hagmeyer and Gimbel, and Bandini and Vezzani observed an increase in rejection for an increase in feed concentration of $CaCl_2$. Bowen observed the rejection of both $MgCl_2$ and $MgSO_4$ increasing with concentration (Bowen and Welfoot, 2002b). All of the workers used a Desal 5 DK nanofiltration membrane, and none of them explained their findings for this surprising phenomenon. Peeters observed the rejection of $CaCl_2$, for 21 different NF membranes (not including Desal 5 DK), decreasing for increasing feed concentration (Peeters *et al.*, 1998). Therefore, this phenomenon is in contrast to known NF separation mechanisms.

Experiments have been conducted to quantify the rejection of salts at different pH values. Zeta potential measurements have been preformed to gain an insight in to the variation of membranes charge caused by dissociation of ionisable surface groups (Hagmeyer and Gimbel, 1998). Small organic molecules may exhibit rejection mechanisms that are dependent on pH. This group of molecules includes amino acids, humic acids, lactic acids and other simple organics that can be charged to different extents, or neutral depending on the pH of the solution. Other factors could cause a change in the membranes electrical characteristics that would affect the rejection behaviour, such as interactions between divalent cations and the membrane (Childress and Elimelech, 1996) and fouling (Nyström *et al.*, 1995). Thus, the feed conditions can be modified to tailor the charge properties of the membrane and the molecules for a particular separation.

## 2.3 Nanofiltration of amino acids

In recent years, several membrane processes have been developed and applied in the dairy industry. The main area of interest in the dairy industry was the separation of proteins, peptides and amino acids (Timmer *et al.*, 1998). This lead to work that was concerned with the prediction and characterisation of NF membrane rejection properties for high value products such as amino acids (Li *et al.*, 2003, Gotoh *et al.*, 2004 and Wang *et al.*, 2002). Other sections of the food industry also use NF and RO membranes for processing fruit juices, tea, coffee and sugar solutions (Merry, 2001).

Since amino acids contain both an acidic and a basic group, they undergo an intramolecular acid-base reaction and exist in the form of a dipolar ion or zwitterion. Amino acid zwitterions are internal salts and they have many of the physical properties associated with ordinary salts. They have large dipole moments, are soluble in water but insoluble in hydrocarbons, and are crystalline substances with high melting points. Amino acids are also amphoteric; they react as acids or bases, depending on the environment. In aqueous acidic solution, an amino acid zwitterion is a base that accepts a proton to yield a cation; in aqueous base solution, the ion was an acid that lost a proton to form an anion. The pH at which the amino acid is balanced between anionic and cationic forms and exists as a neutral dipolar zwitterion is called the isoelectric point. The isoelectric point of an amino acid depended on its structure and therefore its $pK_\alpha$ values (data given in Chapter 4). From the $pK_\alpha$ values, the fraction of protonated, neutral and deprotonated forms in solution for a given pH was calculated by the Henderson-Hasselbalch equation:

$$\log\frac{[A^-]}{[HA]} = pH - pK_\alpha$$

where $[A^-]$ is the proton acceptor and $[HA]$ is the proton donor. An example calculation of the fraction mean charge of an amino acid is shown in Appendix A.5 and the charge calculation results are given in Chapter 4.

Separation of amino acids with molecular mass in the region of 200-1000 g/mol is very difficult. This is due to the fact that the differences in physicochemical

characteristics between the components are moderate because of their small number of inorganic or hydrophobic groups (Garem *et al.*, 1997). Therefore, the separation of amino acids requires a process that is highly selective to small differences in charge, size and hydrophobicity Popular separation processes have been chromatography (Ding *et al.*, 2002; Horie and Kohata, 2000) and ion-exchange membranes (Bobreshova *et al.*, 2002; Elisseva *et al.*, 2002; Minagawa *et al.*, 1997; Sato, 2002). In spite of chromatography's efficacy, their utilisation at the industrial scale creates problems with productivity and prohibitive costs (Garem *et al.*, 1997). The ion-exchange method has attained high yields but produces a lot of harmful acidic and basic wastes (Wang *et al.*, 2002). Food manufactures have made commitments to reduce the amount of chemical additives used in food products and this has lead to a rise in popularity of nanofiltration membranes separations, as these are seen as a "natural" separation that can produce a high purity product without the use of additives. A main area of interest has been the effect of pH on the rejection mechanism for amino acids for NF separations (Garem *et al.*, 1997; Li *et al.*, 2003). Garem discussed the dependence of the rejection behaviour of amino acids at NF membranes on pH through the isoelectric point of the amino acid. Li conducted a series of experiments that examined the effect of pH on rejection for glutamic acid; their data is presented in Figure 2.1.

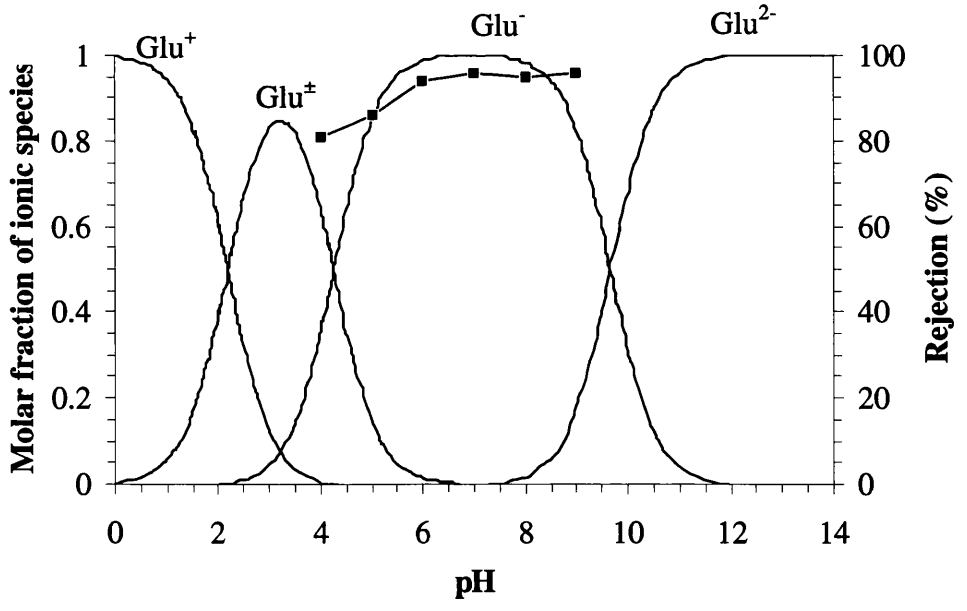


**Figure 2.1 Rejection of Glutamic acid with changing pH Li *et al.* 2003 (1.2 g/l @ 35°C and 1.6 MPa)**

The rejection data presented in Figure 2.1 showed that as the pH was increased from 4 to 9, the rejection increased from 80% to 95%. This was due to the mean net charge of the glutamic acid molecules becoming more negative and increasingly repelled from the negatively charged membrane. At pH 4 the majority of the glutamic acid molecules are at a zero net charge state, with only a few molecules being in the anion state. When considering all of the molecules in solution at pH 4 the mean net charge was –0.34 (electrons per molecule). This mean net charge increased to –1.00 (electrons per molecule) for pH 7 as anion charge predominated. This mean net charge increased further to –1.18 electrons per molecule at pH 9 as both the COOH groups became deprotonated.

An amino acid model was devised for the prediction of rejection of amino acids permeating a nanofiltration membrane that was based on size and charge effects (Garem *et al.*, 1997; Grib *et al.*, 2000; Li *et al.*, 2003; Martin-Orue *et al.*, 1998). This model is presented and examined in Chapter 4.

Li *et al.* (2003) observed that the rejection of glutamate decreased, as expected, for an increase in concentration, for a polymeric NTR7450 NF membranes. For glutamine, the rejection increased for an increase in concentration. The rejection of glutamine was expected to be near zero and independent of the concentration, because the pore size of NTR 7450 membrane is significantly larger than the size of the glutamine molecule. Hong and Bruening (2006) studied multilayer polyelectrolyte nanofiltration membranes for the separation of amino acids and they found that the rejection was influenced by concentration. Li attempted to explain the difference between the experimental results and the expected rejection, by suggesting that glutamine might exist as a dimer or polymer of glutamine. This explanation was tested in the current work and an investigation was conducted into the effect of concentration on rejection for amino acids (Chapter 4).

## 2.4 Models that describe rejection of organic molecules

In this section, several models that describe the rejection of uncharged organic molecules are discussed with reference to their background and transport mechanisms. There are two approaches to the derivation of nanofiltration models, the first

considered a membrane as a black box and has been derived from irreversible thermodynamics. The second method was phenomenological and aimed to provide a transport theory that incorporated a description of each governing mechanism.

### 2.4.1 Theoretical background

A discussion of the transport mechanisms through a nanofiltration membrane was necessary for the description of the retention of uncharged molecules. Transport of uncharged molecules was a combination of diffusion and convection. This was expressed in the transport equations of Spiegler and Kedem (1966) for water flux through the membrane and for the flux of a dissolved component.

$$J_v = L_P(\Delta P - \sigma\Delta\pi) \tag{2.1}$$

$$J_s = \omega\Delta\pi + (1-\sigma)J_v C \tag{2.2}$$

where $J_v$ was the total permeate volumetric flux, $L_P$ was the hydraulic permeability, $\sigma$ was the reflection coefficient, $\omega$ was the mobility of the solute, $c$ was the concentration of the solute and $J_s$ represented the solute flux.

Spiegler and Kedem (1966) stated that when the specific hydraulic permeability $P_1$; the local solute permeability, $P_2$ and the reflection coefficient, $\sigma$, were constant, then equations (2.1) and (2.2) could be applied across a membrane:

$$J_v = -P_1\left(\frac{dp}{dx} - \sigma\frac{d\pi}{dx}\right) \tag{2.3}$$

$$J_s = -P_2\frac{dc_s}{dx} + (1-\sigma)c_s J_v \tag{2.4}$$

The approximate constancy of these three coefficients was brought about by the consideration of local membrane flux. The relationship between local and overall permeability's was summarised by:

$$L_P \equiv P_1/\Delta x \quad \text{and} \quad \omega = P_2/(2RT\Delta x)$$

hence they are normalised for unit membrane thickness.

By consideration of the following conditions (where superscripts ' and " denote the feed and permeate sides of the membrane respectively):

$$C''_s = J_s / J_v \tag{2.5}$$

and

$$R = 1 - \frac{c''}{c'} \tag{2.6}$$

Therefore, solute rejection was defined as:

$$R = \frac{(1-F)\sigma}{1-\sigma F} \tag{2.7}$$

$$\text{where } F = e^{-J_v A},\ A = \frac{1-\sigma}{P_2} \tag{2.8}$$

Equation (2.7) allowed the calculation of solute rejection using reflection coefficient, $\sigma$, and solute permeability $P_2$, determined from osmotic pressure and diffusion measurements. Equations (2.1), (2.2), (2.7) and (2.8) were referred to as the Spiegler-Kedem models (Spiegler and Kedem, 1966). A model for $\sigma$ provided the necessary information about the retention at a relatively high water flux and at high pressure. The resulting curve for the reflection coefficient as a function of the molecular diameter was to estimate the maximal rejection that could be obtained for a given membrane. The models that use $\sigma$ for the prediction of rejection for uncharged molecules were; the steric hindrance pore model, the model of Zeman and Wales (1981), the log-normal model and the adapted log-normal model.

**The Steric Hindrance Model**

In the steric hindrance pore model the reflection coefficient is calculated from the pore size of the membrane and the diameter of the molecule. It is assumed that all the pores in the membrane have the same size. In reality, not every pore has the same cylindrical diameter; the model is an approximation of the membrane's structure. During filtration, the solute molecules encountered a certain amount of steric hindrance and interaction with the pore wall. A molecule that had a diameter smaller than membrane pore was partially retained, while a molecule with the same size as the pore was completely retained by the membrane.

The reflection coefficient was then calculated by;

$$\sigma = 1 - H_F S_F \tag{2.9}$$

with

$$H_F = 1 + \left(\frac{16}{9}\right)\eta^2 \tag{2.10}$$

$$S_F = (1-\eta)^2\left[2-(1-\eta)^2\right] \tag{2.11}$$

$$\eta = \frac{d_s}{d_p} \tag{2.12}$$

where $H_F$ is the 'wall-correction parameter' that represented the effect of the pore wall. $S_F$ is a parameter that represented steric hindrance during transport through the pores. $d_s$ and $d_p$ are the diameters of the molecule and the pore respectively.

Ferry (1936) described the retention of a sphere through a capillary filter as:

$$\sigma = 1 - (\eta(\eta-2))^2 \tag{2.13}$$

The capillaries were assumed to have a uniform cylindrical diameter. Ferry also assumed that a parabolic velocity profile existed within the pore (Ferry, 1936). Zeman and Wales (1981) introduced a term into the Ferry model (equation 2.13) to account for steric hindrance during convective transport. This steric hindrance was assumed to cause a hydrodynamic lag in the membrane pores. Zeman and Wales found by experiment that this hindrance term could be expressed as $\exp(-\alpha\eta^2)$ where $\alpha$ was a dimensionless constant. Equation (2.13) could than be written as:

$$\sigma = 1 - \left[(\eta(\eta-2))^2\right]\exp\left(-\alpha\eta^2\right) \tag{2.14}$$

Martin-Orue *et al.* (1998), Garem *et al.* (1997), Grib *et al.* (2000) and Li *et al.* (2003) all assumed that $\alpha = 0.7146$ for nanofiltration of amino acids. This is discussed further in Chapter 4.

**The Log-Normal Model**

The log-normal model assumed that the membrane pore size was not uniform but that a log-normal distribution pore size existed. No steric hindrance in the pore or hydrodynamic lag was taken into account, but it was assumed that a molecule

permeated through every pore that was larger than the diameter of the molecule. The contribution of diffusion to transport through the membrane was considered to be negligible. The maximal retention was presented by Van der Bruggen *et al.* (2000) as:

$$\sigma(r^*)=\int_0^{r^*}\frac{1}{S_p\sqrt{2\Pi}}\frac{1}{r}\exp\left(-\frac{[\ln(r)-\ln(\bar{r})]^2}{2S_P^2}\right)dr \qquad (2.15)$$

Where $S_p$ was the standard deviation of the pore size distribution and $r$ was the mean pore size. The log-normal model was also expressed in terms of molecular weight (*MW*) and molecular weight cut-off (*MWCO*) (Chapter 5).

**The adapted Log-Normal Model**

The log-normal model was optimized by Van der Bruggen *et al.* (2000) to include the hydrodynamic lag in the pores as given by the Zeman and Wales model. This model is known as the adapted log-normal model. It was assumed that a molecule is completely retained by a pore smaller than the molecules diameter. If the pore is larger than the molecule's diameter, then the molecule is partly retained to the extent that its velocity in the pore is lower than the water velocity. The reflection coefficient is then written as the sum of the fraction of the pores that are smaller than the molecular diameter, and the fraction of molecules that are retained by the pores that are larger than the molecular diameter. The maximal retention given by the adapted log-normal model as presented by Van der Bruggen *et al.* (2000) is:

$$\sigma(r^*)=1-\int_{r^*}^{\infty}\exp\left(-\alpha\left(\frac{r^*}{r}\right)^2\right)\frac{1}{S_p\sqrt{2\Pi}}\frac{1}{r}\exp\left(-\frac{[\ln(r)-\ln(\bar{r})]^2}{2S_P^2}\right)dr \qquad (2.16)$$

Van der Bruggen *et al.* (2000) compared the performance of these four models to experimental results for a range small uncharged organic molecules. The steric hindrance pore model and the Zeman and Wales model were shown to give the poorest fit to the experimental data. This was due to these models being based on an idealised view of the membrane structure. Van der Bruggen *et al.* (2000) considered these two models as not describing a meaningful physical description of the membrane separation. The log-normal and adapted log-normal models both exhibited an excellent fit to the experimental data. The adapted log-normal model accounted for hydrodynamic lag in the pores by defining a supplementary membrane parameter.

Therefore, Van der Bruggen *et al.* (2000) found that the adapted log-normal model was considered the best model for theoretically describing the reflection coefficient. However, the log-normal model, where the hydrodynamic lag was neglected, was considered to be the most practical model to predict the reflection coefficient. This was because the influence of the hydrodynamic lag was found to be negligible (Van der Bruggen *et al.*, 2000), and this model did not require the calculation of the difficult integral equation involved in the adapted log-normal model. The log-normal model consisted of only two parameters (mean pore size and standard deviation from the mean pore size), therefore the log-normal model represented a good semi black box model and has been compared to experimental data in Chapter 5.

### 2.4.2 Extended Nernst Plank Models

An assessment of models suitable for describing nanofiltration rejection would not be complete without a discussion of the theoretical approximations based on the extended Nernst-Plank equation. The most recent derivation was termed the Donnan Steric Partitioning Model (DSPM) was proposed by Bowen *et al.* (1997b). This model assumed a porous membrane structure and that ion transport was described by the extended Nernst-Plank equation modified to include hindered transport:

$$j_i = -D_{i,p}\frac{dc_i}{dx} - \frac{z_i c_i D_{i,p}}{RT} F \frac{d\psi}{dx} + K_{i,c} c_i V \qquad (2.17)$$

where $D_{i,p}$ was the hindered diffusion coefficient of ion $i$ in the pore, $z_i$, and $c_i$ were the valence and concentration respectively of the ion, $\psi$ the electronic potential and $K_{i,c}$ and $V$ were the hindrance factors for convection and the solute velocity. The equilibrium partitioning of ions at the pore inlet and outlet was assumed to be due to a combination of electrical (Donnan) and sieving (steric) mechanisms, resulting in:

$$\frac{c_i}{C_i} = \Phi_i \exp\left(-\frac{z_i F}{RT}\Delta\psi_D\right) \qquad (2.18)$$

where the steric partitioning coefficient was defined (Deen, 1987) as:

$$\Phi = (1-\lambda)^2 \qquad (2.19)$$

where $\lambda$ was given by the relative size of the solute to pore radii ($r_s/r_0$).

With consideration of pore electroneutrality, then equation (2.17) became:

$$\frac{d\psi}{dx} = \frac{\sum_{i=1}^{n} \frac{z_i V}{D_{i,p}} \left( K_{i,c} c_i - C_{i,p} \right)}{\frac{F}{RT} \sum_{i=1}^{n} \left( z_i^2 c_i \right)} \tag{2.20}$$

$$\frac{dc_i}{dx} = \frac{V}{D_{i,p}} \left( K_{i,c} c_i - C_{i,p} \right) - \frac{z_i c_i}{RT} F \frac{d\psi}{dx} \tag{2.21}$$

Equations (2.20) and (2.21) were solved using the boundary conditions of:

$$x = 0,\ C_i = C_{i,f} \text{ and } x = \Delta x,\ C_i = C_{i,p}$$

where subscripts $f$ and $p$ denote the concentration of ion $i$ at the feed side and permeate side of the membrane.

The DSPM model was used to fit filtration rejection data as a function of permeate flux. The model was fitted to the data by manipulation of the three model parameters that represent physical properties of the membrane. These parameters were pore radius, $r_p$, the ratio of membrane thickness to porosity $\Delta x/A_k$, and the membrane charge density, $X_d$.

Schaep *et al.* (2001) applied the DSPM to a system of multivalent cations and found that the models performance was poor when compared to the quality of agreement observed for simple systems of single organic solutes or univalent salts. The poor performance of the DSPM model was attributed to the fact that the three model fitting parameters only had a limited correspondence to the structural and electrical properties of the membrane. Welfoot (2001) adapted the model to account for electrochemical potential (equations 2.22 and 2.23).

$$\frac{dc_i}{dx} = \frac{V}{D_{i,p}} \left[ \left\{ K_{i,c} - Y_i \right\} c_i - C_{i,p} \right] - \frac{z_i c_i}{RT} F \frac{d\psi}{dx} \tag{2.22}$$

$$\frac{d\psi}{dx} = \frac{\sum_{i=1}^{n} \frac{z_i V}{D_{i,p}} \left[ \left\{ K_{i,c} - Y_i \right\} c_i - C_{i,p} \right]}{\frac{F}{RT} \sum_{i=1}^{n} \left( z_i^2 c_i \right)} \tag{2.23}$$

where

$$Y = \frac{D_p}{RT} V_s \frac{8\eta}{r_p^2} \tag{2.24}$$

and

$$\frac{c_i}{C_i} = \Phi_i \exp\left(-\frac{z_i F}{RT}\Delta\psi_D\right)\exp\left(-\frac{\Delta W_i}{kT}\right) \tag{2.25}$$

Equation (2.25) accounted for the relation between bulk solution concentrations, $C_i$ and the pore concentration $c_i$, which was governed by steric and electrostatic partitioning effect and the solvation energy barrier ($\Delta W_i$).

### 2.4.3 Summary of models

Having considered two different approaches of modelling nanofiltration behaviour, it was useful to follow this with a comparison of the two modelling methods.

The DSPM model was devised to model rejection as a function of applied pressure. To obtain a set of data for rejection as a function of concentration required the DSPM to be rearranged and therefore would not be used as it was intended. The DSPM two parameter model also required the quantification of specific membrane properties such as membrane charge $X_d$, which was used as a fitting parameter. In contrast, the log-normal model relied on a value known as the reflection coefficient. This represented the maximal rejection of a solute for a membrane at infinite pressure. The value of the reflection coefficient varied with respect to the solute but was a constant for the membrane. It was therefore concluded that a model that treated the membrane as a black-box or semi black-box was the best solution for modelling concentration dependant rejection. Hence, the log-normal model was used to fit the experimental data considered in this work.

## *2.5 Membrane properties and membrane chemistry*

Most materials acquire a surface electric charge when brought into contact with a polar (e.g. aqueous) medium. The charging mechanisms are:

- Ionisation;
- ion adsorption;
- ion dissolution.

The surface charge influences the distribution of nearby ions in the polar medium. Ions of opposite charge (*counter-ions*) are attracted towards the surface and ions of like charges (*co-ions*) are repelled away from the surface (in this case, nanofiltration membranes). This, together with the mixing tendency of thermal motion, leads to the formation of an electrical double layer made up of the charged surface and a neutralising excess of counter-ions over co-ions distributed in a diffuse manner in the polar medium. The theory of the electric double layer deals with the distribution and magnitude of electrical potentials occurring at a membrane surface. Double layer theory is an important first step towards understanding experimental observations concerning the electrokinetic properties membrane filtration.

### 2.5.1 Origin of charge at the membrane surface

**Ionisation**

Amino acids acquire their charge mainly through the ionisation of carboxyl and amino groups to give $-CO_2^-$ and $-NH^+_3$ groups. The ionisation of these groups, and the net molecular charge, depends strongly on the pH of the solution. At low pH, an amino acid molecule is positively charged and at high pH, it will be negatively charged. The pH at which the net charge (and electrophoretic mobility) is zero is the isoelectric point

**Ion Adsorption**

The membrane active layer contains an inherent surface charge, for example the NTR 7450 membrane's active layer material is sulfonated polyether sulfone; the sulfonic acid group ($-SO_3^-$) produces a relatively high negative charge (Schaep and Vandecasteele, 2001). Therefore at neutral and high pH there will be a preferential tendency to adsorb positive counter-ions.

Adsorption is often referred to as occurring in three stages, as the concentration increases. Firstly, a single layer of molecules builds up over the surface of the

membrane. This monolayer may be chemisorbed and will be associated with a change in free energy, which is a characteristic of the forces that hold it. As the fluid concentration is further increased, second, third etc., layers form by physical adsorption (Bowen, 2001a). The number of layers that form may be limited by the sizes of the pore. It is possible for counter-ion adsorption to cause a reversal of surface charge (Shaw, 1980)

**Ion Dissolution**

The dissociable groups occurring in the membrane active layer are strong acidic groups (sulfonic acid groups $-SO_3^-$) and weak acid groups (carboxylic groups $-CO_2^-$). The sulfonic acid groups, which are present on NTR 7450 membrane, are almost completely dissociated over nearly the entire pH range (pH 3-7), while carboxylic groups, which may be present on polyamide and cellulose acetate membranes, will not be dissociated at low pH (Schaep and Vandecasteele, 2001). Figure 2.2 shows a hypothetical polymeric NF membrane with carboxylic groups attached to the surface of the membrane, which is brought in contact with an aqueous solution of an electrolyte. The presence of the dissociated carboxylic groups on the membrane surface ($R-CO_2^-$) cause the occurrence of an active layer charge. This charge repels large $SO_4^{2-}$ ions and allows the passage of smaller $Cl^-$ ion through the NF membrane.

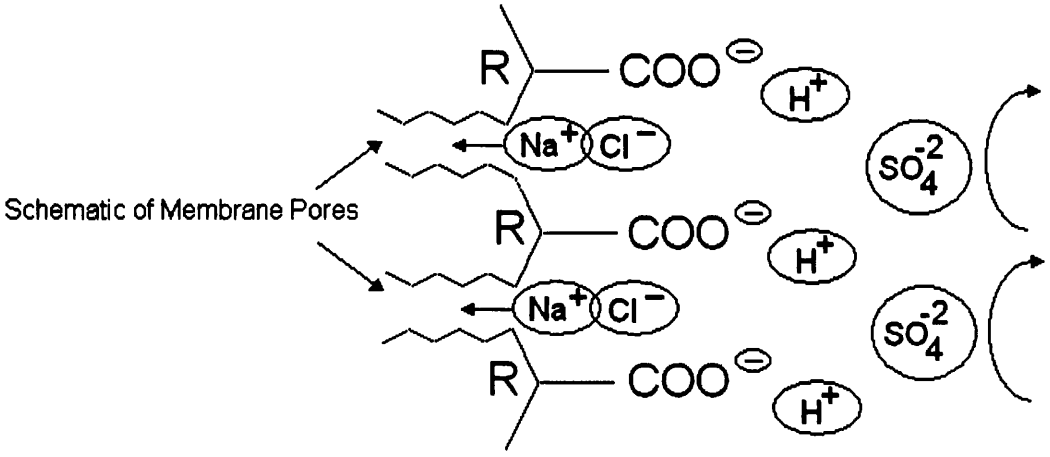


**Figure 2.2 Surface charge effects for a hypothetical polymeric nanofiltration membrane (Bessarabov and Twardowski, 2002)**

Models of the surface dissociation process are very useful for describing polymer latex systems, which often have carboxylic, sulphate, and sulphonate groups on their surfaces and which can also be made with zwitterionic surfaces (Elimelech and O'Melia, 1990).

## 2.6 The diffuse double layer

The electrical double layer can be regarded as consisting of two regions; an inner region which may include adsorbed ions; and a diffuse region in which ions are distributed according to the influence of electrical forces and random thermal motion. The electrical double layer is an extremely complex mechanism, and in order to fully understand and appreciate this phenomenon, a detailed knowledge of particle electrochemistry and molecular dynamics is required. Quantitative treatment of the electrical double layer presents difficult, and in some respects, an unsolved problem. The basis of the theoretical description to be adopted has been described in detail elsewhere (Shaw, 1980) (Hunter, 1986) (Israelachvill, 1991), so only the most important expressions are presented here. The intention of this work is not to further develop electrical double layer theory, but provide the reader with an understanding of the complex issues involved.

The simplest quantitative treatment of the diffuse part of the double layer is that due to Gouy (1910) and Chapman (1913), which is based on the following model:

1. The surface is assumed to be flat, or infinite extent and uniformly charged
2. The ions in the diffuse part of the double layer are assumed to be point charges distributed according to the Boltzmann distribution
3. The solvent is assumed to influence the double layer only through its dielectric constant, which is assumed to have the same value throughout the diffuse layer.
4. A single symmetrical electrolyte of charge number $z$ will be assumed

The electric potential will be $\psi_0$ at a flat membrane surface and $\psi$ at a distance x from the membrane surface in the electrolyte solution. Taking the surface to be positively charged (Figure 2.3) and applying the Boltzmann distribution,

$$n_+ = n_0 \exp\left[\frac{-ze\psi}{kT}\right] \qquad n_- = n_0 \exp\left[\frac{+ze\psi}{kT}\right] \tag{2.26}$$

where $n_+$ and $n_-$ are the respective numbers of positive and negative ions per unit volume at points where the potential is y (i.e., where the electric potential energy is $ze\psi$ and $-ze\psi$, respectively), and $n_0$ is the corresponding bulk concentration of each ionic species.

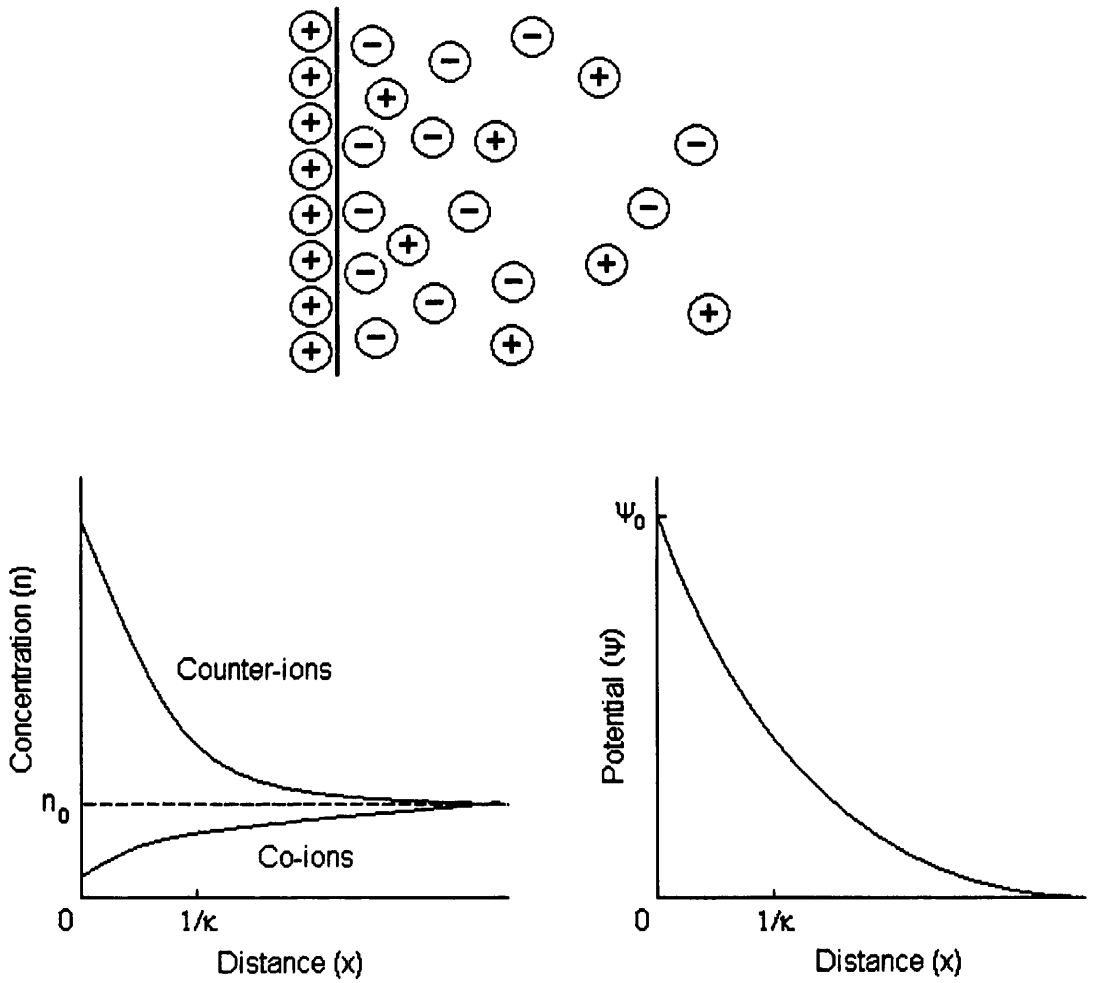


**Figure 2.3 Schematic representation of a diffuse electric double layer (Shaw, 1980)**

The net volume charge density ρ at points where the potential is $\psi$ is, therefore, given by

$$\begin{aligned}\rho &= ze(n_+ - n_-) \\ &= zen_0\left(\exp\left[\frac{-ze\psi}{kT}\right] - \exp\left[\frac{+ze\psi}{kT}\right]\right) \\ &= -2zen_0 \sinh\frac{ze\psi}{kT}\end{aligned} \tag{2.27}$$

$\rho$ is related to $\psi$ by Poisson's equation, which for a flat double layer takes the form

$$\frac{d^2\psi}{dx^2} = -\frac{\rho}{\varepsilon} \tag{2.28}$$

where $\varepsilon$ is the permittivity (the dielectric constant of a material is equal to the ratio between its permittivity and the permittivity of a vacuum).

Combination of equations (2.27) and (2.28) gives

$$\frac{d^2\psi}{dx^2} = \frac{2zen_0}{\varepsilon}\sinh\frac{ze\psi}{kT} \tag{2.29}$$

The solution of this expression, with the boundary conditions ($\psi = \psi_0$ when $x = 0$; and $\psi = 0$, $d\psi/dx = 0$ when $x = \infty$) taken into account can be written in the form

$$\psi = \frac{2kT}{ze}\ln\left(\frac{1+\gamma\exp[-\kappa x]}{1-\gamma\exp[-\kappa x]}\right) \tag{2.30}$$

where

$$\gamma = \frac{\exp[ze\psi_0/2kT]-1}{\exp[ze\psi_0/2kT]+1} \tag{2.31}$$

and

$$\kappa = \left(\frac{2e^2n_0z^2}{\varepsilon kT}\right)^{1/2} = \left(\frac{2e^2N_Acz^2}{\varepsilon kT}\right)^{1/2} \tag{2.32}$$

where $N_A$ is Avogadro's constant and $c$ is the concentration of electrolyte.

If $ze\psi_0 / 2kT \ll 1$ ($kT / e$ = 25.6 mV at 25°C, (Shaw, 1980)), the Debye-Hückel approximation

$$\exp\left[\frac{ze\psi_0}{2kT}\right] \approx 1+\frac{ze\psi_0}{2kT} \tag{2.33}$$

can be made and equations (2.30) and (2.31) simplify to

$$\psi = \psi_0\exp[-\kappa x] \tag{2.34}$$

This shows that at low potentials the potential decreases exponentially with distance from the charged surface. Close to the charged surface, where the potential is likely to be relatively high and the Debye-Hückel approximation inapplicable and the potential is predicated to decrease at a greater than exponential rate.

The potential $\psi_0$ can be related to the charge density $\sigma_0$ at the surface by equating the surface charge with net space charge in the diffuse part of the double layer (i.e., $\sigma_0 = -\int_0^\infty \rho\, dx$) and applying the Poisson-Boltzmann distribution. The resulting expression is

$$\sigma = (8 n_0 \varepsilon k T)^{1/2} \sinh \frac{ze\psi_0}{2kT} \qquad (2.35)$$

which at low potentials reduces to

$$\sigma_0 = \varepsilon \kappa \psi_0 \qquad (2.36)$$

The surface potential $\psi_0$, therefore, depends on both the surface charge density $\sigma_0$ and (through $\kappa$) on the composition of the medium. If the diffuse part of the double layer is compressed (i.e., $\kappa$ increased), then either $\sigma_0$ must increase, or $\psi_0$ must decrease, or both.

From equation (2.36) it can be seen that, at low potentials, a diffuse double layer has the same capacity as a parallel plate condenser with a distance $1/\kappa$ between plates. It is customary to refer to $1/\kappa$ (the distance over which the potentials decrease by an exponential factor at low potentials) as the *thickness* of the diffuse double layer. For a membrane nanopore, the surface charge potential may be seen in Figure 2.4.

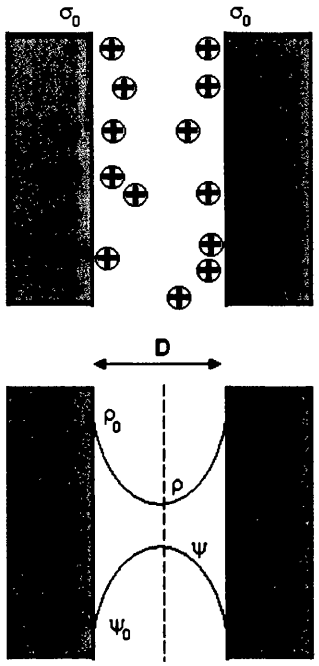


**Figure 2.4 Surface potential in nanopore (Israelachvill, 1991)**

### 2.6.1 The inner part of the double layer

The treatment of the diffuse double layer outlined in the last section is based on an assumption of point charges in the electrolyte medium. The finite size of the ions will, however, limit the inner boundary of the diffuse part of the double layer, since the centre of an ion can only approach the surface to within its hydrated radius without becoming specifically adsorbed. Stern (1924) proposed a model in which the double layer is divided into two parts separated by a plane (the Stern plane) located at about a hydrated ion radius from the surface, and also considered the possibility of specific ion adsorption.

Specifically adsorbed ions are those which are attached (albeit temporarily) to the surface by electrostatic and/or van der Waals forces strongly enough to overcome thermal agitation. The centres of any specifically adsorbed ions are located in the Stern layer (i.e., between the surface and the Stern plane). Ions with their centres located beyond the Stern plane form the diffuse part of the double layer, which is defined by the Gouy-Chapman method.

The potential changes from $\psi_0$ (the surface potential) to $\psi_d$ (the Stern potential) in the Stern layer, and decays from $\psi_d$ to zero in the diffuse double layer. In the absence of

specific ion adsorption, the charge densities at the surface and at the Stern layer ($C_1$) and of the diffuse layer ($C_2$) are given by

$$C_1 = \frac{\sigma_0}{\psi_0 - \psi_d} \qquad \text{and} \qquad C_2 = \frac{\sigma_0}{\psi_d}$$

from which

$$\psi_d = \frac{C_1 \psi_0}{C_1 + C_2} \tag{2.37}$$

When specific adsorption takes place, counter-ion adsorption usually dominates over co-ion adsorption and a typical double layer situation would be that depicted in Figure 2.5

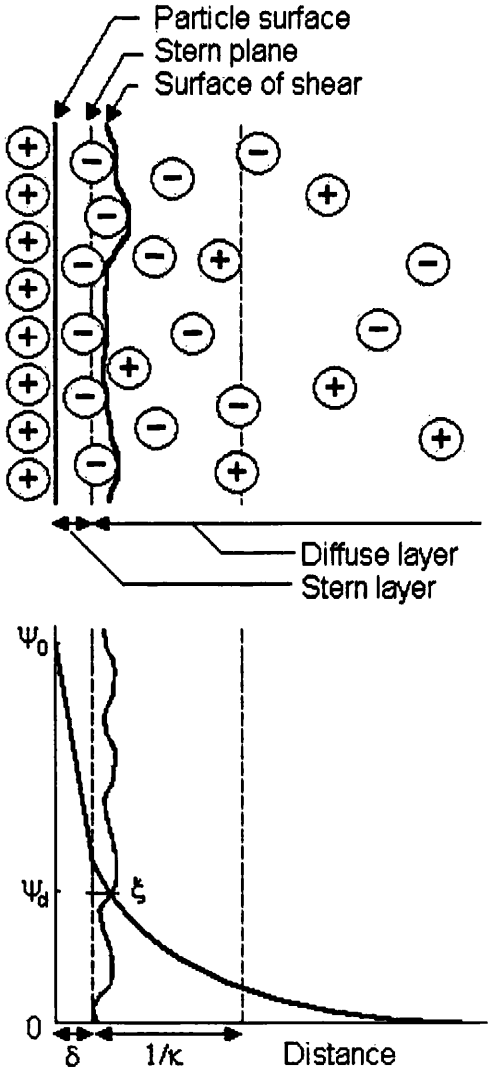


**Figure 2.5 Schematic representation of the structure of the electric double layer according to Stern's theory (Shaw, 1980)**

It is possible, especially with polyvalent or surface active counter-ions, for reversal of charge to take place within the Stern layer (i.e., for $\psi_0$ and $\psi_d$ to have opposite signs), Figure 2.6a. Adsorption of surface-active co-ions could create a situation in which $\psi_d$ has the same sign as $\psi_0$ and is greater in magnitude, Figure 2.6b.

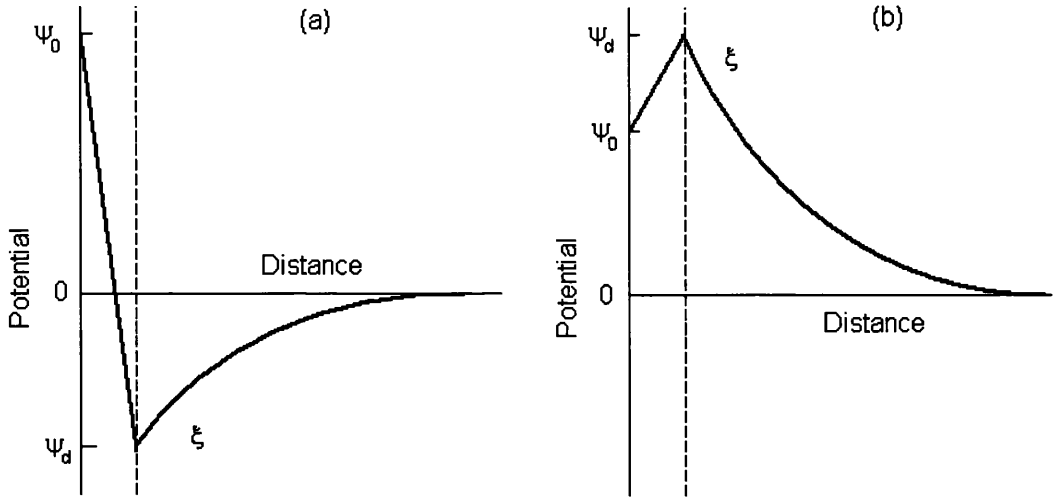


**Figure 2.6 (a) Reversal of charge due to the adsorption of surface-active or polyvalent counter-ions. (b) Adsorption of surface-active co-ions (Shaw, 1980)**

Stern (1924) assumed that a Langmuir-type adsorption isotherm could be used to describe the equilibrium between ions adsorbed in the Stern layer and those in the diffuse part of the double layer. Considering only the adsorption of counter-ions, the surface charge density $\sigma_1$ of the Stern layer is given by the expression

$$\sigma_1 = \frac{\sigma_m}{1+\frac{N_A}{n_0 V_m}\exp\left[\frac{ze\psi_d+\phi}{kT}\right]} \qquad (2.38)$$

where $\sigma_m$ is the surface charge density corresponding to a monolayer of counter-ions and $V_m$ is the molar volume of the solvent. The adsorption energy is divided between electrical and van der Waals ($\phi$) terms.

Treating the Stern layer as a molecular capacitor (condenser) of thickness $\delta$ and with a permittivity $\varepsilon'$,

$$\sigma_0 = \frac{\varepsilon'}{\delta}(\psi_0 - \psi_d) \qquad (2.39)$$

For overall electrical neutrality throughout the whole of the double layer

$$\sigma_0 + \sigma_1 + \sigma_2 = 0 \qquad (2.40)$$

where $\sigma_2$ is the surface charge density of the diffuse part of the double layer.

Substituting from equation (2.39), (2.38) and (2.35) into equation (2.40) gives a complete expression for the Stern model of the double layer

$$\frac{\varepsilon'}{\delta}(\psi_0 - \psi_d) + \frac{\sigma_m}{1 + \frac{N_A}{n_0 V_m}\exp\left[\frac{ze\psi_d + \phi}{kT}\right]} - (8n_0\varepsilon kT)^{1/2}\sinh\frac{ze\psi_d}{2kT} = 0 \qquad (2.41)$$

This expression contains a number of unknown quantities. However, some information can be gained from streaming potential and titrimetric measurements.

## 2.6.2 Effect of concentration on double layer thickness

The charge arrangement at the membrane surface and its extent into the solution depends on the electrolyte concentration: increasing electrolyte concentration causes the diffuse double layer to shrink closer in to the surface, so that the electrostatic potential $\psi_d$ to fall off more quickly with distance (Figure 2.7).

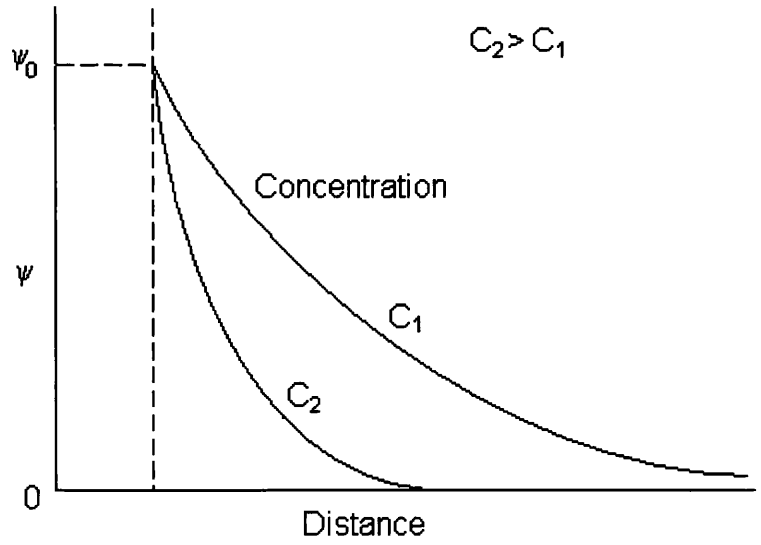


**Figure 2.7 Influence of electrolyte concentration on electrostatic potential (Hunter, 1986)**

For an aqueous solution of a symmetrical electrolyte at 25°C, equation (2.32) became;

$$\kappa = 3.28\times10^{9}\left(cz^{2}\right)^{1/2} \qquad (2.42)$$

For a 1-1 electrolyte the double layer thickness is about 1nm for a $10^{-1}$ mol $dm^{-3}$ solution and about 10 nm for a $10^{-3}$ mol $dm^{-3}$ solution (Shaw, 1980).

### 2.6.3 Dipole moment

An electrical double layer arises due to interactions between solvent/solute dipole moments and the inherent membrane surface charge. The dipole moment ($\mu$) of a molecule is the sum of the permanent dipole moment $\mu^0$ and the induced dipole moment $\mu^{ind}$. The permanent dipole moment is approximately constant but the induced dipole moment is proportional to the electric field. The electric field induced by the charge of the membrane is assumed to be small enough that the induced dipole moment can be neglected and the overall dipole moment is equal to $\mu^0$ (Van der Bruggen *et al.*, 1999). Van der Bruggen *et al.* (1999) stated that an increase in the dipole moment (for an neutral molecule) decreased retention for a neutral permeating a nanofiltration membrane. This effect was further investigated in this thesis.

### 2.6.4 The electroviscous effect

For the case of nanofiltration, the length scales determining separation are only about one order of magnitude grater than atomic dimensions. This is a scale at which macroscopic descriptions of hydrodynamics and interactions are beginning to break down (Bowen and Mukhtar, 1996). It may be asked as to whether it is sensible to describe the transport channels in such membranes as being pores – though recent Atomic Force Microscope studies indicate that, at lest for some membranes, pores may exist (Bowen and Welfoot, 2002a).

When an electrolyte flows through electrically charged pores under pressure gradient, the charges in the mobile part of the double layer near the wall are carried toward one end. This constitutes a streaming current and the accumulation of charge sets up an electric field. The field causes a current flow in the opposite direction through the bulk of the liquid and when the latter conduction current is equal to the streaming current, a steady state is achieved. The resulting electrostatic potential difference between the ends of the pore is the *streaming potential.* This potential will produce a

backflow of liquid by the electro-osmotic effect; that is, the counter-ions in the double layer adjacent to the pore wall will move under the influence of the induced electric field and will draw the liquid along with them. The net effect is a diminished flow in the forward direction. The liquid appears to exhibit an enhanced viscosity if its flow rate is compared with the flow in the absence of double layer effects (at high salt concentration or at the point of zero charge). This increase in apparent viscosity of fluid is termed an *electroviscous effect* (Bowen and Jenner, 1995).

The assumption of bulk solvent properties may not be valid within narrow NF pores. The assumption of bulk water viscosity is likely to overestimate the water permeability since the actual viscosity may be increased due to greater structure caused by orientation of the water molecules at the pore wall. Some work has been preformed on the effects of confinement on water structure, but there still remains a severe limitation on the level of knowledge available. Israelachvili (1991) discussed the layered order of confined water and detailed its behaviour under shear and it was stated that the water structure remains intact under shear. Israelachvili and Pashley measured the structural forces between two surfaces. They found that the structural 'hydration' force is overall repulsive, but for separations below 1 nm, the force becomes highly oscillatory (Israelachvili and Pashley, 1983). Israelachvili, using Surface Force Apparatus, found that the viscosity of water in films as small as 2 nm between mica surfaces was within 10% of its bulk value and that at most, only one layer of water was immobilised at each surface (Israelachvill, 1986).

Bowen and Jenner (1995) investigated theoretically the increase in apparent pore viscosity due to electrokinetic effects within charged capillaries. The apparent viscosity increased with zeta potential and exhibited a maximum at $\kappa r_p \sim 2.5$ for $\zeta <$ 50mV decreasing for both smaller or larger values of $\kappa r_p$. Therefore there is sufficient evidence for an increase in viscosity within the nanopore size range. Experimental evidence suggests the presence of one layer annulus of water molecules adsorbed at the pore wall, with the thickness of one water molecule. Bowen and Welfoot (2002a) showed that the pore viscosity had no direct effect on rejection analysed as a function of $\Delta P$ for uniform pores, and also that even when pore size distribution is included, the effect is not very great (Bowen and Welfoot, 2002a).

### 2.6.5 The Solvation Energy Barrier

The confinement of water molecules within pores will not only affect solvent viscosity. Electrochemical studies of colloidal systems have shown the presence of one layer of water molecules at the colloid-solvent interface with a dielectric constant that is significantly smaller than bulk water (Israelachvill, 1991). Orientation of the water molecules at pore walls will similarly be expected to lead to a reduction in dielectric constant. The reduction of dielectric constant means there is an energy barrier to solvation of ions into the pores (which will increase salt rejection). This mechanism can be expressed theoretically in terms of the model for ion solvation energy proposed by Born (1920):

$$\Delta W_i = \frac{z^2 e^2}{8\pi\varepsilon_0 a_r}\left(\frac{1}{\varepsilon_p} - \frac{1}{\varepsilon_b}\right) \qquad (2.43)$$

where $\Delta W_i$ is the solvation energy barrier.

The small radius of NF pores makes the pore solvent dielectric constant approach that of the membrane, which increases the solvation energy barrier. Bowen and Welfoot (2002a) assumed that the solvation energy barrier is the dominant dielectric exclusion mechanism for most NF operating conditions.

## *2.7 Direct Measurement of surface forces*

There are many different types of measurements that provide information on the forces between particles and surfaces, namely; adhesion; peeling measurement; contact angle measurements; equilibrium thicknesses of thin free films; equilibrium thickness of adsorbed films; inter-particle spacing in liquids; sheet-like particle spacing in liquids and coagulation studies. Most of these methods do not give the force law data (the force as a function of distance) but rather the adhesion force or minimum energy at some particular state e.g., the equilibrium state, of the system. Other methods, such as osmotic pressure measurements, involve the collective interactions of many molecules or particles so that the data gained tend to be of a thermodynamic nature and not directly translatable into a force law. The most

unambiguous way to measure a force-law is to position two bodies close together and directly measure the force between them, e.g., from the deflection of a spring. While the principle of direct force measurement is usually very straightforward, the challenge comes in measuring very weak forces at very small intermolecular surface separations which must be controlled and measured to within 0.1nm (Israelachvill, 1991).

### 2.7.1 Measuring atomic force: the Atomic Force Microscope

The first direct measurements of intermolecular forces were those of Derjaguin and co-workers (Derjaguin and Abrikossova, 1954; Derjaguin *et al.*, 1956). More recently, Bowen successfully used an Atomic Force Microscope (AFM) to image UF membranes (Bowen *et al.*, 1999). Bowen and Welfoot (2002a) have also produced AFM images of NF membranes. Bowen *et al.* (1997a) used an AFM in electrical double layer mode to study the electrical double layer interactions between a silicon tip and two polymeric membranes, one MF (nominally 0.1 μm) and the other UF (25 000 *MWCO*). They observed a number of apparent trends. Firstly, for a high ionic strength, the mean pore diameter decreased with decreasing image force. Secondly, the mean at the highest imaging force increases with decreasing ionic strength. For the UF membrane, the mean diameter obtained by AFM imaging was 5.1 nm. This was greater than the mean diameter (4.5 nm) in $10^{-1}$ M NaCl solution. They concluded, that in electrical double layer imaging in solution the closest approach of the tip may well be with the compact of inner part of the double layer rather than the actual membrane surface (Bowen *et al.*, 1997a). This inner region consists of a layer or possibly layers of dehydrated or hydrated ions (Hunter, 1986). Depending on the exact nature of this inner region, its boundary has been estimated to lie in the region 0.2-0.9 nm from the surface (Senden *et al.*, 1994). Bowen *et al.* (1997a) interpreted force against distance data in the form of isopotential lines for the entrance to a membrane pore. They demonstrated that the potential falls off much faster with distance at higher ionic strength ($10^{-1}$ M NaCl) than at lower ionic strength ($10^{-4}$ M NaCl). This was in agreement with the theory of double layer compression at higher ionic strength.

An important requirement for analysis of AFM data is knowledge of the surface properties of the membrane. These may be acquired by streaming potential and

titrimetric measurements. Direct determination of membrane surface charge is possible by pH surface titration (Bowen and Hughes, 1991; Schaep and Vandecasteele, 2001). However, most studies have focused on the determination of membrane electrokinetic properties, streaming potential or electro-osmosis, with the results often being expressed in terms of membrane zeta potentials (Aguilella *et al.*, 1996; Elimelech *et al.*, 1994; Nyström *et al.*, 1994). If such measurements are made by flow across the top surface of the membrane, the calculation of zeta potential from the experimental data is generally unambiguous (Elimelech *et al.*, 1994). However, the calculation requires more care if measurements are made by flow through the membrane (Aguilella *et al.*, 1996; Nyström *et al.*, 1994).

### 2.7.2 Streaming potential

A streaming potential is the potential difference at zero current caused by the convective flow through a membrane. A streaming potential is generated by exerting a force on the double layer that has been built up in the solution near the charged surface. Since an excess of counter charge is present, movement of those counter charges causes a current. This current which is streaming through the double layer is called the streaming current. The accumulations of counter charges downstream generate a steaming potential across the pore, which in turn causes a conduction current through the capillary in the reverse direction. At steady state, the streaming current equals the conduction current.

The relationship between the measurable streaming potential, $\Delta E_{str}$, and the zeta potential, $\zeta$, is given by the well-known Helmholtz-Smoluchowski equation using the Fairbrother and Mastin approach:

$$\zeta = \frac{\Delta E_{str} \eta \kappa_s R_{el,s}}{\Delta P \varepsilon R_{el}} \qquad (2.44)$$

where $\Delta P$ is the applied pressure, $\varepsilon$ the dielectric permittivity, $\eta$ the viscosity of the solution and $R_{el}$ the electrical resistance of the electrolyte solution. $R_{el,s}$ is the electrical resistance when the measurement cell is filled with a standard solution whose specific conductivity $\kappa_s$ is known (Jacobasch and Schurz, 1988).

### 2.7.3 Titrimetric measurements

Determination of membrane $\zeta$ potential was important in the prediction of membrane permeation rates and membrane rejection during processing. The $\zeta$ potential of membranes may be determined by means of the measurement of the rate of electro-osmosis through the membrane. Streaming potential measurements allow the potential to be determined for some distance away from the membrane surface. However, a detailed knowledge of the membrane/solution interface requires knowledge of the *surface* charge density. This can be determined by means of surface pH titration. Combination of electrokinetic and titration measurements provide a detailed assessment of the nature of the surface properties of a membrane.

Bowen and Hughes (1991) conducted $\zeta$ and titrimetric measurements for aluminium oxide membranes. They used a three-dimensional array to successfully estimate the thickness of the gel layer, the specific adsorption energy of counter-ions and the ratio of functional groups at the membrane surface.

Schaep and Vandecasteele (2001) characterised four nanofiltration membranes by titration. No overall charge density was studied but positively and negatively charged surface groups were determined via a counter-ion exchange method. They concluded that most membranes carry a surplus of negatively charged groups. Only one of the membranes studied carried a net positive surface charge.

### 2.7.4 Osmotic pressure measurement

Osmotic pressure is a colligative property of a solution property that is central to membrane filtration problems. It has been defined as the pressure differential that results when two chambers, separated by a semi permeable membrane and containing two solutions distinguished by the presence in one of a membrane impermeable substance, are allowed to equilibrate (Levine, 1988). Traditionally the apparatus used for this experiment was very simple in arrangement, with the pressure difference measured according to the change of liquid level in each chamber, Figure 2.8.

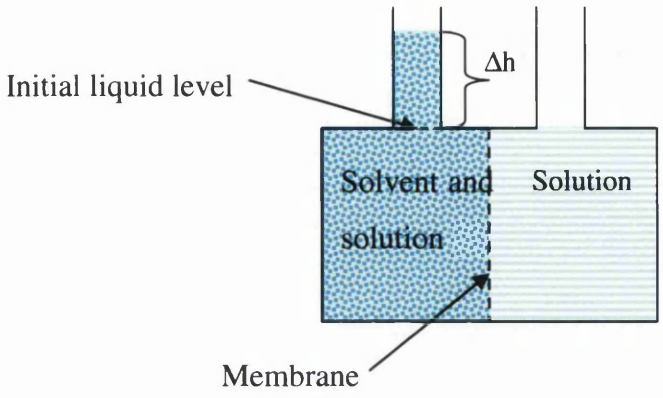


**Figure 2.8 Osmometer schematic**

Figure 2.8 not only presents a practical technique for the evaluation of the osmotic pressure of a solution but is also a general illustration of the fundamentals of osmotic pressure as a phenomenon. Osmosis, a process relied upon by biological systems, has been defined as the flow of a solution from a low concentration zone to one of high concentrations. Driven by the concentration differential, this process endeavours to dilute the high concentration zone such that it becomes equivalent in composition to the low concentration side (Sourirajan, 1970).

Osmotic pressure measurement is one of the standard methods for molecular weight determination. Tanford used osmotic pressure analysis to calculate the molecular weights for macromolecules (Tanford, 1961). Flory also used this method to determine the molecular weight for polymers (Flory, 1943). The osmotic pressure of proteins such as bovine serum albumin has been found to exhibit significant non-ideality. This non-ideality has been attributed to the existence of solute-solute, solute-solvent interactions, and hence, the presence of dimers or higher oligomers (Vilker *et al.*, 1981; Yousef *et al.*, 1998; Yousef *et al.*, 2002).

# 3 Materials and methods

This chapter details the materials and methods used in the experimental work. Firstly, the laboratory scale dead-end batch filtration cell used in all filtration experiments is described in detail. Then the details of the materials used for experimental work will be provided along with the sample analysis methods. Finally, the operation of the High Performance Particle Sizing, osmotic pressure cell, titration, adsorption and electro kinetic potential equipment are described.

## *3.1 Laboratory scale rig*

A stirred SEPA® ST cell supplied by Osmonics (Minnesota, USA) was used for the experimentation in this study (Figure 3.1). The cell had a capacity of 300 ml and supported a membrane disc of 4.9 x $10^{-2}$ m diameter. The effective area of the membrane was 1.69 x $10^{-3}$ $m^2$ and the maximum operating pressure of the cell was 7080 kPa (~ 69 barg) with high-pressure clamps. The cell consisted of a cylindrical body, a membrane support with small channels to allow permeate to flow out, a quick fit base (which held the membrane support and body), a magnetic stirrer assembly that was mounted inside the body, a top cap with a pressure relief valve and an inlet to the body. The design of the body allowed the positioning of the stirrer as close to the membrane surface as possible. The cap and membrane support base were sealed using an o-ring gasket fabricated from silicone rubber. All parts of the cell (apart from the magnetic stirrer follower) were constructed from 316L stainless steel.

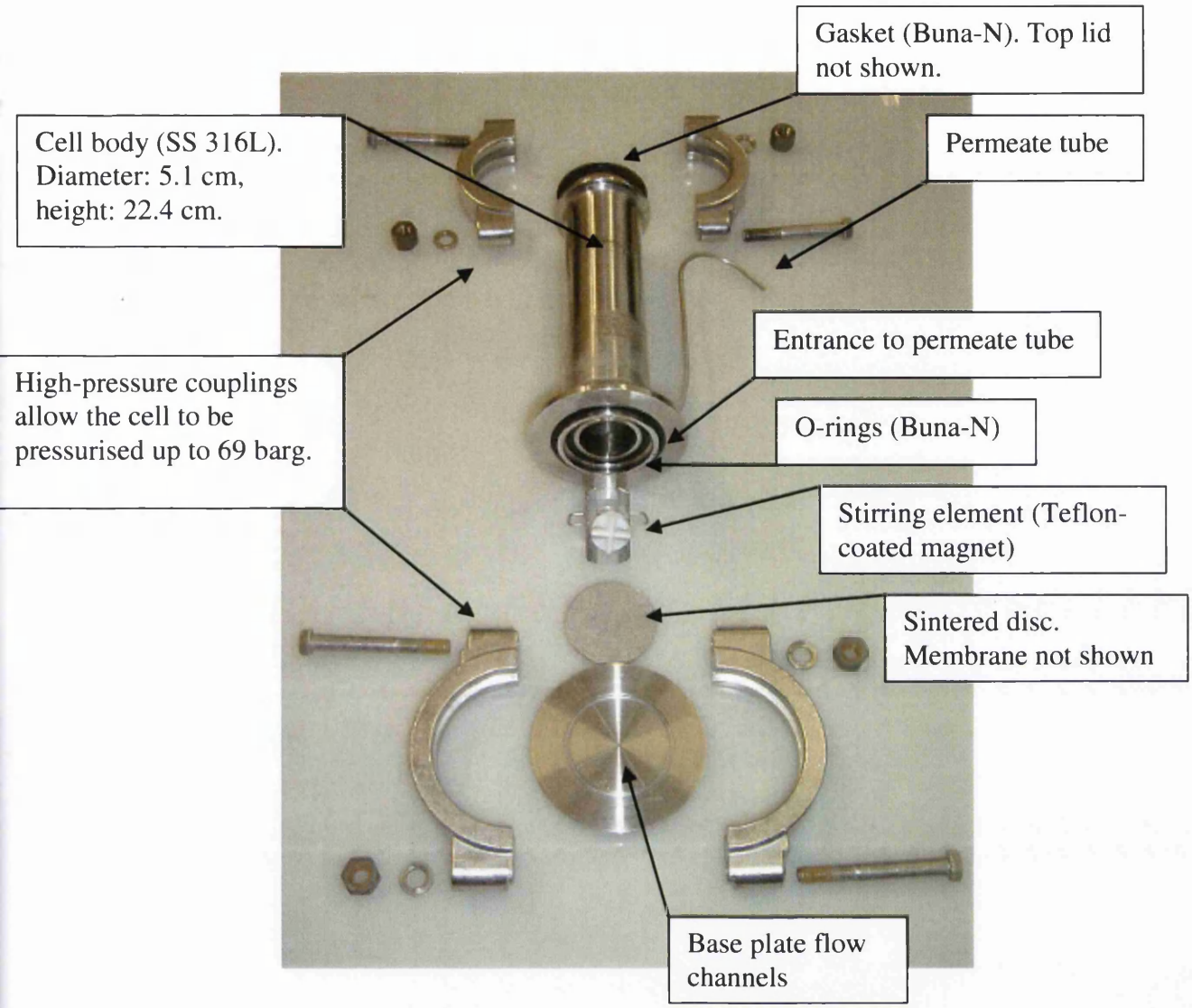


**Figure 3.1 Exploded SEPA® ST Cell**

The filtration cell was immersed in a 3-litre vessel that was fed from a thermostatted bath (manufactured by Grant). This arrangement enabled isothermal operation and is shown in Figure 3.2.

Prior to the filtrations, the cell was flushed at $1690 \pm 10$ kPa ($16.5 \pm 0.1$ barg) with deionised water until 20 ml of water had permeated the membrane. This was carried out in order to avoid any compression effects of the membrane and ensures that operation was always under constant conditions.

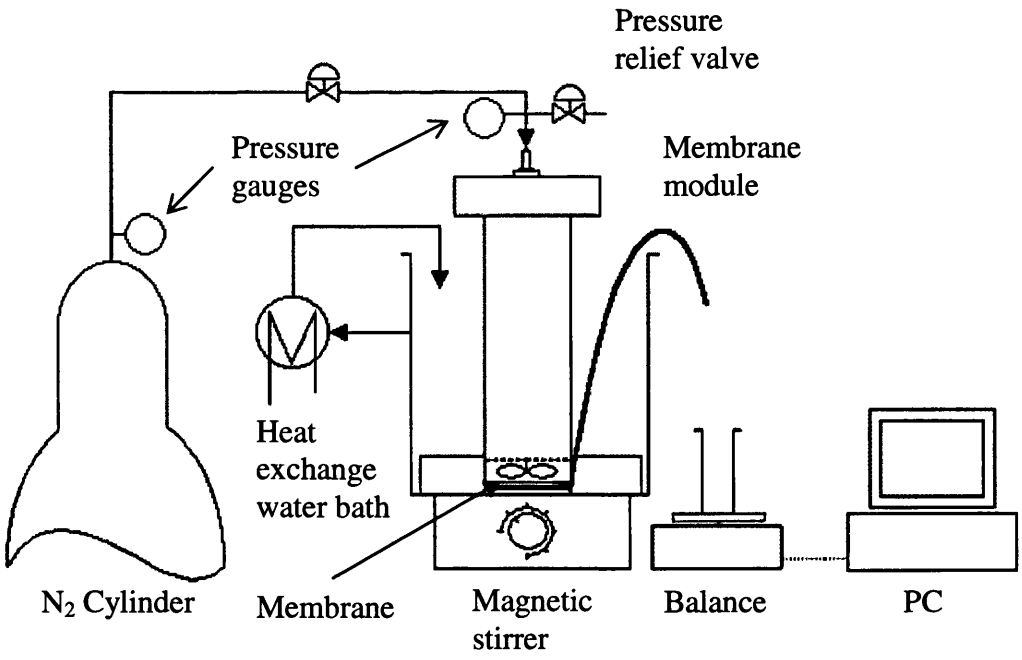


**Figure 3.2 Nanofiltration apparatus**

When operating the cell, the cut and prepared membrane was placed at the bottom of the cell (active layer up), then the porous sintered support disk and base plate were slotted onto the bottom of the cell (Figure 3.1). The o-rings were placed in their seats in the base of the cell, the quick fit base was sealed by tightening the circular couplings (Figure 3.1). The magnetic stirrer was the placed inside the body of the cell and the experimental solution poured in (250 ml of solution was used for all experiments). Next, the top was secured to the body by tightening the top couplings. The sealed cell was placed inside the water bath, on top of a magnetic stirrer (Figure 3.2). The stirring speed was set at 200 rev $min^{-1}$ for all experiments (unless otherwise stated). The pressure relief valve was then closed and the cell was pressurised using compressed nitrogen gas from a freestanding cylinder (Figure 3.2). The applied pressure to the cell was measured using a 0-10260 kPa (1-100 barg) 4-20 mA pressure sensor (Keller), a calibration chart for this sensor is shown in Appendix A.2. This sensor was coupled with a Tracker 221 digital pressure meter supplied by Omni Instruments (UK). A pressure of 1690 ± 10 kPa (16.5 ± 0.1 barg) was used for all experiments. Permeate flux was measured by recording the mass of permeate with respect to time using an electronic balance connected to a computer. The cell was maintained at 35 ± 0.5°C by placing it in a water bath connected to an external water bath (Figure 3.2). On completion of the experiment, the nitrogen gas supply was turned off and the pressure was released from the system by opening the pressure

relief valve (Figure 3.2). The top cap was then removed and the remaining content of the cell (the retentate) was emptied. The cell was also purged with deionised water at the end of experimental runs to flush the membrane. The permeate flux of the deionised water in between experimental runs was measured as an indication of the quality of the membrane. If the membrane quality was reduced (large reduction in pure water permeate flux), then the membrane was replaced.

The hold up volume of the SEPA® ST cell was 1 ml (SEPA® ST instruction manual P/N 5958 Osmonics USA 1994). Therefore the first 5 ml of permeate (i.e. five times the void volume of the apparatus) was discarded and the following 15 ml were fractionated in three test tubes (5 ml each) for analysis. To minimize the concentration change of the feed solution, each filtering operation was terminated before 8% (by volume) of the feed solution was filtered through the membrane. The fractionation of the permeate was used to show that the initial permeate fraction was representational of the filtration. This method is similar to that used by Gotoh *et al.* (2004).

## 3.2 Membranes

The membranes used in this study are summarised in Table 3.1. All membranes used were commercially available thin film composite flat sheet membranes.

| Membrane | Type | Manufacture | MWCO (Da) | Surface chemistry |
|---|---|---|---|---|
| NTR 7450 | NF | Nitto Denko Corporation | 1000 | Sulfonated polyethersulfone |
| LFC 1 | RO | Hydronautics | < 100 | Polyamide |
| NF 200 | NF | Dow | 360 | Polyamide |

**Table 3.1 Membranes and manufactures (properties given by suppler)**

The NTR 7450 NF membrane was used for all nanofiltration experiments. This membrane was selected as it has a high MWCO, putting it at the uppermost limit for nanofiltration membranes. The NTR 7450 membrane had also been used previously for the separation of amino acids and small neutral organic molecules. The LFC membrane was used in the osmotic pressure experiments. The NF 200 membrane was used in the adsorption experiments.

### 3.2.1 Membrane preparation

Although the membranes used had different properties and their active layers were generated from different polymeric compounds, their appearance and mechanical properties were indistinguishable. The membrane sheet had to be cut to the appropriate size for the filtration cell. The membrane support disc was used as a template, from which the membrane could be cut out using a razor blade. Once cut to shape, the membrane was rinsed separately with water and propan-1-ol before being placed in the filtration cell. Rinsing was conducted with the intention of removing manufacturing residues and preservatives from the surface and pores of the membrane. The membranes used were hydrophobic, which meant that the pores had to be opened to allow ingress of water. This was achieved by immersing the membrane in propan-1-ol followed by immersion in water. This cycle was repeated twice before the membrane was ready for use. This method has been tried and tested by Mandale (2005).

## *3.3 Reagents*

All reagents used in this study were analytical grade obtained from Sigma-Aldrich Ltd. (Poole, Dorset, UK). The reagents used are shown in Table 3.2

| Chemical | Structure | Relative molecular mass (g/mol) | Analysis technique | Other information |
|---|---|---|---|---|
| Phenol $C_6H_5OH$ | 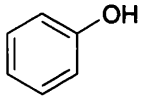 | 94.11 | UV spectroscopy at 270 nm | Toxic<br>Solubility: 8.4/100 parts |
| Benzonitrile $C_6H_5CN$ | 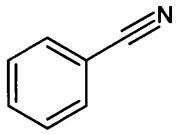 | 103.04 | UV spectroscopy at 271 nm | |
| Benzylalcohol $C_7H_8O$ | 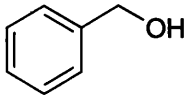 | 108.14 | UV spectroscopy at 257 nm | Solubility: 4.0/100 parts |
| Glycine $C_2H_6NO_2$ | 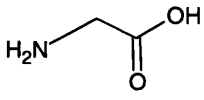 | 75.07 | Ninhydrin reagent visible absorption at 570 nm | Refractive index: 1.685 |

| Chemical | Structure | Relative molecular mass (g/mol) | Analysis technique | Other information |
|---|---|---|---|---|
| Glutamine $C_5H_{10}N_2O_3$ | 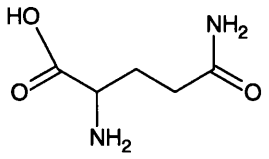 | 146.15 | Ninhydrin reagent visible absorption at 570 nm | Solubility: 4.2/100 parts Refractive index: 1.685 |
| Glutamic acid $C_5H_9NO_4$ | 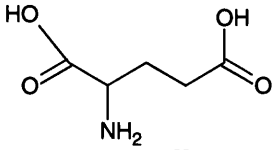 | 147.13 | Ninhydrin reagent visible absorption at 570 nm | Solubility: 0.84/100 parts Refractive index: 1.655 |
| Phenylalanine $C_9H_{11}NO_2$ | 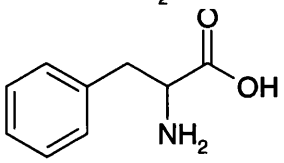 | 165.19 | Ninhydrin reagent visible absorption at 570 nm | Refractive index: 1.682 |
| Lysine $C_6H_{14}N_2O_2$ | 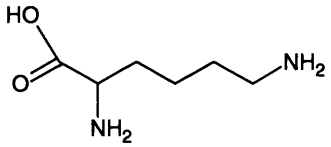 | 146.19 | Ninhydrin reagent visible absorption at 570 nm | Refractive index: 1.615 |
| Caffeine $C_8H_{10}N_4O_2$ | 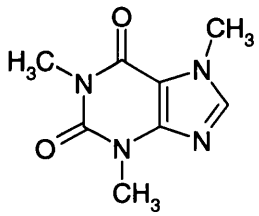 | 194.19 | UV spectroscopy at 275 nm | |
| Glucose $C_6H_{12}O_6$ | 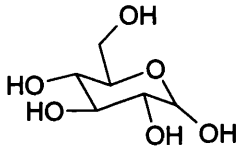 | 180.16 | Phenol - sulphuric acid visible absorption at 490 nm | Solubility: 82/100 parts |
| Sucrose $C_{12}H_{22}O_{11}$ | 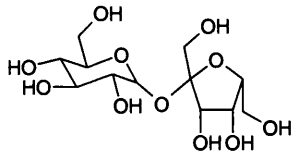 | 342.34 | Phenol - sulphuric acid visible absorption at 490 nm | Solubility: 179/100 parts |
| Raffinose $C_{18}H_{32}O_{16}$ | 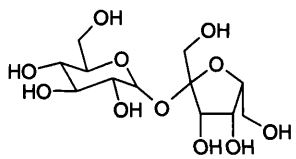 | 342.34 | Phenol - sulphuric acid visible absorption at 490 nm | Solubility: 14.3/100 parts |

**Table 3.2 Organic compounds used in nanofiltration experiments**

The water used in all experiments was produced using a pilot scale reverse osmosis rig and a Dowfilmtec RO-4040-FF membrane. The conductance was < 10 μS.

## 3.4 Chemical analysis

Membrane research focuses on quantifying the performance of the membrane by the amount of solute/solution separation. To make these observations, it was necessary to measure the concentration of solutes in both the feed and the product. To achieve this, techniques of solute concentration measurements were identified for each chemical used. The methods used were:

- UV spectrophotometery
- Visible spectrophotometery
  - Phenol-sulphuric acid technique
  - Ninhydrin reagent technique

### 3.4.1 UV spectrophotometery

This technique was used in the measurement of compounds containing a six membered carbon ring (benzene ring). The presence of the benzene ring is important as it absorbs radiation strongly in the UV region. Peak absorbencies for these compounds were found to be at wavelengths between 200 and 280 nm. The molecules measured by this technique are shown in Table 3.2, they were; phenol, benzonitrile, benzylalcohol, and caffeine. Table 3.2 also shows the wavelength at which each molecule measured. This wavelength represents the point at which the maximum absorption was measured. This point was found by performing a UV absorption scan at different wavelengths. The instrument used was a Unicam UV300 UV-visible spectrometer in UV scanning mode. The results are shown in Appendix A.3. Once the maximum absorption had been found, the concentration calibration graph was constructed by measuring the absorbance of a standard solution at five different dilutions. The instrument used in this case was a Camspec M302 UV-visible spectrophotometer. The spectrophotometer was zeroed against deionised water. Therefore, the concentration of samples produced during an experiment could be calculated by comparing the samples absorbance to the corresponding concentration.

In some cases there was the need for dilution of samples such that saturation was avoided and the resultant measured absorption value fell within the calibrated range.

Saccharides were also found to absorb in the UV region. However, the absorption peak for these compounds existed at around 195 to 200 nm, known to be close to the limits of measurement. The lower wavelength limit of the spectrophotometer is 195 nm as it is here that air will also begin to absorb UV light thus interfering with the result (Mandale, 2005). Hence, a more reliable method of analysis was used for the sugars.

### 3.4.2 Visible spectrophotometery

To absorb light in the visible part of the radiation spectrum it is necessary for the solution to exhibit some colouration. None of the solutions used in this study produced a measurable colour. Thus to permit the measurement of certain components concentration, using visible spectrophotometery, they had to be reacted with appropriate reagents to form a colour that was proportional in intensity (and therefore absorption) to the concentration. Two such methods were used, one to measure saccharides and the other for amino acid analysis.

### 3.4.3 Saccharide analysis using the phenol-sulphuric acid technique

Phenol in the presence of sulphuric acid can be used for the quantitative colorimetric determination of sugars (Dubois *et al.*, 1956). The procedure is to firstly add 1 ml of sample (concentration up to 0.1 g/l) to a test tube. Then 2 ml of 5 wt% phenol was added to the test tube, this was then followed by adding 5 ml of concentrated sulphuric acid to the mixture. Care was taken to avoid adding the acid too quickly and causing the contents to boil and spit out of the top of the tube. After addition of the acid the tube was allowed to stand for ten minutes. After ten minutes, the tube was capped and thoroughly mixed. The tubes were then submerged into a water bath at ~ 20°C, thus cooling the contents. The overall result was that a yellow-orange colour was produced. This colour remained stable for some time. A visible absorption scan reviled that the maximum absorbance of the reaction mixture was at 490 nm (Appendix A.3). The optical density was the measured at this wavelength using the

Camspec spectrophotometer. The spectrophotometer was zeroed against a reagent blank, made in the same way as the other samples, but 1 ml of deionised water was used in place of the sugar solution.

### 3.4.4 Amino acid analysis using the ninhydrin reagent technique

Amino acid analysis was carried out by using ninhydrin colorimetric method which was described by Moore (1968). The ninhydrin reagent solution was supplied by Sigma-Aldrich, UK (product number N7285).

The procedure for the determination of amino acid calibration chart using ninhydrin reagent was as follows. Firstly a stock solution of 0.05 μmoles/ml was prepared. This was diluted into four test tubes as shown in Table 3.3.

| Tube No. | 1 | 2 | 3 | 4 | 5 |
|---|---|---|---|---|---|
| Standard (ml) | 0.0 | 0.5 | 1.0 | 1.5 | 2.0 |
| Water (ml) | 2.0 | 1.5 | 1.0 | 0.5 | 0.0 |
| Ninhydrin reagent (ml) | 1.0 | 1.0 | 1.0 | 1.0 | 1.0 |

**Table 3.3 Amino acid calibration dilutions**

The tubes were then capped and gently mixed. They were then placed into a boiling water bath for exactly ten minute. After ten minute had elapsed, the tubes were allowed to cool to room temperature. Once at room temperature, 5 ml of 95% ethanol was added to each tube. The absorbance of each tube was then read using a spectrophotometer at 570 nm. The resulting colour was stable for approximately 1 hour (Moore, 1968), so no more than twenty samples were produced at any one time to allow sufficient time to take absorbance measurements. The amino acid calibration curves are shown in Appendix A.3. The same procedure was used to determine the concentration for filtration samples. The 2.0 ml of standard solution (tube 5, Table 3.3) was replaced by 2.0 ml of sample. In some cases, there was need for dilution of samples such that saturation was avoided and the resulting measured absorption value fell within the calibrated range.

## 3.5 High Performance Particle Sizing (HPPS)

The particle radius is an extremely important factor for membrane processes. This simple property is difficult to obtain with reliable accuracy from either predictive models or experimental measurements, even more so for very small solutes. Malvern Instruments (Malvern, Worcs. U.K.) has developed the Malvern HPPS 3.1, which has the ability to measure the solute radius of particles as small as 0.3 nm (HPPS Operators Guide, MAN0314, Issue 1.0, Dec 2001). A discussion of the limits of operation for the Malvern HPPS 3.1 is shown in Appendix A.4.

### 3.5.1 Sample preparation

Samples were prepared using deionised water and were filtered with 0.22 μm Millex syringe driven filter unit (Millipore U.K. Ltd.) into a 4.5 ml capacity UV range cuvette obtained from Merck Ltd. This was done to remove any large contaminating particles that would distort the overall result. The samples were loaded into the machine and the measurement sequence was started by computer programme. The results are presented in Chapter 4.

## 3.6 Osmotic pressure measurement

### 3.6.1 Osmometer construction

The osmometer used was based on the modified version of the membrane osmometer cell (Nabetani *et al.*, 1990), first employed by Vilker *et al.* (1981). The configuration of the osmometer is shown in Figure 3.4 and 3.5. The osmosis membrane (diameter: 41 mm) was placed in a vertical position, between two Perspex blocks (Figure 3.4). The two blocks were firmly bolted together and o-rings were used to ensure a good seal (Figure 3.4). The membrane support disc was made of a hastelloy sintered sheet (MOTT Corporation), which was a porous metal media with high strength and low resistance to flow. Both blocks had reservoirs that were used as the solvent cell or the solution cell as shown in Figure 3.5 positions 3 and 7. The solution cell was filled by inserting a needle (connected to a 50 ml syringe) through the valve opening leading to the top of the cell (Figure 3.5 position 2), and emptied by removing the bolt at the bottom of the cell (Figure 3.5 position 5). The solvent cell was filled through the opening at the top of the cell (Figure 3.5 position 9) (which remained open to

atmosphere), and emptied by removing the bolt at the bottom of the cell (Figure 3.5 position 6). Before starting the experiment, the two chambers were filled with solvent or solution and, after ensuring that all bubbles had been removed, the valve was closed. The pressure of the solution was measured with an electronic sensor (Industrial & Process Pressure Transducers – PDCR 910, DRUCK Limited. Figure 3.5 position 1, calibration chart Appendix A.2) interfaced with a DPI 208 SERIES Digital Process Indicator (DRUCK Limited), and recorded with a computer running a GW-Basic data logging program via a RS-232 connection. The temperature was measured by a type K thermocouple (accuracy ± 0.2°C) in the solvent cell (Figure 3.5 position 10). Once the maximum pressure had been reached, opening the valve stopped the experiment. The cells drained, rinsed and filled with solvent. This method allowed the same membrane to be used over and over again.

The osmotic cell was placed in a temperature controlled box held at 30.0 °C in which temperature fluctuations amounted approximately to ± 0.2 °C. This was done to eliminate fluctuations in the solution pressure due to temperature variations. The temperature controlled box comprised of two compartments: one section into which the osmotic pressure cell was placed; the other housed the heating and control elements. The heating element was a 60 W pearl light bulb. A West 6400 Temperature Controller regulated the temperature. The West 6400 Controller had an accuracy of ± 0.25 % of input span. Temperature of the box was measured by a $Pt_{100}$ temperature sensor (accuracy ± 0.1 °C). The air was distributed around the compartments by an 80 mm diameter fan and airflow holes between the two compartments.

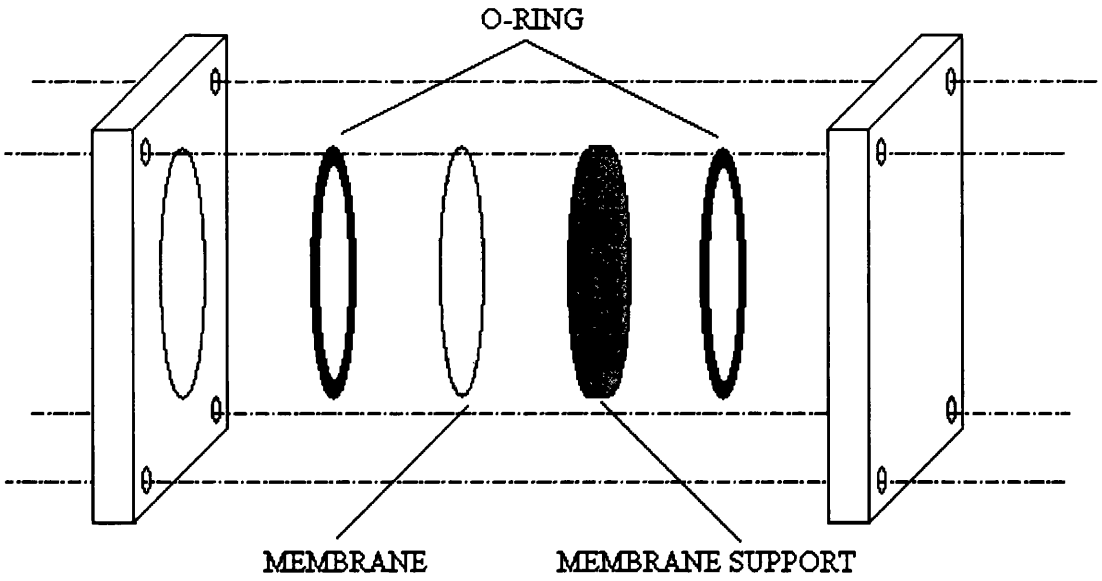


**Figure 3.4 Exploded diagram of Osmometer Cell**

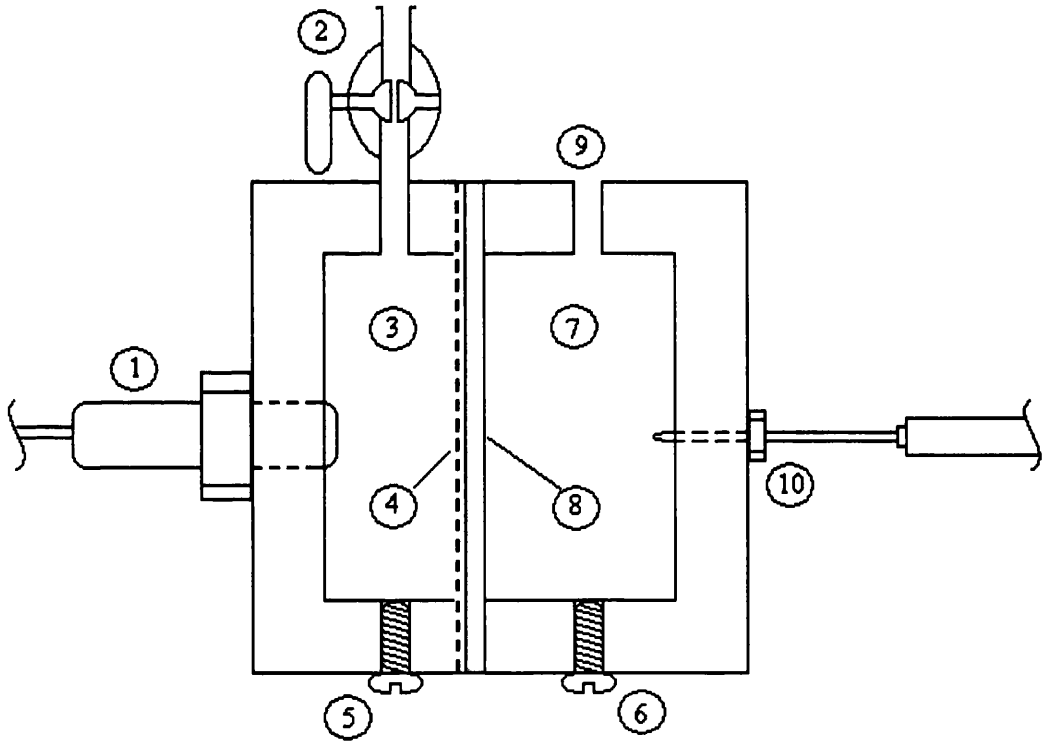


(1) Process Pressure Transducers – PDCR 910
(2) Valve
(3) Solution reservoir (volume 12.45 ml)
(4) Membrane (diameter 41 mm)
(5) Solution drain point and screw
(6) Solvent drain point and screw
(7) Solvent reservoir (volume 16.10 ml)
(8) Membrane support disc
(9) Vent to atmosphere
(10) Thermocouple (Type K)

**Figure 3.5 Elements of the Osmometer**

### 3.6.2 Osmotic cell experimental procedure

A solution of known concentration of the material being studied was loaded in to the solute side of the osmometer; pure water was loaded into the solvent side of the osmometer. After both sides of the osmometer were filled the pressure of the solute chamber was recorded on a data-logging program. The pressure gradually built up and reached a steady state, normally after 5-8 hours. This equilibrium pressure was taken to be the osmotic pressure of the solution at that concentration. Figure 3.6 shows the osmotic pressure results for 40 g/l glucose. The maximum pressure ($P_{max}$) was 437 kPa, which was achived after a time ($t_{max}$) of 7.9 h.

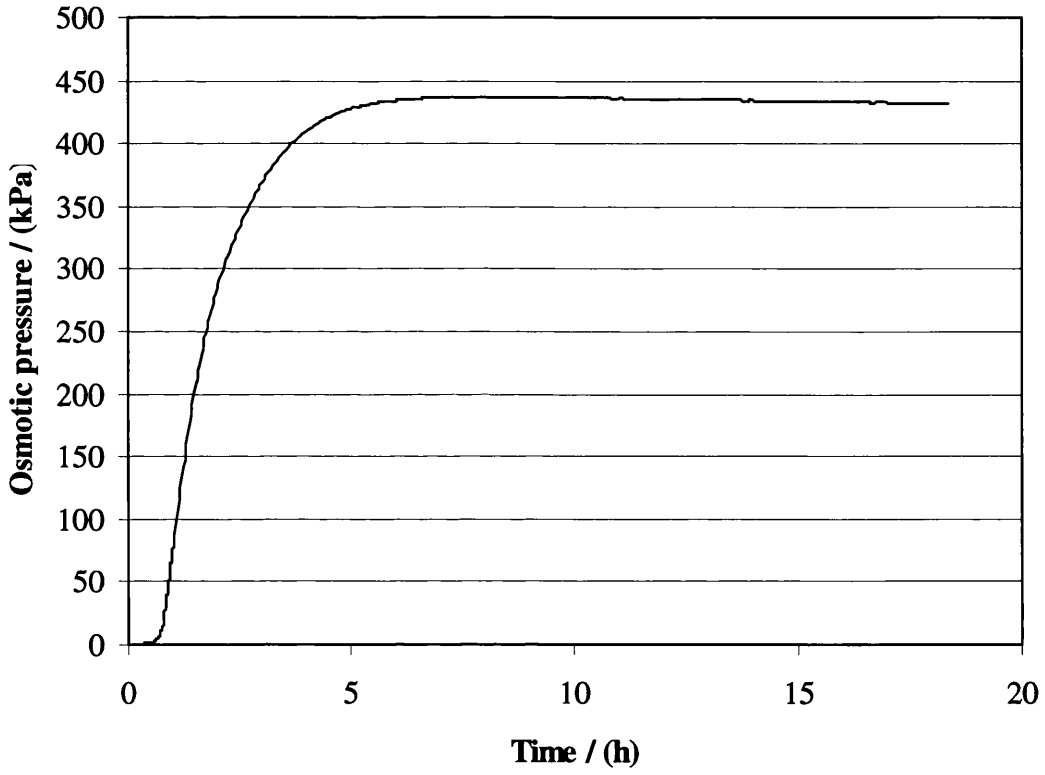


**Figure 3.6 Osmotic pressure of glucose 40 g/l @ 25 °C 437 kPa**

### 3.6.3 Membrane selection

Historically, the measurement of osmotic pressure has been limited due to real RO membranes not being available. In recent years, advances in membrane technology have meant that a wide variety of RO membranes have become available (Nabetani *et al.*, 1992).

One method for membrane selection was to compare an array of membranes through investigation of the maximum osmotic pressure obtained for a specified pure solution. Nabetani investigated the osmotic pressure achieved for Sodium Chloride solutions (Nabetani *et al.*, 1992). Sodium Chloride solutions are useful for investigating the suitability of a membrane, as it is one of the solutes available in terms of its molecular/ionic dimensions.

Nabetani *et al.* (1992) compared a range of membranes with respect to their maximum osmotic pressure $P_{max}$, and the time taken to reach those values, $t_{max}$, for 0.1 M Sodium Chloride solution. The results of this work are shown in Table 3.4.

| Membrane | $P_{max}$ (kPa) | $t_{max}$ (hour) |
|---|---|---|
| NTR 7199 | 320 | 50 |
| NTR 7250 | 37 | 7 |
| NTR 729HF | 0 | - |
| HR 99 | 99 | 4 |
| HR 98 | 199 | 3 |
| CA 960PP | 0 | - |
| DRS 92 | 10 | 12 |

**Table 3.4 Maximum pressure values for 0.1 M NaCl solution achieved with a range of membranes**

From the data shown in Table 3.4, Nabetani selected the HR 98 membrane as it exhibited a good combination of properties $P_{max}$ and $t_{max}$. Nabetani *et al.* (1992) went on to measure the osmotic pressure of glucose and sucrose. A 0.1 M solution of NaCl at 25°C was stated to have an osmotic pressure of 470 kPa (Sourirajan, 1970) but none of the membranes listed in Table 3.4 achieved this pressure with the closest only reaching 68% of this value (NTR 7199). This result was surprising since all the membranes listed were classified as reverse osmosis with salt rejection typically in the region of 99%. However, the figure stated by Sourirajan (1970) was calculated using a measured vapour pressure, this may imply a large discrepancy between theoretical models and actual measurements.

For this work, a LFC 1 membrane was used. This membrane gave reproducible results when tested against the published data for the osmotic pressure of sucrose. The results are shown in Chapter 4.

## 3.7 Membrane charge

Membrane charge is an important factor in solute separations and when considered in conjunction with properties such as molecular weight cut-off (*MWCO*) it becomes possible to make quantitative predictions of membrane separations. Therefore, surface charge measurements were made for the NTR 7450 membrane used in this work.

### 3.7.1 Streaming potential

Zeta potential was evaluated from streaming potential measurements made using an Anton Paar Electrokinetic Analyser. This equipment required the membrane to be cut into two pieces (12.5 cm by 5 cm). One piece had two holes (6 mm diameter) at opposite corners, and two flow channels (6 mm by 22 mm) cut into it. The other piece has two 6 mm holes at opposite corners. This configuration allowed the electrolyte solution to flow in a channel across the surface of the membrane in the electrokinetic analyser cell. Once cut into the specified shape, the membranes were soaked in deionised water and were placed overnight in a refrigerator (at approximately 5°C). This process was in order to remove the stabilizer reagent on the membrane surface and activate the membrane pores.

Streaming potential measurements are known to be influenced by the electrolyte concentration and the pH. In this case, the electrolyte concentrations that were used were 0.1 M, 0.01 M, 0.001 M and 0.0001 M KCl. Approximately 500 ml of KCl solution was placed in a reservoir that was submerged in a water bath at 25°C. This solution was then adjusted to approximately pH 3 by adding HCl solution. The pH was measured by using a pH probe that was regularly calibrated against standard buffer solutions. This solution was then automatically pumped from the reservoir, through the electrokinetic analyser and into the membrane cell, thus creating the streaming potential. The results were logged on a computer. After one streaming potential measurement had been made at a particular pH, the pH was raised by adding

some Sodium Hydroxide solution. The pH was gradually raised in this manner until pH 10 was reached. The process was then repeated for a different concentration of electrolyte.

## 3.8 Titrations

Knowledge of membrane zeta potential is important in the prediction of membrane permeation rates and membrane rejection during processing. The zeta potential of nanofiltration membranes may be determined by means of the measurement of the streaming potential. However, a detailed knowledge of the membrane/solution interface also requires knowledge of the surface charge density. This can be determined by means of surface pH titration.

### 3.8.1 Titration method

Surface pH titrations were carried out using a computer-controlled autotitrator that was designed and built in this laboratory. The main parts of the autotitrator comprised a stirrer unit, a heating block with capacity for three reaction vessels, an analogue pH meter, a peristaltic pump for the delivery of titrant and a computer (Moss, 2001).

The membranes were prepared by rinsing in propan-1-ol in the same manner as that used in the filtration experiments. The membranes were then peeled to remove the support material from the active surface layer. Both of the membrane materials were cut into pieces of approximately 1 x $10^{-4}$ $m^2$. The separated membrane materials were added to 50 ml of 0.001 M NaOH solution in a 100 ml beaker. A small concentration of NaCl (0.001 M) was used to stabilise the pH probe. The pH was lowered by adding 0.1 M HCl. The pH probe was regularly calibrated against standard solutions. The pH probe was connected to an analogue Pye Unicam model 290 pH meter connected to the computer system. All acid and alkali solutions were prepared using pre-packed ConVol solutions (BDH part of VWR International Ltd). The content of the 100 ml beaker was held at 30°C throughout the experiments by automatic control of the heating block. The temperature was measured using a platinum resistance $Pt_{100}$ element. A 25 ml burette was filled with 0.01 M NaOH. This was pumped by a peristaltic pump into the 100 ml reaction vessel. The flow rate of alkali was approximately 1.9 x $10^{-9}$ $m^3/s$ (0.12 ml/min). The resulting pH changes occurring in

the reaction vessel were automatically logged on a computer. This process was repeated for three titrations; 0.001 M NaCl plus active layer, 0.001 M NaCl plus support material and 0.001 M NaCl blank. The support layer was titrated separately to investigate its resulting effect on membrane charge.

## 3.9 Solute adsorption

It is usually accepted that permeate flux decline in the filtration of aqueous solution containing organic molecules is mainly caused by adsorption. However, for nanofiltration, a relationship between flux decline, concentration dependent rejection and adsorption properties has not yet been shown. Moreover, the factors affecting adsorption on the membrane surface or inside the pores are not known. This section outlines a new method that attempts to measure the amount of adsorption occurring on a nanofiltration membrane.

### 3.9.1 Adsorption method

Adsorption on NTR 7450 and NF 200 membranes was determined by batch experiments in which the concentration of an organic compound in aqueous solution was determined after approximately 24 hours contact with the membrane material.

Firstly, the membrane was peeled to remove the back support material from the active surface material. The support and active layer were then cut into disks of a known area, and weighed. This gave the relationship between area and mass for both materials from which irregular pieces of membrane could be weighed to give a surface area value. In the adsorption experiments, a surface area of approximately 0.01 – 0.02 $m^2$ was used. In previous studies, areas of 0.0018 $m^2$ (Van der Bruggen *et al.*, 2002) and 0.003 $m^2$ (Kiso *et al.*, 2000) have been used. However, the method devised in this section allowed a much larger membrane area to be used.

The support and active layer materials were soaked in deionised water overnight in a refrigerator at 5°C. The membrane materials were then cut into pieces of approximately 4 x $10^{-4}$ $m^2$ (2 $cm^2$). A 50 ml organic solution at a concentration of 0.001 M was pipetted into three 250 ml flasks. This concentration was chosen because

of practical considerations; the membrane surface area needed to measure significant adsorption would be much larger with higher concentrations (Van der Bruggen *et al.*, 2002). The active layer was added to one flask, the support layer was added to another and final flask was used as a blank. This blank was used to allow for evaporation. All of the flasks were then capped, placed in a shaker (at 100 rpm) inside an incubator at 30°C. The flasks were left overnight. The concentration difference was measured for the active layer solution and supporting material flask solution against the blank solution.

This method improves on the pervious published adsorption methods for several reasons. Van der Bruggen *et al.* (2002) and Kiso *et al.* (2000) did not remove the porous support material from the active layer. In this study, the support material was removed and studies separately to measure the effect of this material had on adsorption. Van der Bruggen *et al.* (2002) did not stir the organic solution containing the membrane material but Kiso *et al.* (2000) did stir the organic solution. Kiso *et al.* did this by adding 50 ml of solution to the membrane filtration cell (without pressure) that had an integrated stirrer. This method allowed only a small membrane area to be used (0.003 $m^2$). In this study, it was assumed that the most important aspect of this type of experiment was to have the largest membrane area for the smallest volume of solution. Therefore, cutting the membrane into small 4 x $10^{-4}$ $m^2$ pieces and placing them in a shaken flask with 50 ml of solution was found to be the best method. A slow agitation of 100 rpm was used as this was found to give sufficient mixing whilst keeping all of the membrane material wet for all of the time.

### 3.9.2 Desorption

After the concentration difference due to adsorption had been measured, then desorption experiments were conducted. This experiment was similar to that conducted by Schaep and Vandecasteel (2001) who immersed a membrane in CsCl solution. They assumed that the original membrane counter-ions are exchanged for cesium ions. After rinsing the membrane thoroughly in deionised water, Schaep and Vandecasteel (2001) immersed the membrane in $MgCl_2$ solution. The magnesium ions were assumed to occupy the place of the cesium ions as counter-ions and the cesium

ions are then set free in the solution. The measured ceisum ions were said to be equal to the number of negatively charged groups on the membrane surface.

In the present study, this method was adapted to be used after the initial adsorption of organic compounds. The membrane materials were thoroughly rinsed in deionised water and then immersed in 50 ml of 0.1 M KCl, overnight in sealed 250 ml conical flask (shaken at 100 rpm and 30°C). The potassium ions were assumed to ion exchange with the organic compounds which were then measured by UV or visible absorption and compared against a blank 0.1 M KCl solution (no membrane material). This method was used to close the mass balance and check the results of the previous adsorption experiment.

# 4 Nanofiltration of amino acids

## 4.1 Introduction

The effect of concentration on rejection for amino acids filtered through a NTR 7450 membrane was investigated in this chapter.

As amphoteric electrolytes, amino acids act as both basic (proton acceptor) and acidic (proton donor) agents. In the dipolar form of an amino acid, the amino group is protonated ($-NH_3^+$) and the carboxyl group is dissociated ($-COO^-$). The ionisation states of an amino acid varies with pH (Figure 4.1)

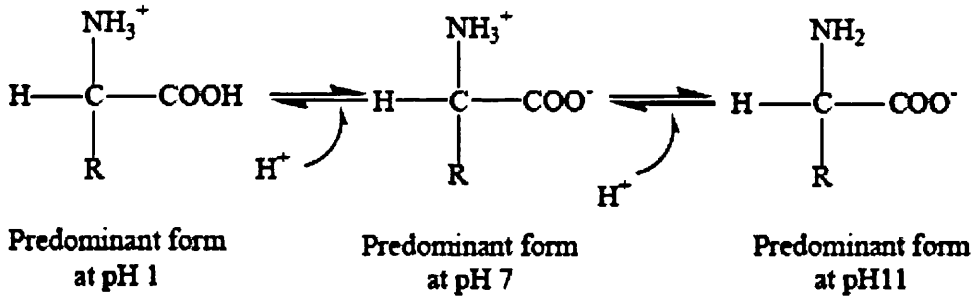


**Figure 4.1 Ionisation states of an amino acid depends on pH**

The relationship between pH and the ratio of acid to base is expressed by the Henderson-Hasselbalch equation (McMurry, 2000):

$$pH = pK + \log\frac{[A^-]}{[HA]} \qquad (4.1)$$

where $[A^-]$ is the concentration of the proton acceptor, and $[HA]$ is the concentration of the proton donor.

The rejection of amino acids by the membrane is determined by both size and charge effect between the amino acid and the membrane. The size (steric) effects depend on the molecular size of the amino acid and the molecular weight cut off (*MWCO*) of the membrane. The charge effect is decided by the ionized states of the amino acids and by the electrical properties of the membrane, both of which are related to the pH of the solution. Therefore pH was controlled in the NF filtrations.

In previous studies, the effect of salt concentration and pH on rejection for a constant concentration of amino acids has been the main area of interest (Garem *et al.*, 1997; Gotoh *et al.*, 2004; Grib *et al.*, 2000; Li *et al.*, 2003; Martin-Orue *et al.*, 1998; Timmer *et al.*, 1998; Wang *et al.*, 2002). This chapter considers the data relating the rejection for changing concentration of pure amino acid solutions at constant pH. The results are then compared against existing amino acid filtration models.

## 4.2 Amino acid results

Five amino acids were studied in this investigation. These were selected to cover a range of parameters that are available out of the twenty most common amino acids. The amino acids used are summarised in Table 4.1.

| Amino acid | Classification (R) | MW | $pK_{\alpha\text{-}COOH}$ | $PK_{\alpha\text{-}NH2}$ | $pK_R$ | Isoelectric point | Working pH | Net charge, z (electrons per molecule) |
|---|---|---|---|---|---|---|---|---|
| Glycine | Neutral | 75 | 2.34 | 9.60 | - | 5.97 | 6.4 | -0.001 |
| Glutamic acid | Acidic | 147 | 2.19 | 9.67 | 4.25 | 3.22 | 4.0 | -0.34 |
| Glutamine | Neutral | 146 | 2.17 | 9.13 | - | 5.65 | 6.5 | -0.002 |
| Phenylalanine | Neutral | 165 | 1.83 | 9.13 | - | 5.48 | 4.0 | 0.007 |
| Lysine | Basic | 146 | 2.18 | 8.95 | 10.53 | 9.74 | 9.74 | 0.000 |

$pK_\alpha$ data from McMurry, 2000

**Table 4.1 Summary of amino acids**

Table 4.1 shows that glutamine, glutamic acid and lysine have approximately the same size but have different classifications due to their chemical structure. The term classification refers to R ($pK_R$) and not the whole molecule. Glycine and phenylalanine are both "neutral" but glycine is one of the smallest and phenylalanine is one of the largest out of the twenty most common amino acids. These five amino acids showed different rejections due to both charge and steric effects.

The first amino acid filtration conducted with the NTR 7450 membrane was that of glutamic acid as shown in Figure 4.2.

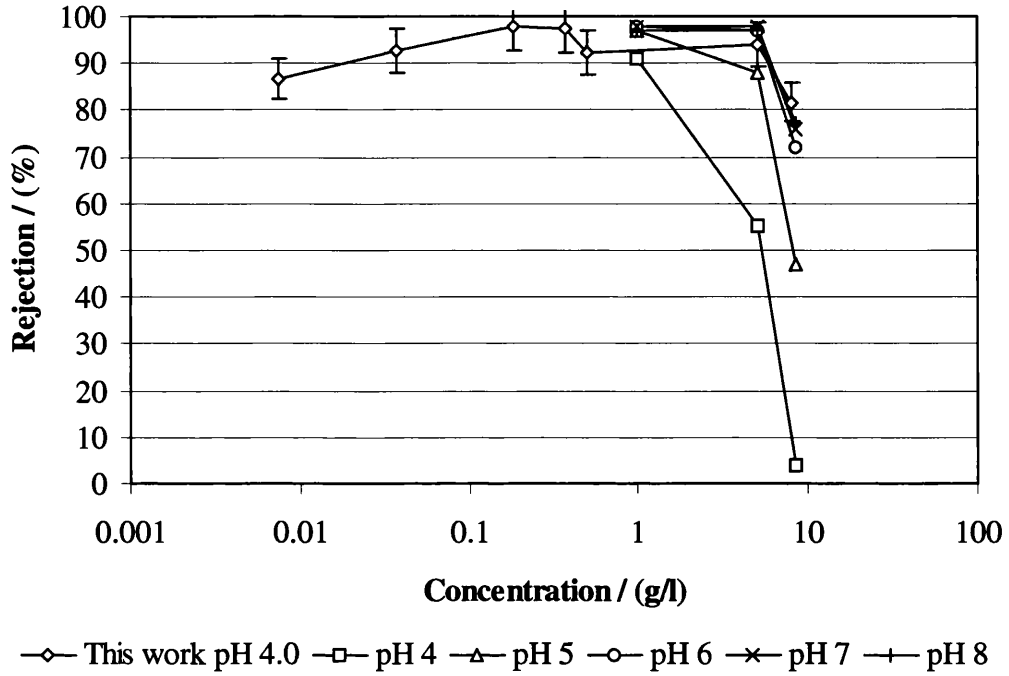


**Figure 4.2 Rejection of Glutamic acid at pH 4.0 for NTR 7450 membrane. The pH data range was re-plotted from Li *et al.* (2003) for NTR 7450 membrane at 0.8 to 30 MPa and 35°C.**

This experiment was conducted as a proof of the experimental equipment and technique. If only the higher concentration part of the graph (0.5 – 10 g/l) is considered, then Figure 4.2 shows that, for this work, as concentration is increased from 0.5 to 8 g/l, the rejection of glutamic acid at pH 4.0 falls from 92.2% to 81.6%. Although this result is not the same as that found by Li *et al.* (2003) for glutamic acid at pH 4.0 (Figure 4.2), the characteristic decrease is in agreement with that of Li *et al.* (2003). The difference may be due to the fact that Li *et al.* (2003) used an applied pressure that ranged from 0.8 – 3.0 MPa, when in this work, the pressure was carefully maintained at a constant 1.69 ± 0.01 MPa (16.5 ± 0.1 barg). This good agreement at higher pH was taken to validate the experimental equipment and technique. Figure 4.2 shows that in the concentration range of 0.5 – 10 g/l, the rejection of glutamic acid increases with pH. As the pH is increases from 4 to 8, then the average charge over all the glutamic acid molecules decreased from -0.34 to -1.02 electrons per mole respectively. An example of amino acid charge calculation is shown in Appendix A.5. It was reported that the NTR 7450 membrane had an inherent negative charge (Nyström *et al.*, 1995; Schaep and Vandecasteele, 2001). Therefore the more negative the charge on the amino acid molecule, the greater the

charge repulsion, resulting in a higher rejection. Figure 4.2 shows that, in the range 0.5 – 10 g/l, as the concentration is increased for glutamic acid (at constant pH) the rejection decreased. This is a typical phenomenon if electrostatic interactions are involved in the rejection mechanism; Hagmeyer and Gimbel (1998), Garba *et al.* (2003) and Mohammad and Takiiff (2003) reported this for divalent salts. As concentration increased, the membrane's fixed charge became increasingly neutralised by the counter-ions in solution, resulting in lower rejection. Thus, the importance of the Donnan mechanism became progressively diminished with increasing feed concentration. For the experimental data presented in Figure 4.2, the rejection dropped more rapidly with increased concentration for glutamic acid at pH 4 more than any other pH. This was due to glutamic acid having a more neutral average charge over all the molecules at pH 4. Therefore the Donnan mechanism diminishes more readily at a lower pH, and hence a lower charge on the molecule.

Now if the lower concentration range (0.007 – 0.5 g/l) on Figure 4.2 is considered, then it shows rejection increasing with concentration. This is an unexplained phenomenon. Figure 4.2 shows that the rejection of glutamic acid increases form 86.7% to 97.8% for a concentration range of 0.007 g/l to 0.18 g/l. Before any speculation was made to what might cause this behaviour, the data had to be evaluated to check that the filtration results indicated an actual property of membrane-solution systems, and not an artefact of errors. Thus this possibility had to be ruled out by evaluation of the experimental error.

### 4.2.1 Error

Amino acid concentration was measured by Ninhydrin Reagent analysis (Chapter 3). The error was evaluated by two methods. The first considered the accumulated error related to the preparation of a sample for measurement in the spectrophotometer. The second assessed the statistical error determining the deviation in repeated analysis of the sample or by the consideration of the deviation of the data points from the straight line fitted to the calibration data.

### Accumulated error

Several steps were required in the Ninhydrin reagent analysis of amino acids. The first step was to dilute the sample so that its concentration was within the analysis range. The second step was the addition of two reagents, and the final step was an adsorption measurement in a spectrophotometer. The errors associated with each step are summarised in Table 4.2.

| Source of error | Maximum condition | Absolute error ± | Units |
|---|---|---|---|
| Variable pipette | 1 | 0.006 | ml |
| Variable pipette | 5 | 0.03 | ml |
| Volumetric flask | 25 | 0.04 | ml |
| Volumetric flask | 500 | 0.25 | ml |
| Spectrophotometer | 2 | 0.005 | - |
| Balance | 200 | 0.00005 | g |

**Table 4.2 Error sources and magnitudes for amino acid analysis using Ninhydrin Reagent method**

The accumulated error associated with sample preparation and measured was found to be ± 2% (Appendix A.1).

### Statistical error

The statistical error was evaluated by two methods. The first was a study of the standard deviation in a set of repeated adsorption measurements and the second was a study of the standard deviation of these repeated measurements when compared to a calculated best-fit value. Both methods are shown in Appendix A.1 for glutamic acid analysis. The largest error was found to be 3.6% for the best-fit calculation. The value was chosen as the associated error in glutamic acid analysis as it was of a higher magnitude than the accumulated error. This error implied that for a concentration of 5.0 gl/l of glutamic acid, the rejection was 94 ± 5%. The error bars were determined for all data points and plotted in Figure 4.2. Particular consideration was paid for amino acids with significant increase in rejection with increasing concentration. It may be seen from the error bars plotted on Figures 4.2 to 4.6 that the errors in rejection cannot account for the observed increase in rejection with concentration. For example, the rejection of 1.0 g/l glycine was 67 ± 3%, when the measured increase in rejection was from 25% to 72%. On the basis of this discussion, it is possible to

conclude that the phenomenon was a real observation and not due to experimental error.

### 4.2.2 Amino acid filtrations

A series of experiments was conducted to examine this phenomenon further. Figure 4.3 shows the rejection of glutamine for a NTR 7450 membrane.

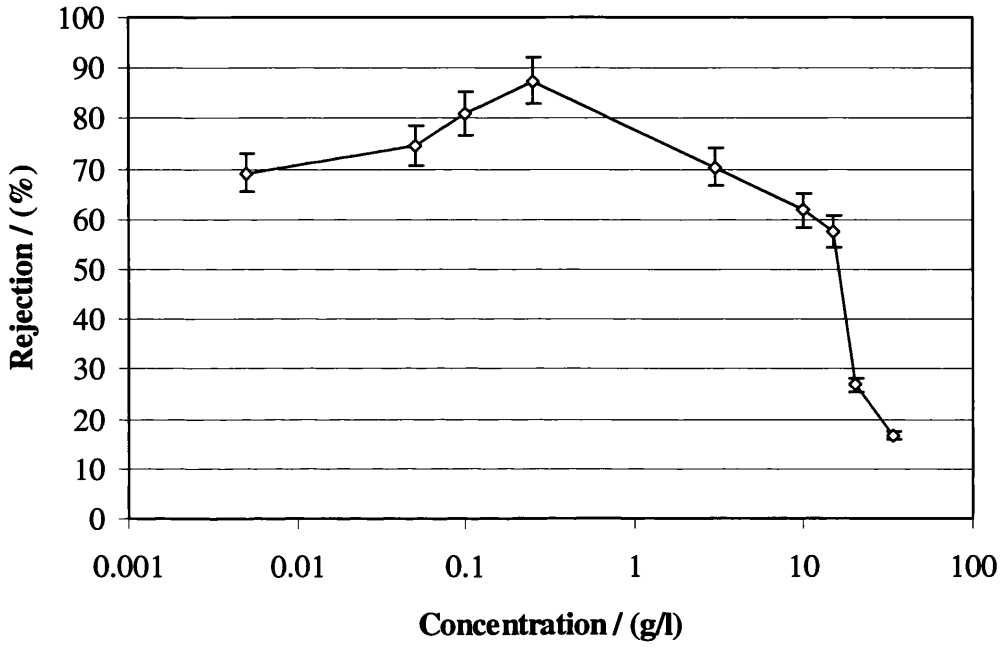


**Figure 4.3 Rejection of glutamine at pH 6.5 for NTR 7450 membrane**

Figure 4.3 shows that the rejection of glutamine increases from 69.2% to 87.5% for a concentration rise of 0.005 g/l and 0.25 g/l respectively. The rejection then progressively falls to 16.7% for a further concentration increase to 33.5 g/l. Although glutamine and glutamic acid have a similar MW (Table 4.1), the overall rejection of glutamine is lower than that for glutamic acid. Glutamine at pH 6.5 carries a very small mean negative net charge of –0.002 electrons per molecule (Table 4.1), therefore the maximum rejection of 87.5% is not as high as that for glutamic acid (maximum glutamic acid rejection was 97.8%) which is due to the fact that glutamine carries a higher mean net charge than glutamic acid, and therefore Donnan repulsion is less.

Figure 4.4 shows the rejection of glycine for a NTR 7450 membrane

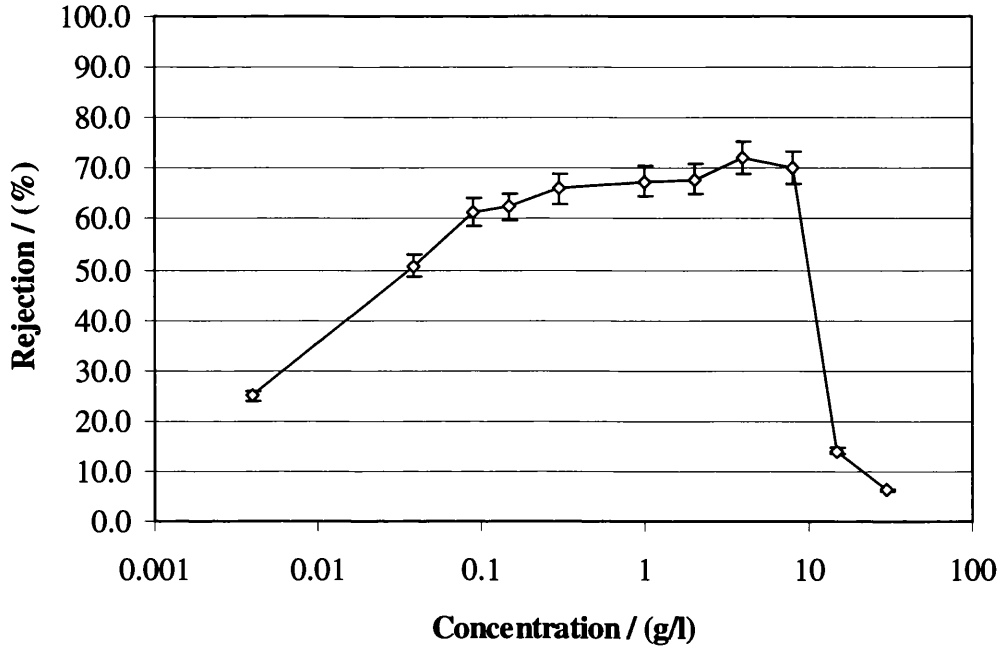


**Figure 4.4 Rejection of glycine at pH 6.5 for NTR 7450 membrane**

Figure 4.4 shows that the rejection of glycine increases from 24.9% to 72.2% for a concentration rise from 0.004 g/l to 4 g/l respectively. The rejection then falls rapidly to 6.3% for a concentration of 30 g/l. Although glycine and glutamine have a similar net charge (Table 4.1), the overall rejection of glycine is lower than that for glutamine. This is due to the fact that glycine has a much smaller MW than glutamine (Table 4.1), therefore the steric effects are smaller for glycine. The molecules that have shown rejection with concentration have all carried a negative charge. With the next experiments, the effect of positive (Figure 4.5) and neutral (Figure 4.6) mean charges were investigated.

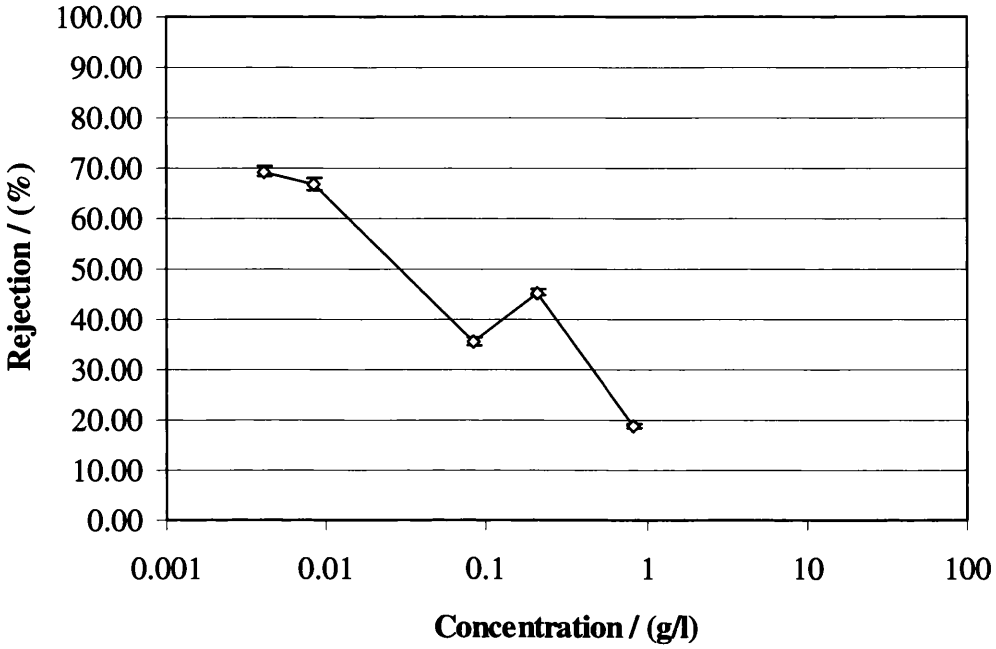


**Figure 4.5 Rejection of phenylalanine at pH 4.0 for NTR 7450 membrane**

Figure 4.5 shows that the rejection of phenylalanine decreases from 69.4% to 18.9% for 0.004 g/l and 0.83 g/l respectively. Phenylalanine at pH 4.0 carries a mean small positive net charge of 0.007 electrons per molecule (Table 4.1). Therefore the phenylalanine molecule will experience an attraction towards the negatively charged membrane, and will readily permeate the membrane. Figure 4.5 shows that a positively charged phenylalanine molecule does not exhibit the increasing rejection with concentration that the previous negatively charged molecules showed. The effect of a neutral charge on the behaviour was then investigated.

Lysine was filtered through the NTR 7450 membrane at its isoelectric point (pH 9.74), at this pH the lysine molecule carries no net charge. The results are shown in Figure 4.6.

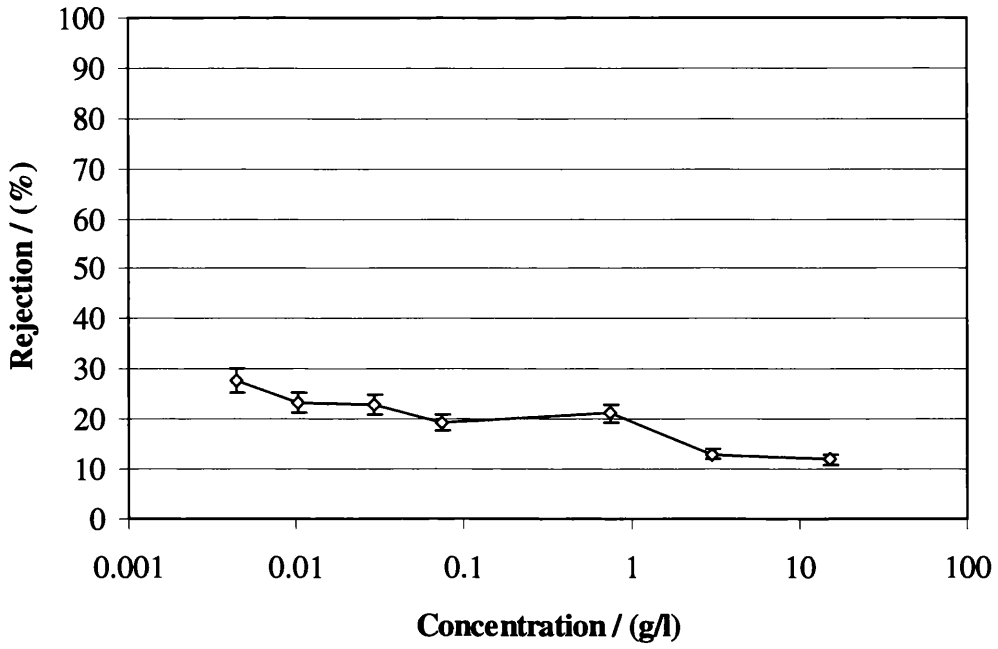


**Figure 4.6 Rejection of lysine at pH 9.74 for NTR7450 membrane**

Figure 4.6 shows that the rejection of lysine remains around 20%. The rejection does show slight decrease from 27.8% to 11.9% for 0.004 g/l and 15 g/l respectively. As the lysine molecule carries no net charge, the rejection is purely steric and relatively constant with changing concentration. This result is similar to that found by Li *et al.* (2000). They stated that for a single amino acid in net charge zero state, the behaviour in the NF process is not completely clear. The rejection could be determined by steric effects. However, some deviation of neutral solute behaviour of the amino acid could occur because it is not a truly neutral molecule, but has two opposite charge sites (Li *et al.*, 2000).

Li *et al.* (2003) has previously observed the rejection increasing with concentration for an amino acid. They stated that this was due to dimers forming in the amino acid solution. This claim was investigated further in this work.

## *4.3 Concentration-size effects*

Li *et al.* (2003) observed that the rejection of glutamic acid decreased, as expected, for an increase in concentration, for a polymeric NTR 7450 NF membrane. For glutamine, the rejection increased with an increase in concentration. Li *et al.* (2003)

stated that the rejection of glutamine was expected to be near zero and independent of the concentration, because the pore size of NTR 7450 membrane is significantly larger than the size of glutamine (Chapter 3, Table 3.2). Li *et al.* (2003) attempted to explain the difference between the experimental results and the expected rejection, by suggesting that glutamine might exist as a dimer polymer of glutamine in solution where the concentration is high and near the saturated solubility of glutamine. They stated that the hydrogen bonds between amide (-NH) and carbonyl (-CO) groups make glutamine more likely to associate together into a dimmer or polymer, thereby increasing the observed molecular weight of glutamine.

### 4.3.1 Peptide bond

A peptide bond is a chemical bond formed between two molecules when the carboxyl group of one molecule reacts with the amino group of the other molecule, releasing a molecule of water. This is a dehydration synthesis reaction, and usually occurs between amino acids. The resulting C-NO bond is called a peptide bond. A peptide bond can be broken by amide hydrolysis. The peptide bonds in proteins are metastable and will break spontaneously in water releasing about 10 kJ/mol of free energy. Living organisms also employ enzymes to form peptide bonds as this process requires free energy. Therefore the glutamine molecules may not freely associate together as energy of formation is required. Therefore it was necessary to test if glutamine molecules do form dimmers (or polymers) at very high concentration (near the saturated solubility), as suggested by Li *et al.* (2003).

### 4.3.2 Determination of the hydrodynamic radii

A High Performance Particle Sizing (HPPS) instrument (Malvern Instruments, Worces. U.K.) was used to measure the size of both glutamine and glutamic acid. The HPPS is capable of measuring the solute radius of particles as small as 0.3 nm ± 10% (as discussed in Appendix A.4), but is at the operational limit. Table 4.3 shows the measured hydrodynamic diameter for glutamine by HPPS measurement.

| Concentration % (wt/wt) | Diameter (nm) |
|---|---|
| 0.5 | 0.52 |
| 1.0 | 0.45 |
| 2.0 | 0.52 |
| 3.0 | 0.70 |

**Table 4.3 HPPS measurement of hydrodynamic diameter of glutamine**

Table 4.3 shows that the HPPS was capable of giving an approximate value the diameter of glutamine, as the average measured diameter was 0.55 nm which is comparable to the published diameter 0.56 nm (Li *et al.*, 2003). The spread of measured diameters (Table 4.3) are likely due to the high experimental error associated at radii ~ 0.3 nm (Appendix A.4). Table 4.3 shows that there was no significant increase in glutamine diameter with concentration, which is a strong indication of no dimers (or polymers) being present at higher concentration. This may be more clearly seen in Figure 4.7. Figure 4.7 shows that for all measurements, only one peak was observed, indicating only one species was present. If a dimmer were present (in significant quantities – enough to change the rejection characteristics as observed by Li *et al.* (2003)), then a secondary peak on the shoulder of the monomer peak would be observed. If dimmers were present, then the secondary peak would be expected to be in the 0.74 nm region (0.74 nm is the diameter of a glutamine dimmer molecule, calculated by the Schnabel *et al.* (1988) correlation used by Li *et al.* (2003)).

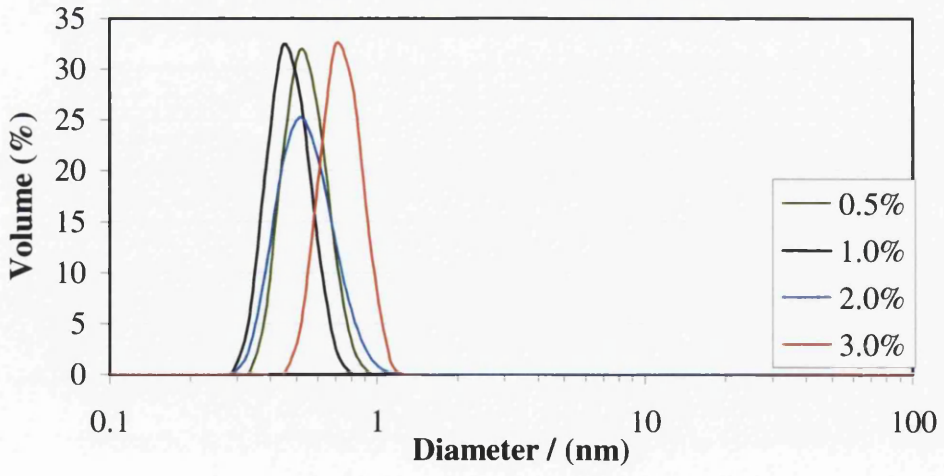


**Figure 4.7 Hydrodynamic radii of glutamine by HPPS measurement**

The effect of concentration on size of glutamic acid molecules was also investigated using the HPPS instrument. Li *et al.* (2003) observed a decreased in rejection for glutamic acid passing through a NTR 7450 NF membrane. They concluded that glutamic acid molecules are less likely associate to form dimmers than glutamine molecules and that charge effects are much more significant than steric effects for glutamic acid. Table 4.4 shows the measured hydrodynamic diameter for glutamic acid by HPPS measurement.

| Concentration % (wt/wt) | Diameter (nm) |
|---|---|
| 0.01 | 0.13 |
| 0.05 | 0.13 |
| 0.10 | 0.12 |
| 0.20 | 0.18 |
| 0.40 | 0.81 |
| 0.80 | 0.51 |

**Table 4.4 Measured hydrodynamic diameter of glutamic acid by HPPS measurement**

Table 4.4 shows a spread of results, which are probably due to the HPPS measuring at its limit of operation (Appendix A.4). Table 4.4 does show an increase in glutamic acid diameter with concentration, however the results below 0.40% (wt/wt) have a diameter below 0.56 nm (the size of a glutamic acid monomer, Li *et al.*, 2003), which is impossible. Figure 4.8 show that for all measurements, only one peak was observed, indicating that only one species was present, hence no dimers or polymers were present. However, the results shown in Table 4.4 and Figure 4.8 highlight the limitations of HPPS measurement at a radii of around 3 nm.

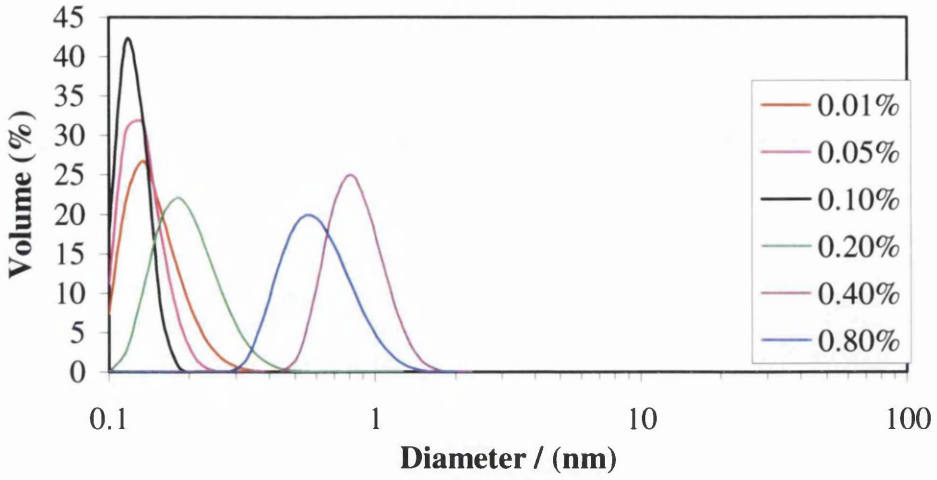


**Figure 4.8 Hydrodynamic radii of glutamic acid by HPPS measurement**

Although the HPPS measurements for glutamine and glutamic acid have their limitations, they do appear to signify that dimmers do not exist and no general trend could be found. However, the instrument used was at the limits of its operating range and another method, namely osmotic pressure analysis, will help to clarify the HPPS findings.

## *4.4 Osmometer results*

The osmometer used in this study was shown to produce reliable values of osmotic pressure (Cao, 1999). Cao used this osmometer to measure the osmotic pressure of Bovine Serum Albmin suspensions, which contain particles of high molecular weights. As a result, they found that no great care was required over the selection of the membrane and a tight ultrafiltration membrane was found to be acceptable. By the same token, a reverse osmosis membrane (Dow Filmtech LFC 1) was assumed to be suitable for the osmotic pressure measurement of solutions of small (100-200 Da MW) organic compounds.

### 4.4.1 Osmotic pressure versus time

In the osmotic pressure experiments, the pressure of the solute chamber was monitored with time. Usually the pressure built up quickly at first, then the rate of change slowed down and gradually arrived at an equilibrium state (Figures 4.9 and 4.10), which was the osmotic pressure. The rate at which the pressure arrived at the

equilibrium pressure was dependent on solute temperature (Figure 4.9) and concentration.

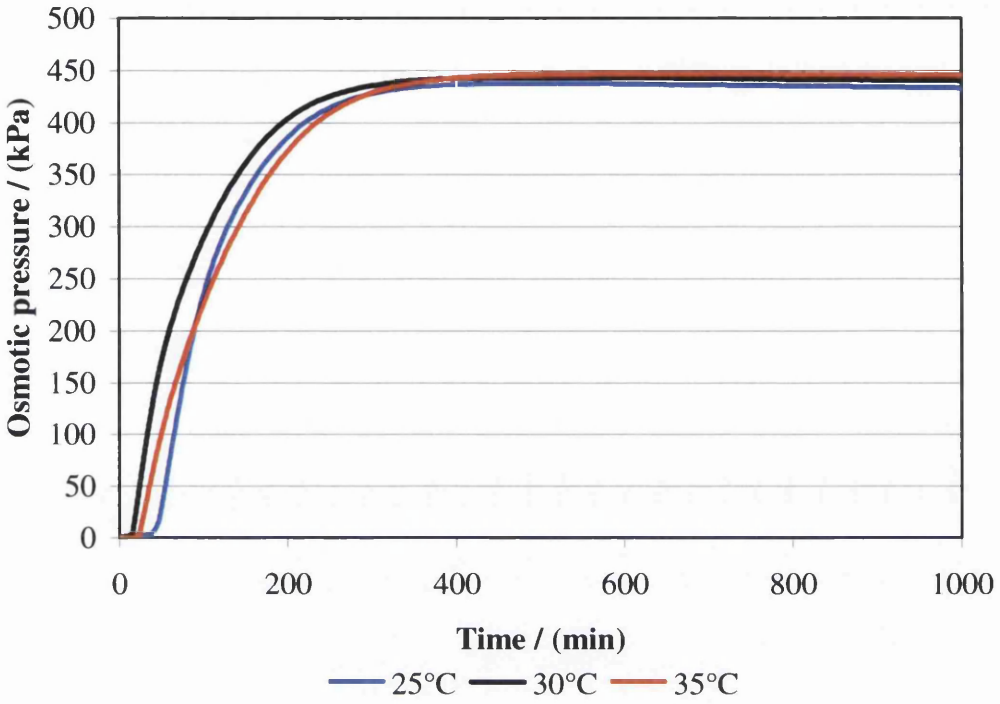


**Figure 4.9 The effect of temperature on the osmotic pressure of glucose 40 g/l (LFC RO membrane)**

Figure 4.9 shows that the osmotic pressure is influenced by temperature: the osmotic pressure of glucose 40 g/l at 35°C is 447 kPa, this is reduced to 437 kPa at 25°C. Therefore the heating box, in which the osmometer was enclosed, was temperature controlled to within ± 0.2°C. Figure 4.9 shows that for each run there was a "lag-phase" occurring within the first 20 minutes of the experiment. This is most probably due to dissolution of micro-bubbles; it did not appear to influence the final result. It can be seen in Figure 4.10 that although the shape of the plot is different, the equilibrium point is the same.

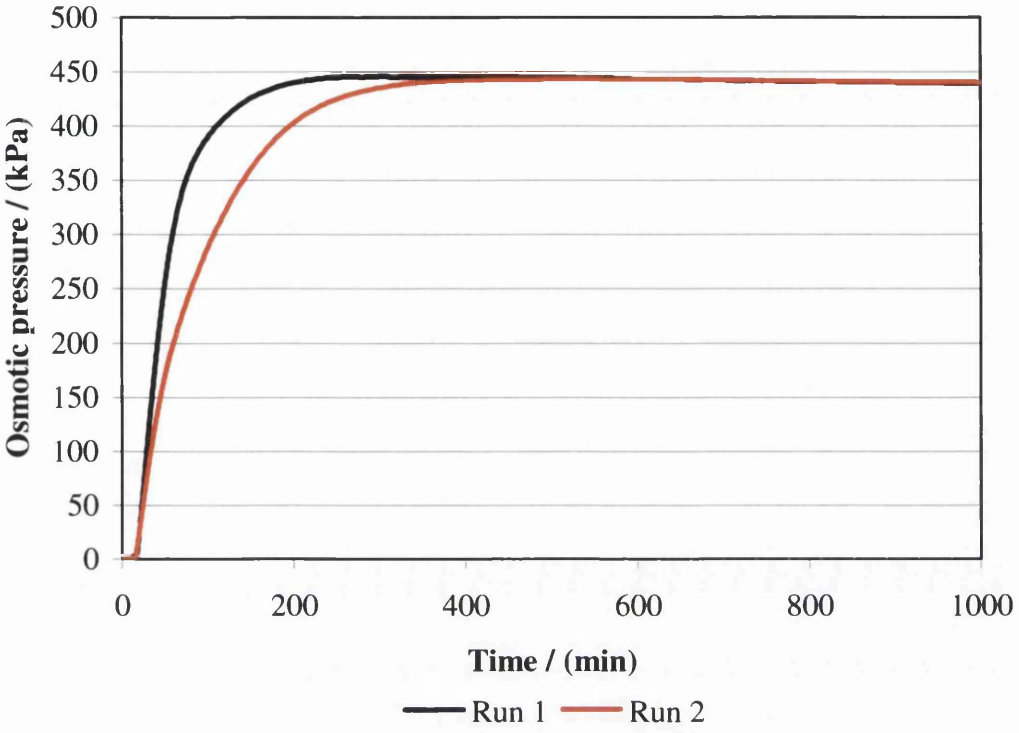


**Figure 4.10 Experimental determination of the osmotic pressure of glucose 40 g/l at 30°C (LFC RO Membrane)**

Figure 4.10 shows that the osmotic pressure of glucose 40 g/l at 30°C is 443 kPa and that the equipment is capable of reproducible results.

To enable comparison with osmotic pressure correlations from other sources; International Critical Tables (Garner, 1929) and Van't Hoff, a series of osmotic pressure values were measured for several solute concentrations. The osmometer used in this study was limited in operation due to the material of construction and the pressure transducer having a maximum range of 0 to 700 kPa. As a result, only a small amount of the range presented in the literature could be measure. The results are shown in Figure 4.11.

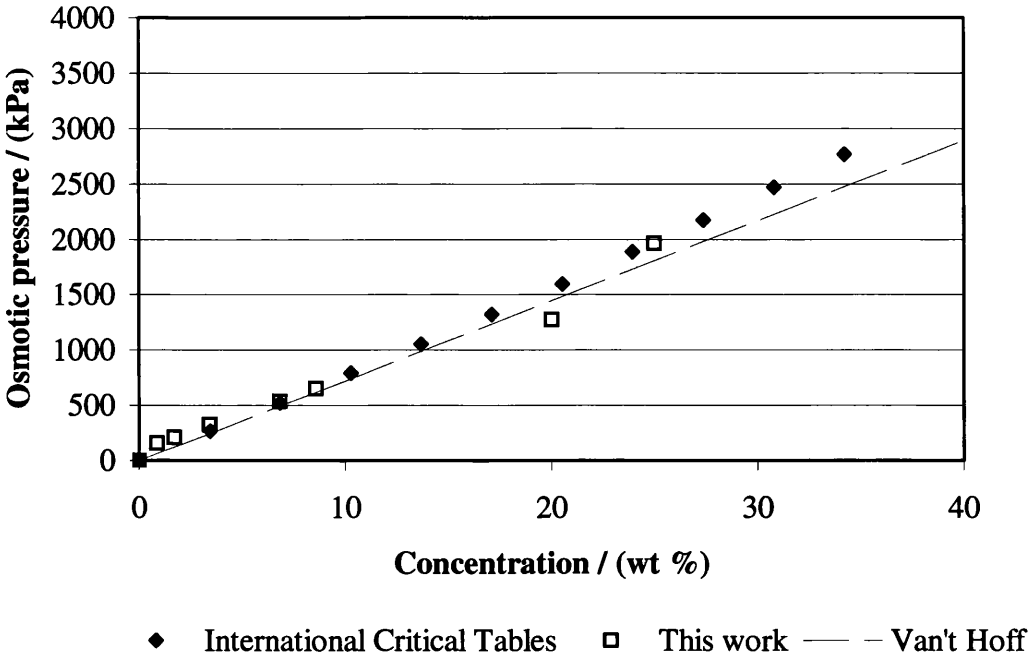


**Figure 4.11 Relationship between solute concentration and osmotic pressure for sucrose at 25°C**

Figure 4.11 shows a very good agreement between the measured data and the published data for the osmotic pressure of sucrose at 25 °C. The region of 0-30 wt% is a linear relationship between osmotic pressure and concentration. Figure 4.11 includes the Van't Hoff approximation; this approximation provides a theoretical description of osmotic pressure and was defined as:

$$\pi = cRT \tag{4.2}$$

where $\pi$ is the calculated osmotic pressure, $c$ is the concentration of the solution, $R$ is the gas constant and $T$ is the temperature of the system. When using the Van't Hoff relationship, it is assumed that the solution is ideal and that there is no particle association. Typically, the Van't Hoff relationship is applied to dilute solutions with a concentration less than 1% (Alvarez *et al.*, 1997). The osmotic pressure may also be expressed in a simplified form that was derived from the thermodynamic description of the osmotic pressure (Sourirajan, 1970), which stated:

$$\pi = -\frac{RT}{V_w} \ln a_s \tag{4.3}$$

where $a_s$ was the activity coefficient and $V_w$ the partial molar volume of water. The values $a_s$ and $V_w$ were known to be very difficult to evaluate hence the simplification presented by equation (4.2). The Van't Hoff equation (equation 4.2) is strictly valid for dilute solutions. It is generally accepted that pressure data that deviate from equation (4.2) and (4.3) is a result of non idealities due to solute-solute, solute-solvent and other interactions that are often accounted for in the activity coefficients in equation (4.3).

### 4.4.2 Osmotic pressure of amino acids

The osmotic pressure of the four amino acids was measured to assess the amount of interaction occurring between the amino acids. As mentioned in Section 4.3 concentration-size effects, if Li *et al.* (2003) were correct, the observed size of the glutamine would be expected to increase with concentration. This was presumed to be due to the association between the amide (-NH) and carbonyl (-CO) groups to form a dimmer (Li *et al.* 2003). This effect was investigated by measuring the solute diameter by using HPPS. The results of HPPS measurements suggested that dimmers were not occurring, however another method was required due to high error at the operational limit of the HPPS.

The osmotic pressure of proteins such as Bovine Serum Albumin has been found to exhibit significant non-ideality. This non-ideality has been attributed to the existence of solute-solute, solute-solvent interactions, and hence, the presence of dimmers or higher oligomers (Yousef *et al.*, 2002) (Vilker *et al.*, 1981) (Yousef *et al.*, 1998). Vilker *et al.* (1981) plotted reduced osmotic pressure ($\pi/c$) as a function Albumin concentration. From the extrapolated value for the intercept, a molecular weight of 69 000 Da was determined for Albumin. This value is higher than that for monomeric Albumin determined by amino acid sequencing (66 100 Da), and Vilker *et al.* (1981) stated that it could result from the presence of about 5% dimmers or higher oligomers. This method cannot be used for molecular weight determination of amino acids due to relatively high inaccuracies at low molecular weights and it is limited to use with macromolecules (~ $10^4 < 10^6$ Da). However, a nonlinear relationship between a plot of $\pi$ and $c$ indicates solute-solute interactions are occurring. Therefore a study of $\pi$ with respect to concentration for single amino acids was conducted.

### 4.4.3 Osmotic pressure as a function of concentration

The osmotic pressure as a function of concentration is plotted in Figure 4.12. Figure 4.12 shows the measured osmotic pressure for the four amino acids used in nanofiltration. The results are plotted over a small concentration range (0-1.0 g/l) as this is the region in which the interesting rejection phenomenon was occurring on the concentration rejection charts (Section 4.2 Amino acid results). Figure 4.12 show that the osmotic pressure for the amino acid is linearly proportional to concentration. This implies that the amino acid solution exhibits an ideal behaviour over the measured concentration range and crucially, no dimerisation was present.

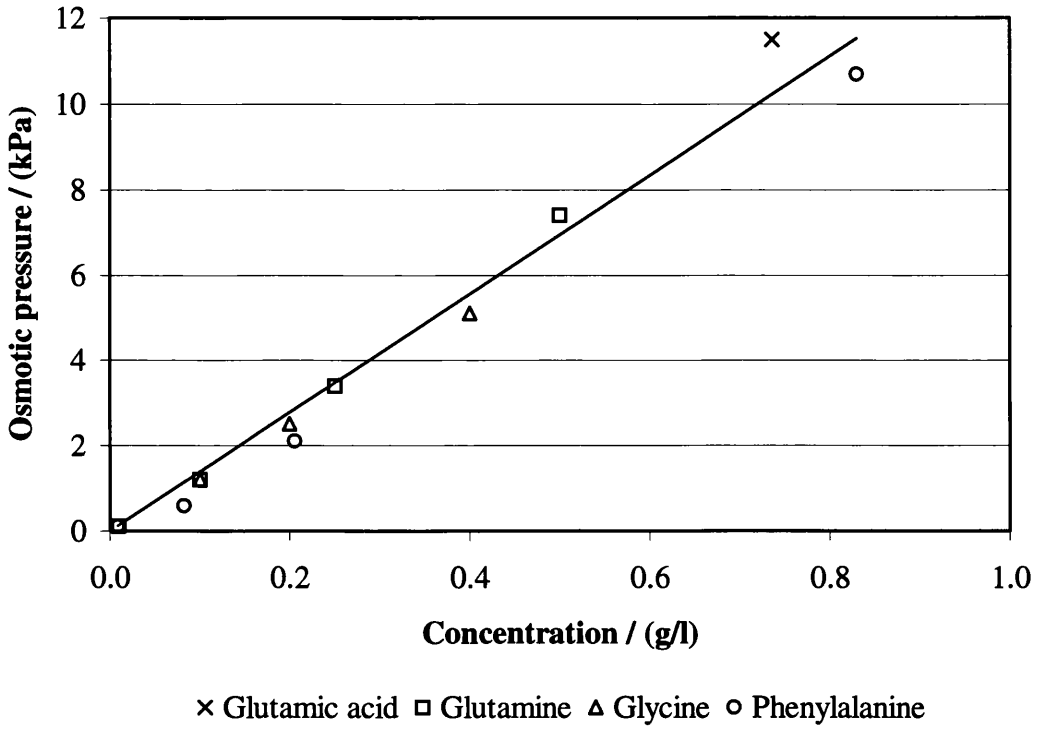


**Figure 4.12 Osmotic pressure of amino acids (low concentration range). The data is fitted with a best-fit straight line for illustrative purpose only**

The osmotic pressure was then studied over the whole concentration range used for nanofiltration of glutamine and glutamic acid; the results are shown in Figure 4.13.

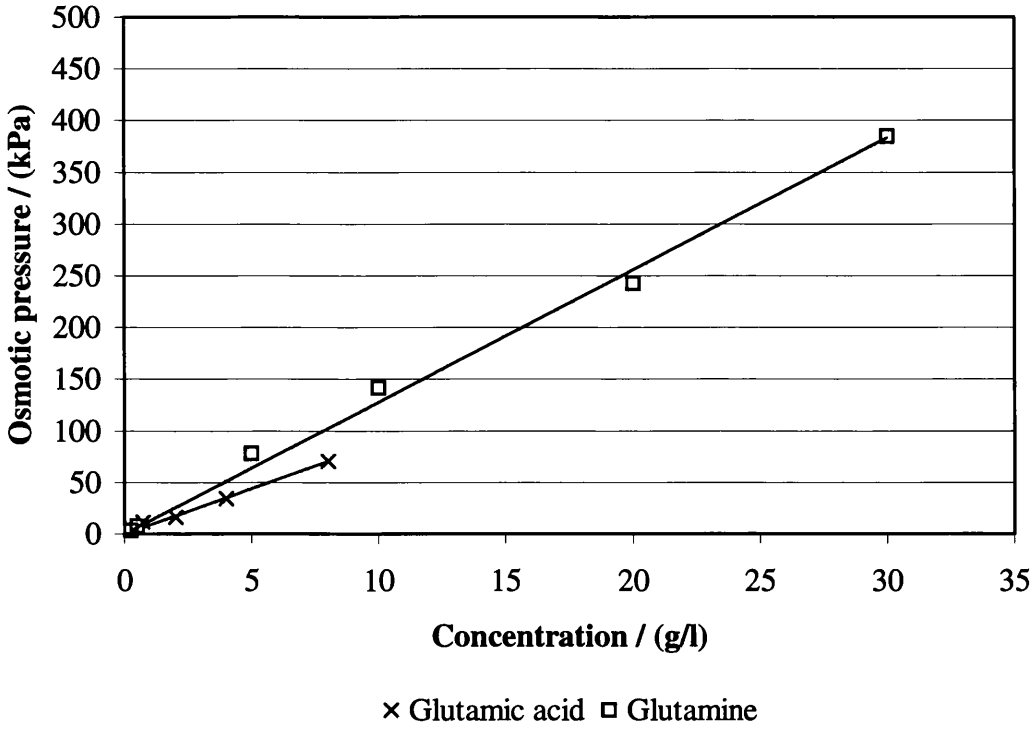


**Figure 4.13 Osmotic pressure of amino acids (high concentration range). The data is fitted with a best-fit straight line for illustrative purpose only**

Figure 4.13 again shows a linear relationship between $\pi$ and $c$. Therefore no nonlinear solute-solute interactions were occurring over the concentration range of nanofiltration. This result combined with the HPPS data clearly demonstrated that dimerisation was not occurring. Therefore, the rejection increasing with concentration for nanofiltration membrane was due to another process.

## 4.5 Amino acid nanofiltration model

For a charged NF membrane in which applied pressure is the driving force, the solute transfer is the result of two steps

1. firstly, a distribution of ionic species at the selective interface as a function of their charge
2. and secondly, transfer by a combination of diffusion / convection / electrophoretic mobility through the membrane.

Solute flux ($J_s$) has been described by the extended Nernst-Plank equation:

$$j_i = -D_{i,p}\frac{dc_i}{dx} - \frac{z_i c_i D_{i,p}}{RT} F \frac{d\psi}{dx} + K_{i,c} c_i V$$

Coefficients $D_{i,p}$ and $K_{i,c}$ are the solute hindered diffusivity in the membrane and the solute hindrance factor for convection inside the membrane respectively. Both $D_{i,p}$ and $K_{i,c}$ are a function of the solute radius/pore radius ratio. Therefore, NF membrane rejection is due to both the size and charge of solutes (Rautenbach and Gröschl, 1990). Garem *et al.* (1997) assumed that the transmission of a solute ($Tr$) through a NF membrane was the product of two independent terms, $Tr_s$ and $Tr_c$, related to the size and charge effects respectively.

In the case of a solution containing a single amino acid, Garem *et al.* (1997) applied Donnan theory to the solute concentrations in both sides of the membrane to model the amino acid transmission. The transmission of an amino acid alone in solution is a function of its molecular weight, $MW$, its net charge, $z$, the membrane molecular weight cut-off ($MWCO$) and the membrane charge density, $M$ (Kimura and Tamano, 1984) (Yaroshchuk and Staude, 1992) (Tsuru *et al.*, 1994). Depending on the values of $z$ and $M$, two different situations may occur.

### 4.5.1 An uncharged amino acid or a membrane with no charge

In this case, amino acid transmission through the NF membrane is solely dependent on the size exclusion effects between the membrane and the amino acid (Garem *et al.*, 1997). For this operating state, the transmission can be expressed as:

$$Tr = Tr_s$$

Where $Tr$ is the actual amino acid transmission, and $Tr_s$ is the transmission of the amino acid due to steric effects. The influence of size on transmission was described by Ferry (1936) and corrected by Zeman and Wales (1981). They assumed that the membrane was composed of perfectly cylindrical and parallel pores with radius $r_p$, for which the solvent velocity follows Poseuille's law with a parabolic profile. The amino acids are considered as non-adsorbing hard spheres with radius $r_s$ (Ferry, 1936) (Zeman and Wales, 1981). The theoretical $Tr_s$ value is calculated according to:

$$Tr_s = \left(1-(\lambda(\lambda-2))^2\right)\exp\left(-0.7146\lambda^2\right) \tag{4.4}$$

where, $$\lambda = \frac{r_s}{r_p} \tag{4.5}$$

However, a discrepancy in published $\lambda$ calculations has been observed. Garem *et al.* (1997), Grib *et al.* (2000) and Li *et al.* (2003) state $\lambda$ as that defined by equation 4.5, where the solute radius ($r_s$) is given by the Schnabel *et al.* (1988) correlation:

$$r_s = 0.038 MW^{0.4} \tag{4.6}$$

where $MW$ is the molecular weight of the solute.

Grib *et al.* (2000) calculated solute radius by using:

$$r_s = r_p\left(\frac{MW}{MWCO}\right)^{\frac{1}{3}} \tag{4.7}$$

where $MWCO$ is the molecular weight cut-off for the membrane. Equation (4.7) is a rearrangement of a correlation stated by Martin-Orue *et al.* (1998), namely:

$$\lambda = \left(\frac{MW}{MWCO}\right)^{0.33} \tag{4.8}$$

Martin-Orue *et al.* (1998) did not state how equation (4.8) was derived. However, if the assumption is made that

$$r_p = 0.038 MWCO^{0.4} \tag{4.9}$$

from Schnabel *et al.* (1988) correlation, then by substituting equations (4.6) and (4.9) into equation (4.5) gives:

$$\lambda = \left(\frac{0.038 MW^{0.4}}{0.038 MWCO^{0.4}}\right) = \left(\frac{MW}{MWCO}\right)^{0.4}$$

This equation differs from equation (4.8) given by in Martin-Orue *et al.* (1998) and Grib *et al.* (2000). This implies that a different and unknown correlation, other than Schnabel *et al.* (1988), was used for determining solute and pore radius. The Schnabel *et al.* (1988) correlation has been used numerous times in the literature and this

correlation has been used for the determination of amino acid solute radius (Li *et al.*, 2003, Garem *et al.*, 1997, Grib *et al.*, 2000, Hong and Bruening, 2006), and has been tested in this work by light scattering size analysis for amino acids. Although the *MW* is not a direct measure of the dimensions of a molecule, it still reflects the overall molecular size.

Grib *et al.* (2000) stated that the steric rejection for amino acids might be given by:

$$R_s = \left(1 - \lambda(\lambda - 2)^2\right)\exp\left(-0.7146\lambda^2\right)$$

where, $R_s = 1 - Tr$

Curiously, neither this equation nor equation (4.4) can be used to calculate Grib *et al.* (2000) published size retentions coefficients ($R_s$) for alanine, phenylalanine, glutamic acid and arginine, implying that some unknown method was used. For these reasons, all size exclusion calculations were determined by the use of equations (4.4), (4.5) and (4.6).

### 4.5.2 Single charged amino acid confronted with a charged membrane

In an amino acid-membrane system, charge effects result from interactions located at the solid/liquid interface. When the amino acid net charge ($z$) and membrane charge density ($M$) are of the same sign, the transmission has to take into account both size and electrical repulsion effects. Thus

$$Tr = Tr_s \times Tr_c \qquad \text{(Garem } et\ al.\text{, 1997)}$$

The relationship for the total exclusion as a function of both the size and charge coefficients has also been written as:

$$R = R_s + R_c - R_s R_c \qquad \text{(Grib } et\ al.\text{, 2000) (Li } et\ al.\text{, 2003)}$$

recalling that: $R_s = 1 - Tr$

$Tr_c$ can be described by referring to Donnan theory, which states that under equilibrium conditions, electroneutrality and equality of electrochemical potentials are maintained throughout the system (Donnan, 1911).

In the case of binary electrolyte solution of an amino acid with its counter-ion, *X*, Garem *et al.* (1997) formalized the following system of equations:

$$\ln(\upsilon_{ct} C_r)=\ln([X]_m)+z_{ct}\Psi_D$$

$$\ln(\upsilon_{AA} C_r)=\ln([AA]_m)-z\Psi_D$$

which gives,

$$\Psi_D=\frac{1}{z_{ct}}\ln\left(\frac{\upsilon_{ct} C_r}{[X]_m}\right)=\frac{-1}{z}\ln\left(\frac{\upsilon_{AA} C_r}{[AA]_m}\right) \qquad (4.10)$$

where $\Psi_D$ is the Donnan potential; $\upsilon_{AA}$ and $\upsilon_{ct}$ are the stoichiometric coefficients for the membrane and its counter-ion; $z$ and $z_{ct}$ represent the charge of the amino acid and its counter-ion; $[AA]_m$ and $[X]_m$ are the concentration inside the membrane for the amino acid, and its counter-ion. In the limiting case, system selectivity takes place only in the high-pressure side of the membrane, therefore Garem *et al.* (1997) showed that:

$$Tr_c(AA)=\frac{[AA]_m}{\upsilon_{AA} C_r} \qquad (4.11)$$

The requirement for electroneutrality within the membrane gives:

$$M + z[AA]_m = z_{ct}[X]_m \qquad (4.12)$$

If the pressure is sufficiently high that the amino acid in the membrane is forced into the nanofilter, its concentration inside the membrane $[AA]_m$ is far below that of the membrane fixed charge, *M*. Also, if the counter-ion concentration in the membrane phase, $[X]_m$, is practically equal to *M*.

Thus, combining equations (4.10), (4.11) and (4.12) gives:

$$Tr_c(AA)=\left(\frac{\upsilon_{ct} z_{ct} C_r}{M}\right)^{\frac{z}{z_{ct}}} \qquad (4.13)$$

Therefore equation (4.13) is the overall equation used to calculate the charge exclusion coefficient for an amino acid system.

### 4.5.3 Determination of size exclusion coefficients

The size transmission for each amino acid was calculated by using equation (4.4), the results are presented in Table 4.5.

| Amino acid | $MW$[1] (Da) | $r_s$[2] (nm) | $\lambda$ | $Tr_s$ (%) |
|---|---|---|---|---|
| Glycine | 74 | 0.21 | 0.35 | 60.6 |
| Glutamic acid | 147 | 0.28 | 0.46 | 42.1 |
| Glutamine | 146 | 0.28 | 0.46 | 42.3 |
| Lysine | 146 | 0.28 | 0.46 | 42.3 |
| Phenylalanine | 165 | 0.29 | 0.49 | 38.7 |

[1] (McMurry, 2000) [2] (Schnabel *et al.*, 1988)

**Table 4.5 Calculated size transmission coefficients**

Table 4.5 shows that as the $MW$ of the solute increases from 74 Da for glycine, to 165 Da for phenylalanine, the calculated transmission reduces from 60.6% to 38.7% for glycine and phenylalanine respectively. This result is expected for purely steric rejection mechanisms; as the solute radius increases, its transmission through the NF membrane is reduced. Now, when the steric model (equation (4.4)) is compared to experimental results for lysine (Figure 4.14), then it can be seen that purely steric rejection can describe the rejection behaviour of a neutral amino acid.

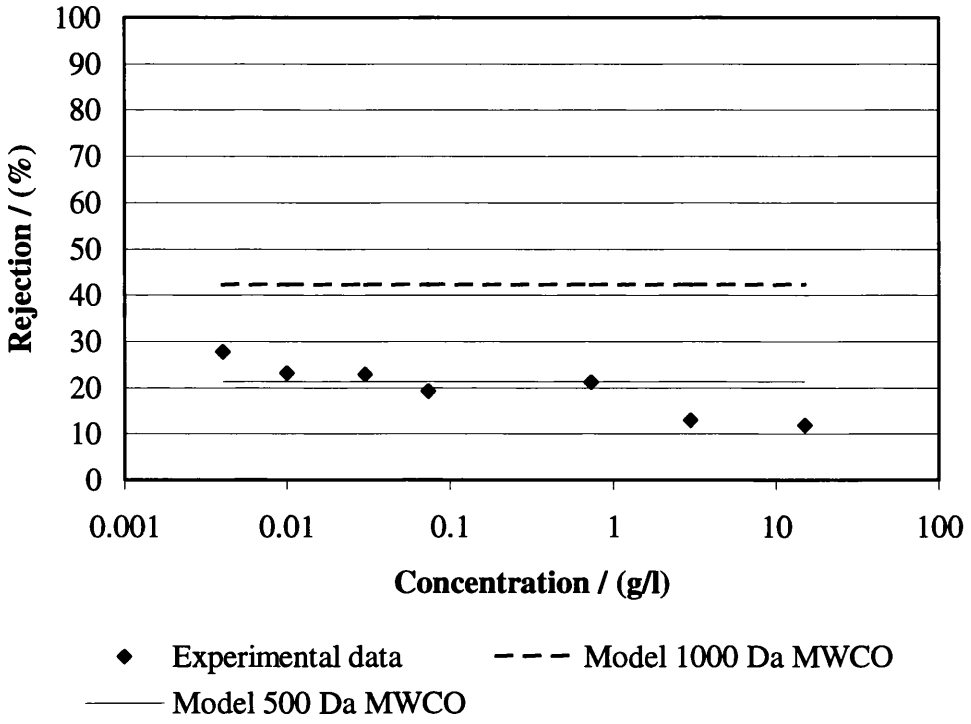


**Figure 4.14. Comparison between experimental rejection and the steric partitioning model for lysine at pH 9.74 and a NTR 7450 NF membrane**

Figure 4.14 shows that the calculated rejection (equation (4.4)) remains constant at 42.3% (dashed line Figure 4.14). This rejection value was calculated using a *MWCO* of 1000 Da in equation (4.5). There are numerous reports that the *MWCO* of NTR 7450 membrane is 1000 Da (Timmer *et al.*, 1998) (Gotoh *et al.*, 2004). However, Figure 4.14 clearly shows that the 1000 Da model over estimates the rejection of lysine. As *MWCO* is the only variable in the steric model, then this could be manipulated to bring the calculated rejection in line with the experimental rejection, the result is shown by the solid line in Figure 4.14. If the *MWCO* of the membrane were halved to 500 Da, then the steric model could describe some of the experimental rejection of lysine. Lysine has a *MW* of 146 Da and it is unclear why this would coincide with the model using 500 Da *MWCO* as a parameter. Therefore the *MWCO* of the NTR 7450 membrane will need to be separately investigated and quantified.

After comparing Figures 4.2 to 4.4 and Table 4.5, it became clear that the steric model could only be used to describe the rejection of lysine, as it was a neutral molecule. Figure 4.4 shows that the experimental rejection data for glycine varies considerably as a function of concentration, whereas the calculated rejection remains constant at

39.4% (Table 4.5). The glycine molecule carries a very small negative charge of -0.001 at pH 6.5 (Table 4.1). The charge appears to have a significant effect on the rejection. Hence, the effect of electrostatic rejection was investigated.

### 4.5.4 Charge rejection model

The amino acid charge rejection model (equation 4.13) takes into account the stoichiometric coefficient ($\upsilon_{ct}$), charge of the counter-ion inside the membrane ($z_{ct}$), amino acid concentration ($C_r$), membrane charge density ($M$), and the amino acid net charge (z).

A zeta potential of 11.4 mV at pH 6.5 (0.01 M KCl, Chapter 6) was used to calculate the membrane surface charge density at the shear plane $\sigma_s$ using equation (4.14) (Schaep and Vandecasteele, 2001):

$$\sigma_s = \frac{\varepsilon\zeta}{\lambda_{Deb}} \tag{4.14}$$

The Debye-length $\lambda_{Deb}$ can be calculated according to:

$$\lambda_{Deb} = \sqrt{\frac{\varepsilon\varepsilon_0 kT}{e^2 I}} \tag{4.15}$$

with the ionic strength:

$$I = \frac{1}{2}\sum_i z_i^2 c_i \tag{4.16}$$

All parameters are shown in the nomenclature list.

The number of charged groups per membrane surface area, expressed in eq/m$^2$, is then calculated by equation (4.17)

$$N = \frac{\sigma_s}{F} \tag{4.17}$$

where $F$ is Faraday's constant.

In this case, for NTR 7450 membrane, the membrane charge density, M, is dependent on pH. At pH 4 and 6.5 the charge density is –9.4 x 10$^{-6}$ eq/m$^2$ and –2.7 x 10$^{-5}$ eq/m$^2$ respectively (Chapter 6)

The net charge of the amino acid is calculated from the pH and the relevant $pK_\alpha$ values (example calculation shown in Appendix A.5). The mean net charges for the amino acid molecules are shown in Table 4.1

Therefore, the only unknown quantity in the charge rejection model (equation 4.13) is the charge of the counter-ion inside the membrane ($z_{ct}$). This coefficient, $z_{ct}$, was used in this work as a fitting parameter, a value of $z_{ct} = 0.001$ gave the "best fit" of the charge model to the experimental model, shown in Figure 4.15. The complete rejection model shown in Figure 4.15 was calculated by combining both the steric and charge rejection coefficients, the method used for this was that suggested by Grib *et al.* (2000) and Li *et al.* (2003), namely:

$$R = R_s + R_c - R_s R_c \tag{4.18}$$

where $R_s$ and $R_c$ represent the rejection coefficients for steric and charge rejection respectively.

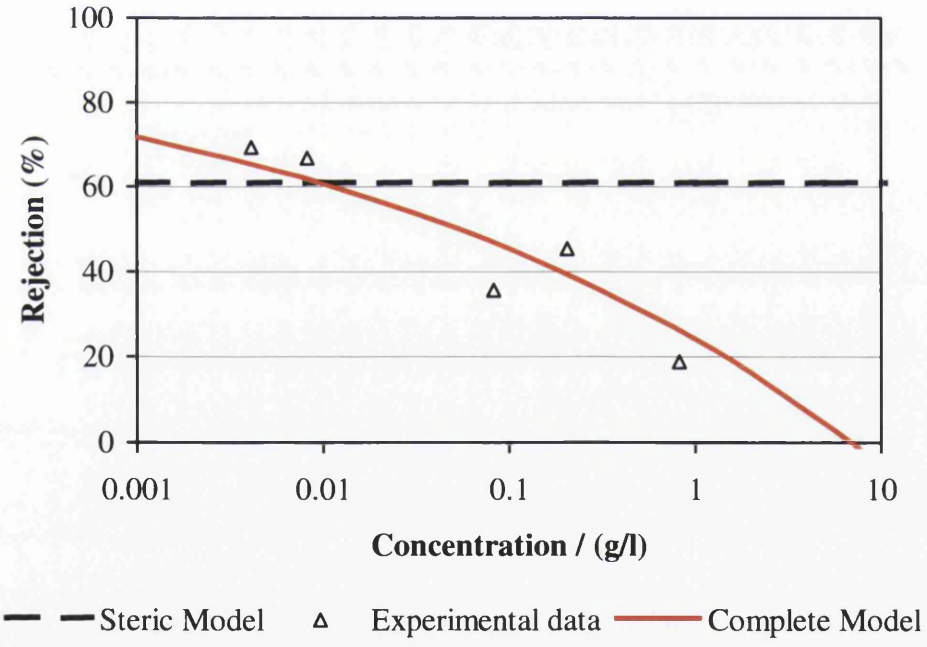


**Figure 4.15 Comparison of complete charge/steric amino acid model to the experimental rejection for phenylalanine at pH 4.0**

Figure 4.15 shows that the complete amino acid model (equation 4.18) is capable of describing the experimental rejection of phenylalanine. The experimental data shows a gradual decrease in rejection from 69.4% to 18.9% for 0.004 g/l and 0.83 g/l respectively. This is a typical phenomenon when electrostatic interactions are

involved in the rejection mechanism. As concentration increases, the membrane's fixed charge becomes increasingly neutralised by the counter-ions in solution, resulting in a lower rejection. The dashed line (Figure 4.15) represents the steric model (equation (4.4)). The steric model remains constant (at 61%) and independent of concentration, which would predict the rejection of a neutral molecule (Timmer *et al.*, 1998). But the phenylalanine molecules have a mean positive charge of 0.007 electrons per molecule at pH 4.0 and therefore, do not behave as a neutral molecule. The complete amino acid charge rejection model was then fitted, using $z_{ct}$ = -0.0001, against the experimental rejection of glycine. The results are shown in Figure 4.16.

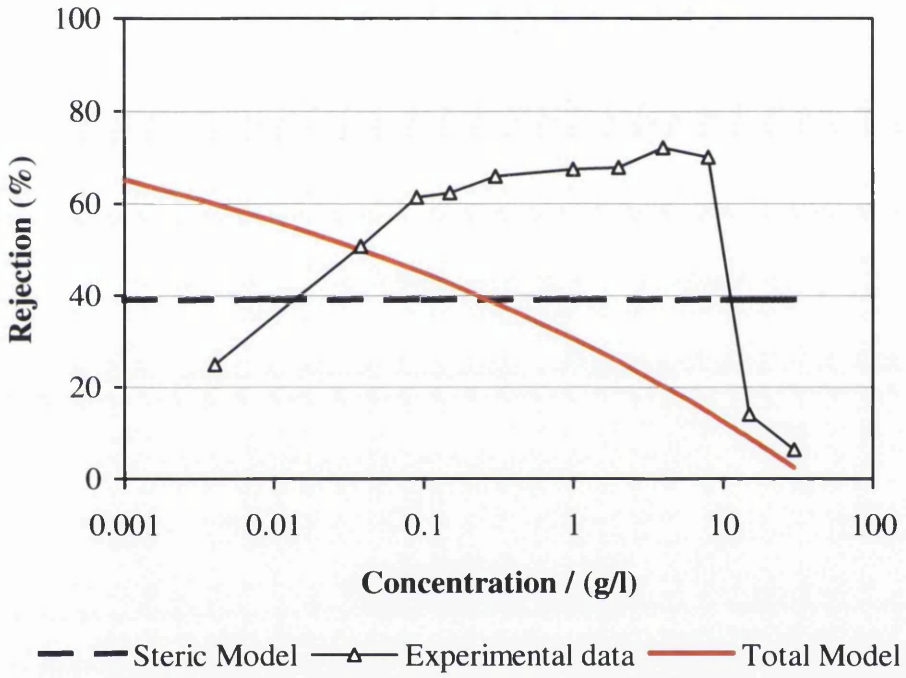


**Figure 4.16 Comparison of complete charge/steric amino acid model to the experimental rejection for glycine at pH 6.5**

The complete rejection model shown in Figure 4.16 was believed to be the best fit because at high concentration of amino acid (>10 g/l), the model best describes the experimental rejection data. At this high concentration, it is believed that classical charge rejection is occurring. However, at low amino acid concentration (<10 g/l), the complete rejection model is inadequate to describe the experimental rejection of glycine at a net charge of –0.001 electrons per molecule. This result suggests that another mechanism is occurring.

# 5 Molecular weight cut-off

In this section, the results of experiments to investigate the effect of concentration on the molecular weight cut-off (*MWCO*) of a NTR 7450 membrane are discussed. The *MWCO* is an important membrane parameter that is used for the selection of membrane for a specific filtration. The *MWCO* is also used as a parameter in various membrane models. The membrane's *MWCO* was investigated by filtration experiments and calculation of the rejection of neutral molecules with a range of molecular weight. The results are compared to a reflection coefficient model. The effect of concentration on *MWCO* has not been investigated in the published work. In this section it is shown that increasing the solute concentration decreased the *MWCO*, indicating that the *MWCO* is not a constant parameter but dependent on concentration. The dipole moment of a molecule was also found to have an effect on the membranes *MWCO*. Filtering molecules with a range of dipole moments through the NTR 7450 nanofiltration membrane and observing their rejection was used to investigate this dipole moment effect. The results showed that molecules with a large dipole moment caused rejection to increase with concentration.

## *5.1 Rejection of uncharged molecules*

Spiegler and Kedem proposed a transport model, based upon the thermodynamics of irreversible processes, which presented a "black-box" description of the solute flux through a membrane. This model was composed of a diffusion term and a convection term, with the convection term controlled by the solvent flux, $J_v$.

In the context of this work the theory had two uses; the first was to provide a means of predicting the rejection of uncharged solutes, and the second was to determine membrane properties. To evaluate coefficients that represented key properties of the membrane such as solute permeability and molecular weight cut-off it was necessary to fit the relevant models to data obtained by experiment.

### 5.1.1 Theoretical background

In general, the transport equation for components through a nanofiltration membrane consisted of two components: a diffusion component and a convection component (Van der Bruggen and Vandecasteele (2002)). This is reflected by the transport equation of Spiegler and Kedem (1966):

$$j_s = -P_s \Delta x \frac{dc_s}{dx} + (1-\sigma) j_v c_s \qquad (5.1)$$

where $P_s$ was the solute permeability, $x$ the distance perpendicular to the surface of the membrane, $\sigma$ was the reflection coefficient and $c_s$ was the solute concentration at the membrane.

On the basis of Hagen-Poiseuille's law solvent flux, $j_v$, was represented by:

$$j_v = \frac{A_k r}{8\eta\tau} \frac{\Delta P}{\Delta x} \qquad (5.2)$$

where $A_k$ represents the porosity, $r$ the pore radius, $\eta$ the viscosity, $\tau$ the tortuosity $\Delta P$ the trans-membrane pressure and $\Delta x$ the membrane thickness.

At non-infinite pressures, equation (5.1) can be solved to calculate rejection as a function of reflection coefficient, $\sigma$, and the solute permeability $P$. The result of this calculation is:

$$R = \frac{(1-F)\sigma}{1-\sigma F} \qquad (5.3)$$

where

$$F = \exp\left(-\frac{1-\sigma}{P_s} J_v\right) \qquad (5.4)$$

The diffusion parameter described a general property of the membrane and allowed prediction of the solute permeability on the basis of solute size, hence equation (5.5).

$$P_s = \frac{\rho}{d_s} \qquad (5.5)$$

where $\rho$ is the specific diffusion parameter. In this work $\rho = 2.07 \times 10^{-15}$ $m^2 s^{-1}$ (Van der Bruggen and Vandecasteele 2002), and $d_s$ is the diameter of the solute.

Historically these two equations, (5.3) and (5.4), were fitted to experimental data to obtain values for the solute permeability, $P_s$, and the reflection coefficient, $\sigma$.

Van der Bruggen *et al.* (2002) conducted an extensive review of the theoretical "black-box" models that utilise the Spegler and Kedem parameters, namely reflection coefficient and solute permeability. The models considered were: the steric hindrance pore model (SHP model); the Zeman and Wales model; the log-normal model and the adapted log-normal model. Van der Bruggen *et al.* (2002) concluded that the reflection coefficient was best represented by the log-normal model. This log-normal model considered the reflection coefficient to be controlled by a logarithmic function of the pore radius and standard deviation, and the size of the solute molecules. The log-normal model can be manipulated to express the size characteristics as both molecular weight (*MW*) (equation (5.6)) and effective molecular diameter (equation (5.7)). The log-normal model as a function of molecular weight (*MW*) and molecular weight cut-off (*MWCO*) was given by:

$$\sigma(MW_s) = \int_0^{MW_s} \frac{1}{s_{MW}\sqrt{2\pi}} \frac{1}{MW} \exp\left[-\frac{(\ln(MW)-\ln(MWCO)+0.56s_{MW})^2}{2s_{MW}^2}\right] dMW \quad (5.6)$$

Log-normal model as a function of effective molecular diameter ($r$) and molecular diameter cut-off ($\bar{r}$) was given by:

$$\sigma(r^*) = \int_0^{r^*} \frac{1}{S_p\sqrt{2\Pi}} \frac{1}{r} \exp\left(-\frac{[\ln(r)-\ln(\bar{r})]^2}{2S_p^2}\right) dr \quad (5.7)$$

where $S_{MW}$ and $S_p$ are the standard deviation for molecular weight and effective diameter respectively. The relationship between molecular weight and effective diameter was stated by Van der Bruggen (2002) to be:

$$d_s = 0.065(MW)^{0.438} \quad (5.8)$$

which was similar to the correlation derived by Schabel *et al.* (1988), equation (4.9).

The pressure dependency of the retention, implicated through inclusion of the solvent flux in the transport model (equation (5.4)), was evaluated through experiment by Van der Bruggen and denoted as a coefficient of water permeability, *K*. Although equation (5.2) indicated that water permeability was a function of the membrane porosity, pore

radius, and tortuosity as well as the membrane thickness and the solution viscosity, this coefficient was determined from an experimental investigation of the variation of pure solvent flux with trans-membrane pressure and was given as flux per unit of applied pressure. In this work, a value of $K = 4.72 \times 10^{-6}$ $m^3m^{-2}s^{-1}bar^{-1}$ was used as calculated by Van der Bruggen and Vandecasteele (2002) for NTR 7450 nanofiltration membrane.

The reflection coefficient represented a maximal condition of the membrane system: the rejection at infinite pressure. However, infinite pressure is an idealised condition and as such is impossible to achieve. Van der Bruggen and Vandecasteele (2002) conducted an experiment in which the effect of pressure on the rejection for maltose was investigated. They found that for system pressures over 10 bar, there was minimal pressure effect on rejection. Therefore, the filtrations in this work conducted at 16.5 bar were suitable for fitting with the reflection coefficient.

### 5.1.2 Application of the theory

The results of the curve fitting procedure are given in Figure 5.1. MathCad was used to provide a numerical solution to the differential equation, equation (5.6) and was used for the execution of a fourth-order Runge-Kutta numerical technique

In the tuning of the model parameters (*MWCO*, $S_{MW}$ and $\rho$) an observation of the influence and therefore importance that each parameter had within the model was made. Van der Bruggen and Vandecasteele (2002) defined molecular weight cut-off as corresponding to the molecular weight of molecules whose rejection was greater than 90%, but Bowen defined this as being 95% (Bowen, 2001b)). The *MWCO* value dictated the location of the curve in relation to the *x*-axis. However, the value of the model *MWCO* parameter only bore a vague resemblance to the observed *MWCO*. The standard deviation of molecular weight retention ($S_{MW}$) determined the slope of the main (central) part of the curve.

*MWCO* charts are often plotted as molecular weight (*MW*) against *R*, where *R* represents reflection coefficient and rejection, (the difference between these two

parameters was dealt with in a separate case later in this section) or effective molecular diameter against *R*. Some examples of *MWCO* charts are:

- *MW* verses *R* and effective diameter verses *R* (Van der Bruggen and Vandecasteele (2002))
- Effective diameter verses *R* (Van der Bruggen *et al.* (2000))
- *MW* verses *R* (Boussu *et al.* (2006) and Mandale (2005))

From analysis of the Van der Bruggen and Vandecasteele (2002) publication and data from this work, it became obvious that effective molecular diameter against *R* is the better case. The *MWCO* model parameter used to fit the experimental data to the curve in Figure 5.1 was 210 Da, where the *MWCO* from analysing the experimental data is about 260 Da. From Figure 5.2 the diameter cut-off model parameter used to produce the curve was 0.85 nm, which agreed with the observations made in this work.

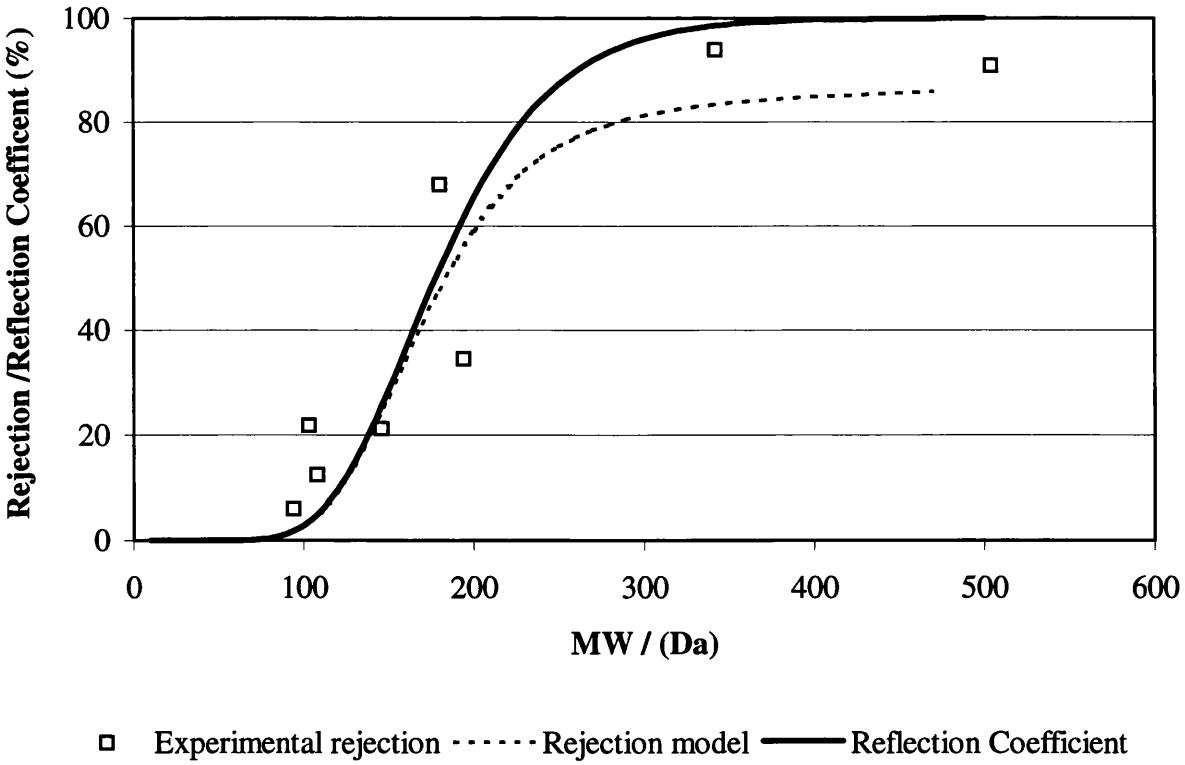


**Figure 5.1 NTR 7450 molecular weight cut-off (3 mmol/l)**

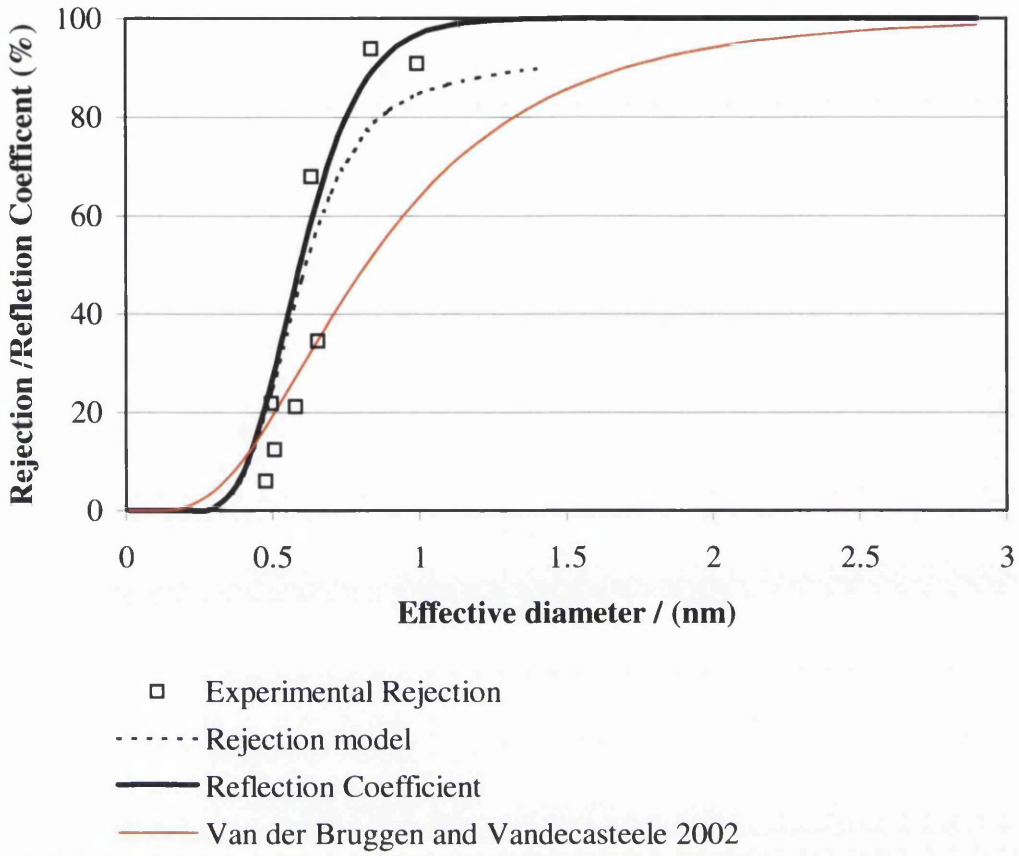


**Figure 5.2 NTR 7450 molecular diameter cut-off (3 mmol/l)**

The better result for the effective diameter verses *R* curve (Figure 5.2) was due to the fact that the correlation for $d_s$ as a function of *MW* (equation (5.8)) has the effect of reducing the data spread, this could be seen in Figures 5.1 & 5.2. Van der Bruggen and Vandecasteele (2002) arrived at the same conclusion and they added that a size parameter is more realistic than a relative value of molecular weight.

In this section, both rejection and reflection coefficient have been plotted on the same axis (Figures 5.1 and 5.2), this has been done to easily compare *MWCO* data from different sources. Boussu *et al.* (2006) and Mandale (2005) have presented their *MWCO* results with respect to rejection, whilst Van der Bruggen and Vandecasteele (2002) and Van der Bruggen *et al.* (2000) have presented their *MWCO* results with respect to reflection coefficient. Strictly speaking nether method is completely correct. This point is highlighted in Figures 5.1 & 5.2. The experimental data is a rejection value, but the reflection coefficient is not a true rejection value. It is a component of

the log-normal model that can be used to calculate the theoretical rejection by using equations (5.3) and (5.4). The difference between the reflection coefficient and the rejection calculated from the refection coefficient is shown in Figures 5.1 & 5.2. In both cases, the reflection coefficient can be manipulated to better fit the experimental data than the calculated rejection. Also, the calculated rejection reaches a limit of validity when the reflection coefficient is equal to 1. When the reflection coefficient is equal to 1, $F$ becomes equal to 1 (equation (5.4)). This reduces $R$ to 0/0 (given in equation (5.3)), which is not mathematically defined.

### 5.1.3 Importance of solute parameters

The importance of the selection of compounds used for *MWCO* determination was considered. The molecule selection process as suggested by Van der Bruggen *et al.* (1999) was to use non-dissociating neutral (uncharged) molecules with low dipole moments. The list of molecules that fit these requirements and have a range of molecular weights was found to be surprisingly few, so some compromise had to be made. The lists of molecules used in this work for *MWCO* determination are shown in Table 5.1.

| Solute | Molecular weight, *MW* (Da) | Dipole moment, $\mu^0$ (Debye) |
|---|---|---|
| Phenol | 94 | 1.45[a] – 1.7[b] |
| Benzonitrile | 103 | 3.99 – 4.08[a] 3.9[b] |
| Benzylalcohol | 108 | 1.59 – 2.48[a] 1.7[b] |
| Lysine | 146 | (NA) |
| Glucose | 180 | 14.1[a] |
| Caffeine | 194 | 3.7[a] |
| Sucrose | 342 | 12.4 – 14.3[a] |
| Raffinose | 504 | (NA) assume 14 |

[a](McClellan, 1974) [b]Van der Bruggen et al. (1999)
(A range of $\mu^0$ values as the permanent dipole varies due to different solvents/conditions)
(Raffinose assumed $\mu^0 = 14$ as same family groups as sucrose and glucose)

**Table 5.1 List of molecules used in MWCO experiments**

Phenol, benzonitrile and benzylalcohol fit the selection criteria very well as they are neutral with very small dipole moments. These three molecules were used by Van der Bruggen *et al.* (1999) with good results. Lysine is an amino acid and can therefore be a zwitterion (having one positive and one negative group). Lysine was not an ideal

molecule for use in this study, but Mandale (2005) used phenylalanine, another amino acid, with good results for *MWCO* experiments. The lysine molecule was filtered at its isoelectric point (pH 9.74) and was previously shown in the amino acid filtration section (Section 4.2.2) that it behaved as a neutral molecule. Mandale (2005) also used caffeine and again recorded useful results. Caffeine was a good molecule for *MWCO* experiments as it had a low $\mu^0$ and is relatively large and therefore present on the sharp slope part of the *MWCO* curve. Both Van der Bruggen et al. (1999) and Mandale (2005) used raffinose. Van der Bruggen did not include raffinose in the statistical analysis as it was stated to be a "charged" molecule, but had obtained good results in other studies (Van der Bruggen *et al.* (2000), Van der Bruggen and Vandecasteele (2002)), and referred to raffinose as a "neutral" molecule in which the rejection was only due to steric effects (Van der Bruggen et al. (1999)). If raffinose was neutral and exhibited good behaviour in *MWCO* experiments, then by the same argument, other saccharides, e.g. sucrose and glucose, could be used. Both sucrose and glucose have been shown to give good results in *MWCO* experiments by Mandale (2005).

Although the *MWCO* experiments conducted by Van der Bruggen *et al.* (1999) were very extensive (25 different molecules were used), they did not take into account the effect of concentration. Table 5.2 shows the four molecules used in this study that were also used by Van der Bruggen *et al.* (1999), the concentrations used and the measured rejection.

| Molecule | Van der Bruggen *et al.* (1999) data | | | Data from this study | |
|---|---|---|---|---|---|
| | Concentration | mmol/l | Rejection (%) | mmol/l | Rejection (%) |
| Phenol | 200 mg/l | 2.1 | 0.0 | 3.0 | 6.0 |
| Benzonitrile | 0.01 vol% | 1.0 | 4.9 | 3.0 | 21.8 |
| Benzylalcohol | 0.013 vol% | 1.2 | 29.3 | 3.0 | 12.5 |
| Raffinose | 250 mg/l | 0.5 | 66.7 | 3.0 | 90.8 |

**Table 5.2 Concentrations used by Van der Bruggen *et al.* (1999)**

Table 5.2 shows that Van der Bruggen used a range of concentrations (2.1 to 0.5 mmol/l) for the various compounds used for *MWCO* experiments. In this work the concentration was kept constant (3.0 mmol/l) for comparison between molecules, as

the molecules used have a wide range of molecular weights. Also keeping the molar concentration constant allowed a comparison of molecular interactions.

The results presented in Figure 5.2 show that the *MWCO* curve presented by Van der Bruggen and Vandecasteele (2002) exhibits a more diffuse cut-off than the predicted curve fit for the experimental data. This could be due to the fact at Van der Bruggen and Vandecasteele (2002) generally used lower concentrations. The effect of concentration was investigated further.

## 5.2 Concentration Effect

As stated in Section 5.1.3, the molar concentration was held constant for a set of *MWCO* experiments, but this concentration was then varied to produce a surprising range of curves for *MWCO* (Figures 5.3 to 5.6).

Due to the reduced distribution range of results of molecular diameter graphs (due to the bunching effect of the diameter correlation) the results are shown as a function of molecular weight.

Figure 5.1 has already described the *MWCO* for a NTR 7450 membrane at a concentration of 3 mmol/l. The concentration was increased to 20 mmol/l and the results for a new set of *MWCO* experiments are presented in Figure 5.3.

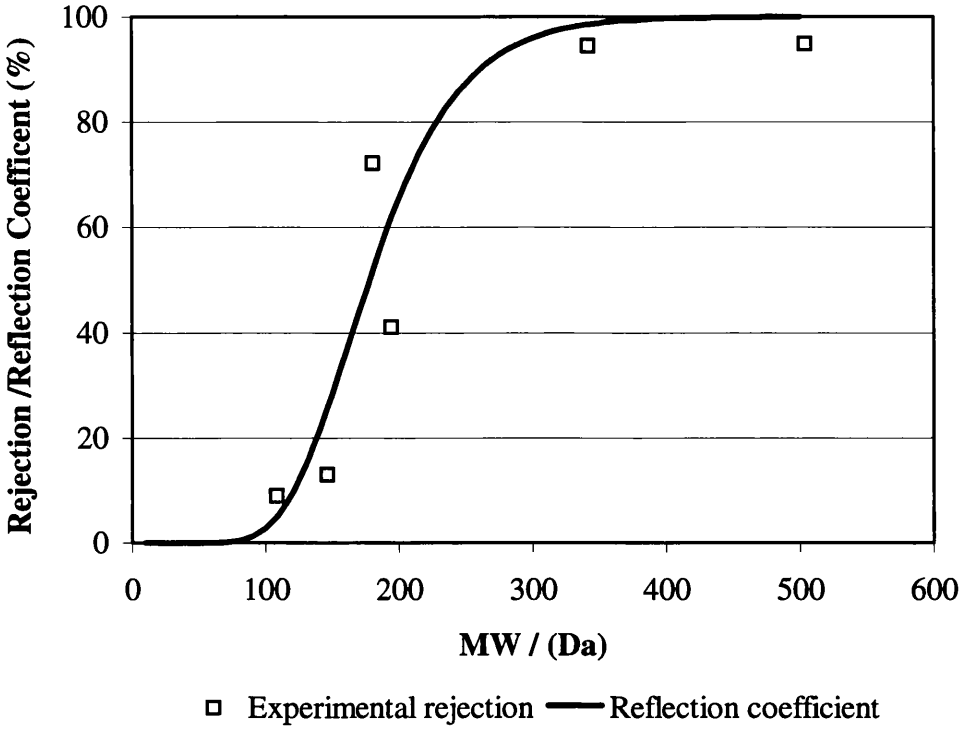


**Figure 5.3 NTR 7450 molecular weight cut-off (20 mmol/l)**

The experimental results presented in Figure 5.3 show that the *MWCO* for 20 mmol/l was similar to that observed for the experiments conducted at a concentration of 3 mmol/l; the same model coefficients were used in both cases to fit the reflection coefficient model to the experimental data (*MWCO* = 210 Da, $S_p$ = 0.3, Table 5.3). This result implied that a minimum *MWCO* limit had been reached and that raising the concentration above 3 mmol/l had little or no effect on the *MWCO* of the membrane.

The effect of lowering the concentration was investigated and the results are presented in Figures 5.4 to 5.6.

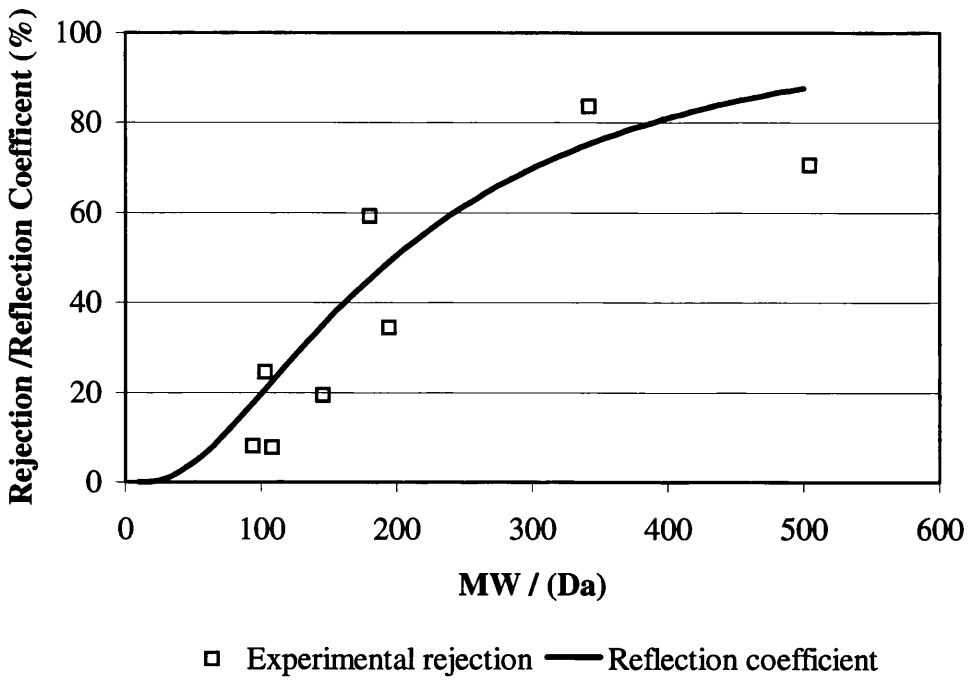


**Figure 5.4 NTR 7450 molecular weight cut-off (1 mmol/l)**

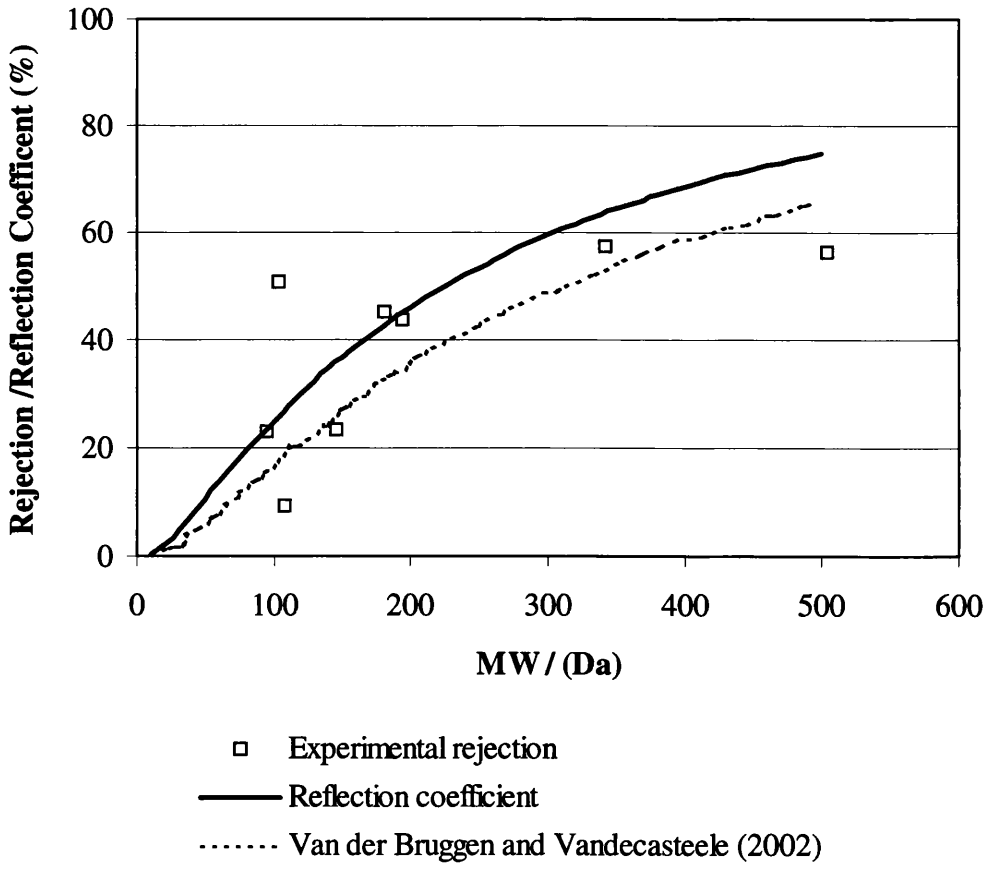


**Figure 5.5 NTR 7450 molecular weight cut-off (0.1 mmol/l)**

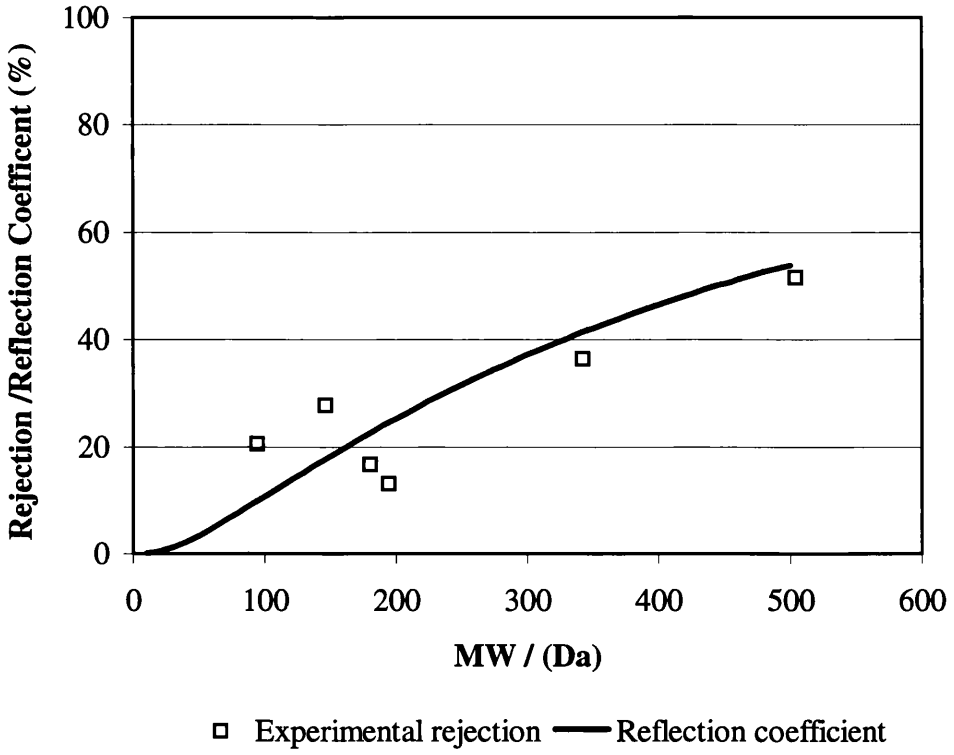


**Figure 5.6 NTR 7450 molecular weight cut-off (0.02 mmol/l)**

Figures 5.4, 5.5 & 5.6 show the *MWCO* for concentration 1.0 mmol/l, 0.1 mmol/l and 0.02 mmol/l respectively. The fitted values for each curve are stated in Table 5.3.

| Concentration (mmol/l) | *MWCO* (Da) | Standard deviation ($S_p$) |
|---|---|---|
| 20 | 210 | 0.3 |
| 3 | 210 | 0.3 |
| 1 | 310 | 0.8 |
| 0.1 | 440 | 1.2 |
| 0.02 | 870 | 1.2 |

**Table 5.3 Summary of coefficients used to fit MWCO curves for five different concentrations**

The results presented in Figures 5.1, 5.3, 5.4, 5.5 & 5.6 and Table 5.3 show that as the concentration is reduced from 3 mmol/l to 0.02 mmol/l, the *MWCO* increases from 210 to 870 Da. This result implied that the *effective* pore size changed as a function of concentration and reduced with increased concentration. Figures 5.1, 5.3, 5.4, 5.5 & 5.6 also show that the *MWCO* becomes more diffuse as the sharpness of the cut-off reduces with decreasing concentration. The more diffuse cut-off for 0.1 mmol/l is similar to that observed by Van der Bruggen and Vandecasteele (2002) for NTR 7450

nanofiltration membrane (Figure 5.5), as this concentration range was similar to that used by these workers. Also this larger diffuse *MWCO* is similar to the published estimated *MWCO* of 600-800 Da. Figures 5.1, 5.3, 5.4, 5.5 & 5.6 also show that experimental rejection for the solutes varied with concentration. All of the solutes studied observed some change in rejection with changing concentration, however the most pronounce change occurred for the molecules with higher dipole moments. The rejection for raffinose ($\mu^0$ ~ 14 Debye) at 3 mmol/l (Figure 5.1) was 90.8%, which reduced to 56.2% at 0.1 mmol/l (Figure 5.4). On the other hand, the rejection of benzylalcohol exhibited a small change; *R* was 12.5% for 3 mmol/l and 9.4% at 0.1 mmol/l (Figures 5.1 & 5.5). Therefore, the concentration influenced the dipole moment interaction, which in turn affected the solute rejection.

## 5.3 Effect of dipole moment

It has been stated that molecules with relatively high dipole moments should be excluded from *MWCO* experiments (Van der Bruggen *et al.* (1999)). The reasons for this statement will now be considered.

An investigation into the effect of dipole moment on rejection was conducted for the species shown in Table 5.4. The results for solutes with low dipole moments are shown in Figure 5.7 to 5.10. The rejection results for filtrations of lysine solutions are also presented in Figure 5.11. The concentration range of the species investigated was kept as wide as possible, with the exceptions of phenol and benzonitrile. The maximum phenol concentration used was 0.28 g/l (Figure 5.8), this was due to the fact that phenol is toxic and therefore handling issues became the determining factor. Benzonitrile was found to dissolve the active layer of the NTR 7450 NF membrane at concentrations of approximately 1-3 g/l. Therefore, the maximum benzonitrile concentration used was 0.4 g/l (Figure 5.10)

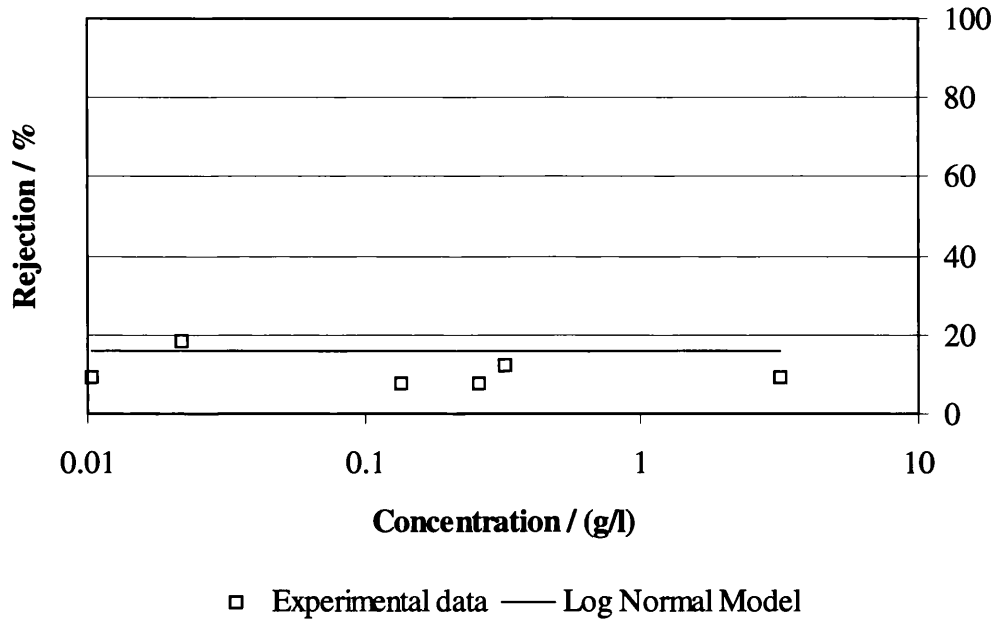


**Figure 5.7 Experimental rejection of benzylalcohol ($\mu^0$ = 1.7 Debye) for NTR 7450 NF membrane**

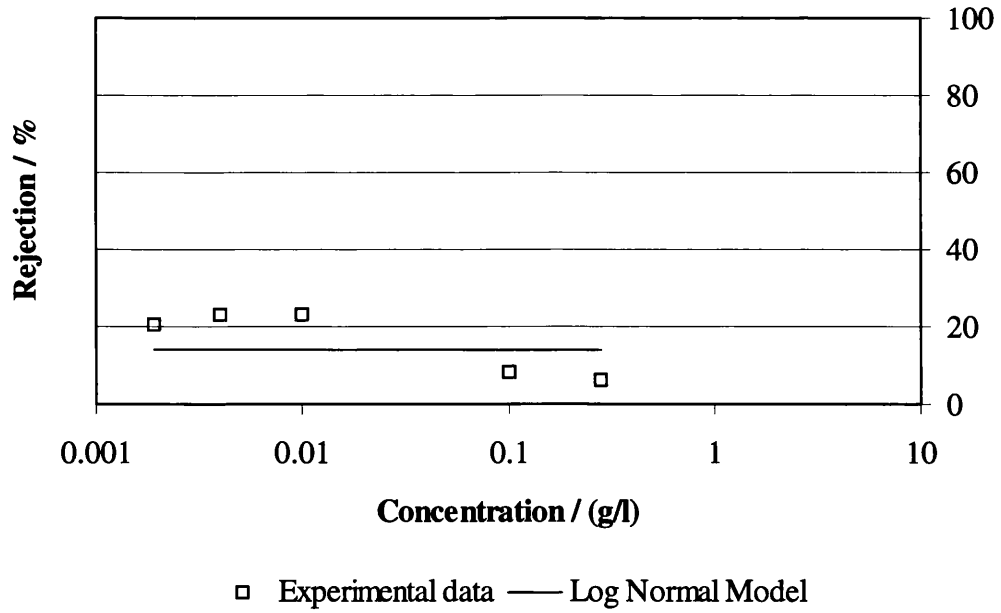


**Figure 5.8 Experimental rejection of phenol ($\mu^0$ = 1.7 Debye) for NTR 7450 NF membrane**

Figures 5.7 to 5.10 show that the Log-Normal Model, suggested by Van der Bruggen *et al.* (2000), can be used to describe the rejection of neutral organic species with low dipole moment (<4 Debye). The reflection coefficient (equation (5.6)) and the subsequent calculated rejection (equation (5.3)) are independent of concentration. This fact is highlighted in Figures 5.7 to 5.10 as the rejection calculated by the Log-Normal Model is linear with no dependence on concentration.

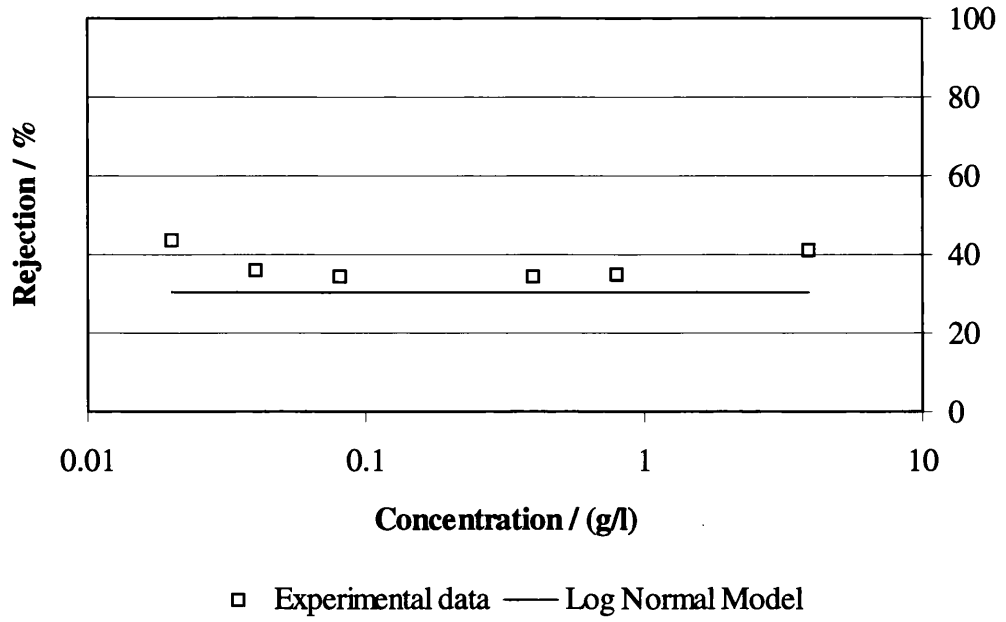


**Figure 5.9 Experimental rejection of caffeine ($\mu^0$ = 3.7 Debye) for NTR 7450 NF membrane**

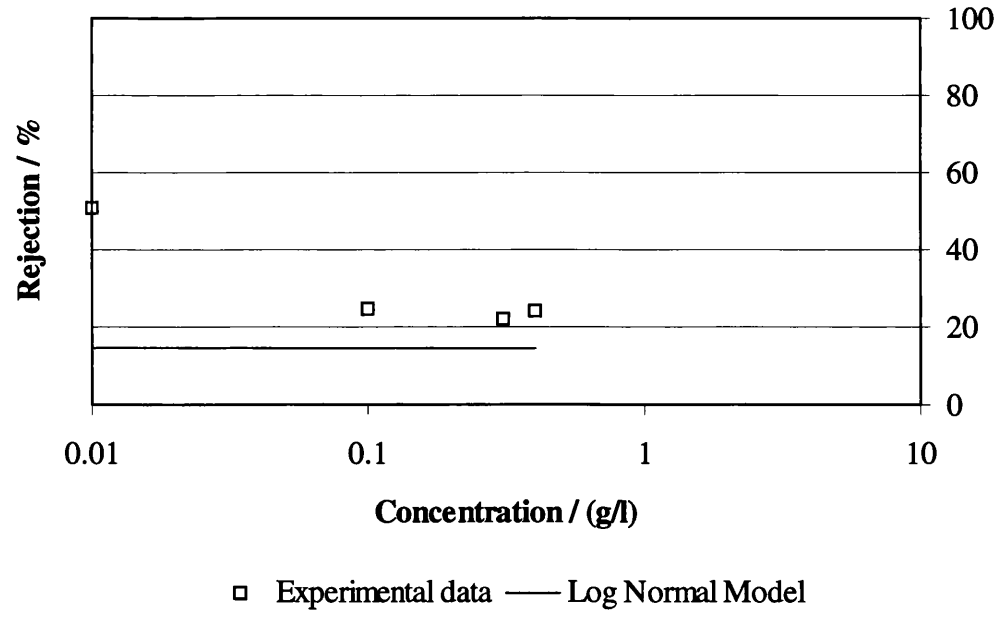


**Figure 5.10 Experimental rejection of benzonitrile ($\mu^0$ = 3.9 Debye) for NTR 7450 NF membrane**

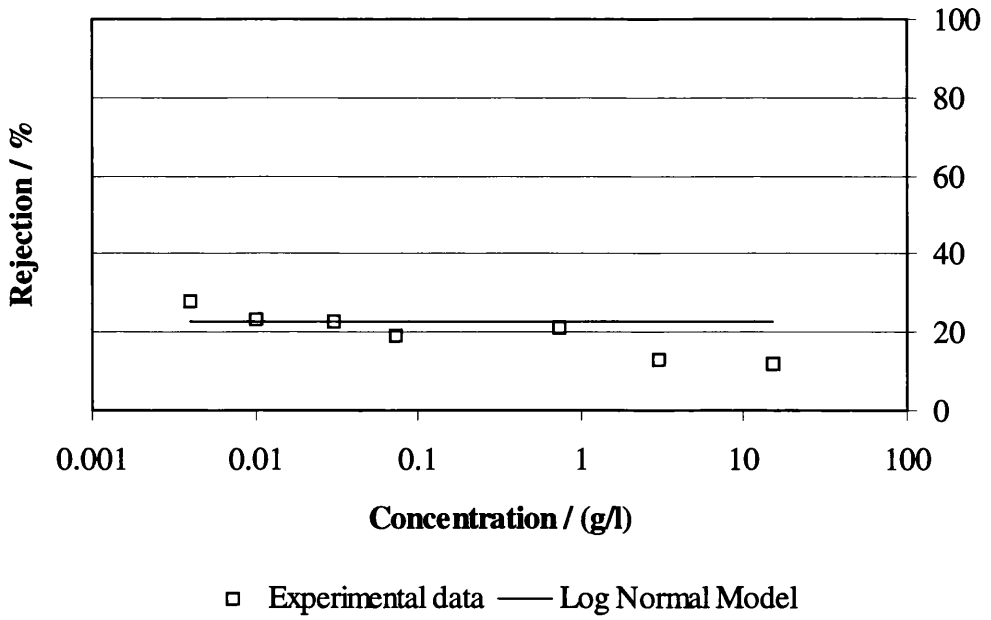


**Figure 5.11 Experimental rejection of lysine for NTR 7450 NF membrane**

Generally, it was observed that the experimental rejection slightly decreased for low dipole moment species. Benzonitrile (Figure 5.10) reduced from a rejection of 50.7% to 24.2% for a concentration of 0.01 g/l and 0.4 g/l respectively. Caffeine (Figure 5.9) exhibits a reduction in rejection from 45.4% at 0.01 g/l to 34.9% at 0.8 g/l. The rejection for phenol reduced from 23% to 6% for a concentration change from 0.004 g/l to 0.28 g/l (Figure 5.8). However, benzylalcohol doesn't show any clear change in rejection with increasing concentration, as the rejection remains approximately constant at around 9% for a concentration range 0.01 – 3.2 g/l (Figure 5.7).

The reasonably good fits between the Log-Normal Model and the experimental data on Figures 5.7 to 5.10, indicate that the rejection of species with low dipole moments is predominantly due to steric effects. The reflection coefficient used in the Log-Normal Model was based upon size exclusion and it is assumed that the molecules pass through every pore that is large enough.

The Log-Normal Model parameters, namely molecular diameter cut-off and $S_p$ used in Figures 5.7 to 5.10 were based upon the findings of Van der Bruggen and Vandecasteele (2002). The values of molecular diameter cut-off and $S_p$ were 1.62 nm and 0.52 respectively. These were used as Van der Bruggen used 13 different species, all with dipole moment below 3 Debye. As found in the previous section, molecules

with low dipole moments did not exhibit major change in *MWCO* with respect to concentration. Therefore, Van der Bruggen's model showed a better fit to the experimental data presented in Figures 5.7 to 5.10 than the Log-Normal Model using parameters derived in the previous section. However, the Log-Normal Model overestimates the rejection of benzylalcohol ($\mu^0$ = 1.45 Debye, Figure 5.7), and the initial part of the phenol results ($\mu^0$ = 1.7 Debye, Figure 5.8). The Log-Normal Model also underestimates the rejection of benzonitrile (Figure 5.10) and caffeine (Figure 5.9), their dipole moments are 3.9 and 3.7 Debye respectively. Benzonitrile (*MW* 103 Da) and benzylalcohol (*MW* 108 Da) have very similar molecular weights. However, for every concentration, the rejection of benzonitrile is substantially larger that that exhibited by benzylalcohol. This indicates that dipole moment is a parameter that influences the rejection in NF. Van der Bruggen *et al.* (1999) suggested a plausible explanation for the effect of the dipole moment is that by electrostatic attraction, the dipole is directed towards the membrane charge in such a way that the side of the dipole with the opposite charge is closer to the membrane. Hence, the molecule is directed toward the pore and enters more easily into the membrane structure. However, the results presented here suggest that another mechanism is also occurring.

The experimental rejection results for lysine at its isoelectric point (pH 9.74) are presented in Figure 5.11. These results were included to examine the quality of agreement for the reflection coefficient to the experimental data for an amino acid with a zero net charge. The lysine rejection results presented in Figure 5.11 show that the reflection coefficient was able to describe the experimental data; the experimental rejection data was observed to be between 10 & 30%, the reflection coefficient was calculated to be constant at 23%. The reflection coefficient exhibited better agreement for the experimental data that the amino acid model presented in Section 4.5.3. The amino acid model (which is similar to the Zeman and Wales Model) had to be manipulated by adjusting the *MWCO* parameter to fit the experimental rejection data. The reflection coefficient presented in Figure 5.11 was fitted using the model parameters that describe the membrane. Therefore, the reflection coefficient was able to describe the rejection of a net neutral amino acid, and was shown to give a better fit that the amino acid model.

The effect of higher dipole moments is presented in Figures 5.12 to 5.14. These graphs show that the Log-Normal Model was not capable of describing the rejection of pure filtrations of glucose, sucrose and raffinose.

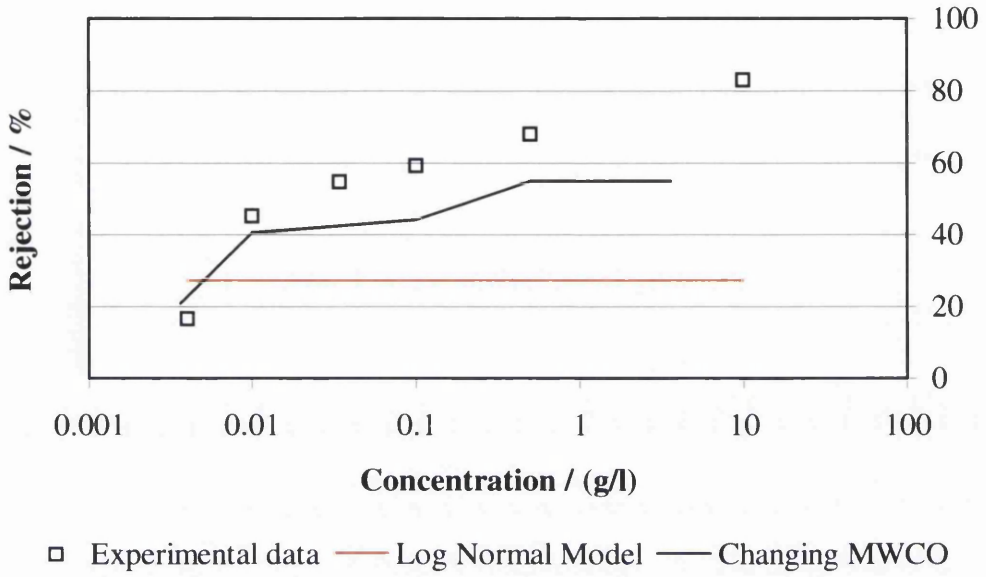


**Figure 5.12 Experimental rejection values for glucose ($\mu^0$ = 14.1 Debye) with NTR 7450 NF membrane**

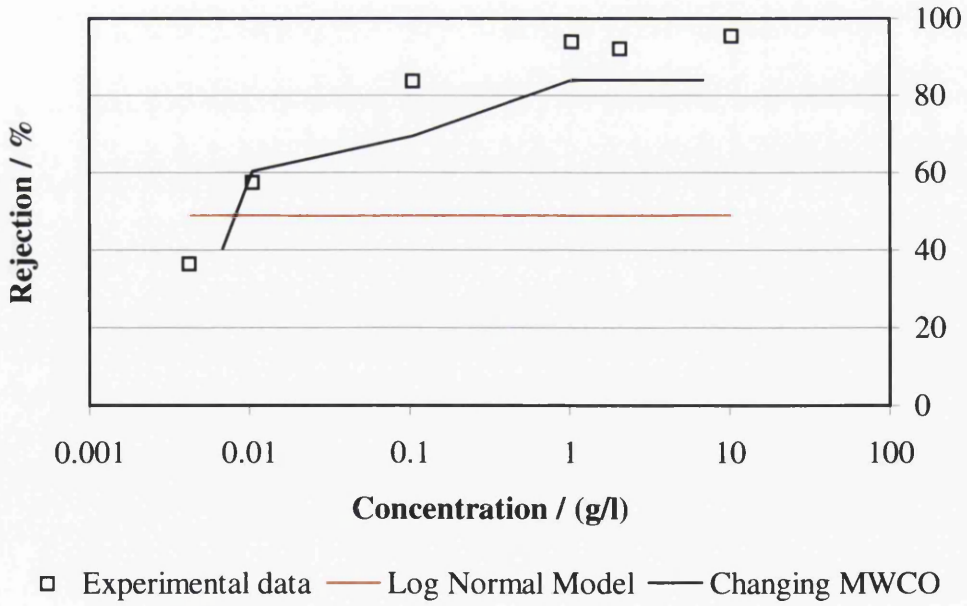


**Figure 5.13 Experimental rejection values for sucrose ($\mu^0$ = 14 Debye) with NTR 7450 NF membrane**

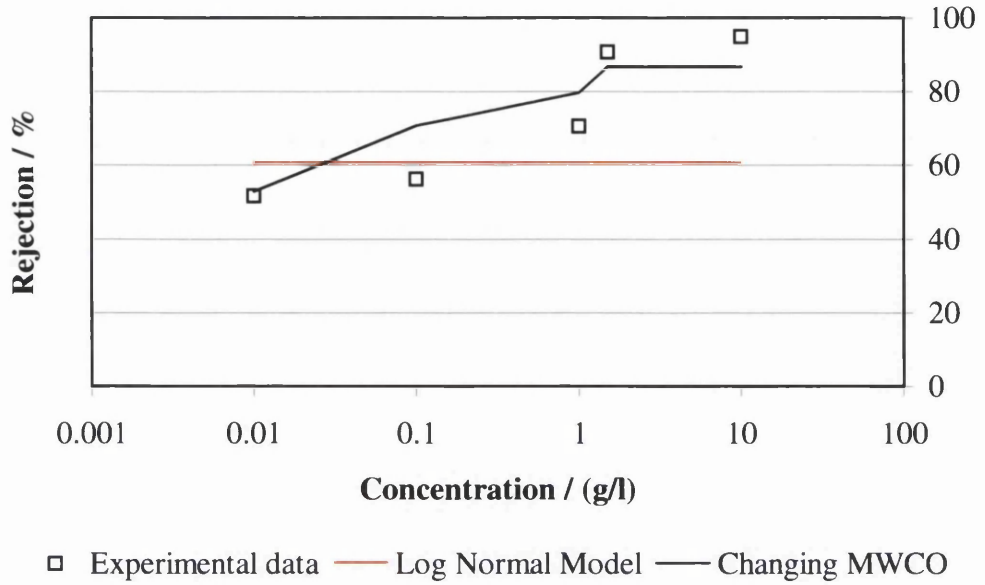


**Figure 5.14 Experimental values of raffinose rejection for NTR 7450 NF membrane**

The Log-Normal Model predicts rejections in which the mechanism is solely steric, and therefore independent of concentration. However, glucose, sucrose and raffinose all exhibit rejection increasing with concentration (Figure 5.12 to 5.14). The steric effects can be seen to have a role in the rejection mechanism, as the rejection of sucrose ($MW$ = 342 Da, Figure 5.13) is always higher than glucose ($MW$ = 180 Da, Figure 5.12) for all concentrations. The rejection of glucose (Figure 5.12) at 0.004 g/l is 16.7%, the rejection of sucrose (Figure 5.13) at the same concentration is 36.4%. These rejections increase to 83% and 95.4% at 10 g/l for glucose and sucrose respectively. A similar result was observed for raffinose (Figure 5.14).

A suggested explanation for the increase in rejection as a function of concentration was the increase in osmotic pressure and subsequent decrease in trans membrane flux at elevated concentrations. For a sucrose concentration of 0.004 g/l, the osmotic pressure was 0.03 kPa (calculated by Van't Hoff method). The resulting flux was $1.36 \times 10^{-5}$ $m^3m^{-2}s^{-1}$ when the system pressure was 16.5 bar. The flux reduced to $9.11 \times 10^{-6}$ $m^3m^{-2}s^{-1}$ for a concentration of 10 g/l, due to an osmotic pressure of 160 kPa (from experimental measurement) at this concentration. Bowen *et al.* (2004) conducted a series of experiments to investigate the effect on rejection with respect to the effective pressure driving force, $\Delta P_e$, given by:

$$\Delta P_e = P - \pi \tag{5.9}$$

where $P$ is the system pressure and $\pi$ is the osmotic pressure. The results of Bowen *et al.* (2004) are presented in Figure 5.15.

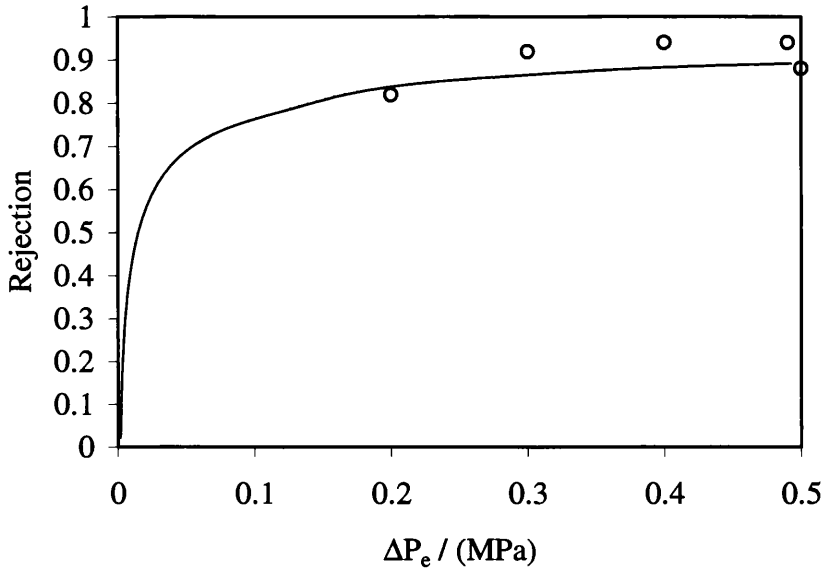


**Figure 5.15 Best-fit data for experimental values of glucose for Nanomax$^{TM}$ –50 membrane (Bowen *et al.* (2004))**

The data within Figure 5.15 showed that as the effective pressure driving force was reduced the rejection decreased. In this case, as the concentration and osmotic pressure increased, the current theory predicts that the rejection should decrease with concentration. However, rejection has been shown to increase with concentration, indicating that another mechanism is occurring.

In Section 5.2 that discussed the effect on *MWCO* with respect to concentration, it was shown that the *MWCO* decreased with increasing concentration. Figure 5.12 to 5.14 are plotted with a modified Log-Normal Model to incorporate a "changing *MWCO*", where the changing *MWCO* are those found in the previous section for 20, 3, 1, 0.1 and 0.02 mmol/l. These parameters were then substituted into the Log-Normal Model at the relevant concentrations to adjust the reflection coefficient accordingly. Figure 5.12 to 5.14 show a poor fit for the modified Log-Normal Model to the experimental data, as only 5 points were available (20, 3, 1, 0.1 and 0.02

mmol/l). However, this approach was useful as a descriptive method and shows that the e*ffective* pores size is reduced with increasing concentration.

The cause of this change in effective pore size was then investigated; the results are presented Chapter 6.

# 6 Solute adsorption

The charge of the NTR 7450 membrane was analysed by titration and streaming potential experiments. The results of the titration experiments showed that acidic groups were present on the surface of the membrane. The streaming potential experiment results showed that the NTR 7450 membrane retained a negative charge for a wide pH range. The effect of this strong negative charge was then investigated by direct and indirect adsorption measurements. The results of the direct technique indicated adsorption occurred at the membrane surface. The indirect observation of adsorption was conducted by measurements of flux decline and rejection as a function of concentration. The results of flux decline and rejection with respect to concentration were shown to give a good fit when modelled with an adsorption isotherm. This in turn highlighted the dominant rejection resistances for various solute systems.

## *6.1 Titration results*

The titration results for the NTR 7450 membrane materials are presented in Figures 6.1, 6.2, 6.3 and 6.4. There are two graphs presented for each case. Presented first (Figure 6.1) are the titration curves for pH against μmoles of acid, and the second (Figure 6.2) presents the first derivative of that curve. The number of peaks in the derivative data gave an indication of the number of different kinds of ionisable groups present. The derivative curves were obtained through use of the numerical method of Savitzky and Golay (1964), which gave the first derivative calculated over eleven points, assuming a second order polynomial.

The blank and sample titrations (Figure 6.1) were carried out in a 0.001 M sodium chloride solution because the use of the indifferent electrolyte gave improved stability of the pH reading (Moss, 2001).

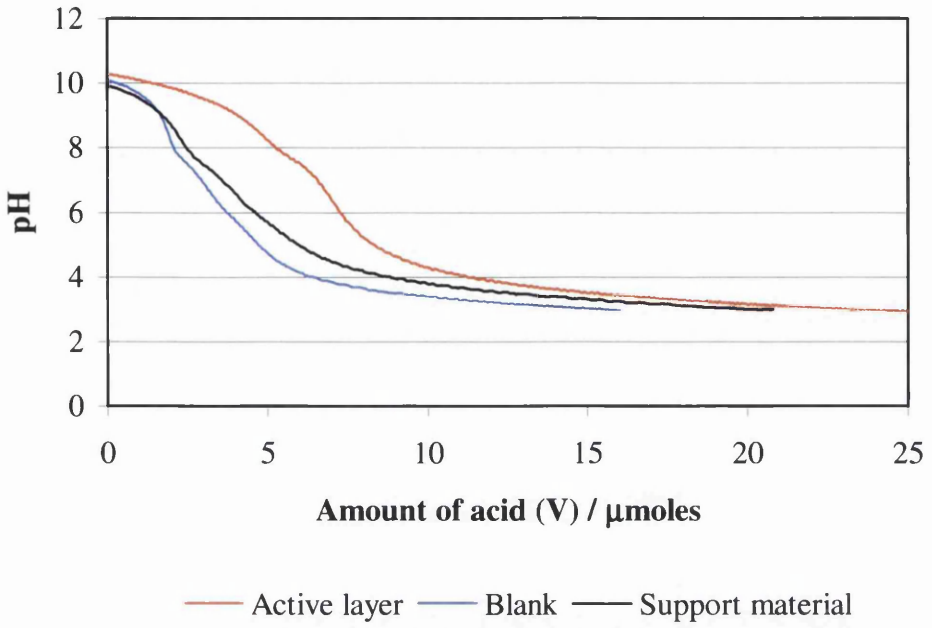


**Figure 6.1 Acid titration of NTR 7450 membrane materials**

The experimental results presented in Figure 6.1 showed that more moles of acid (HCl) were required to lower the pH of the active layer from pH 10 to pH 3, than that required to do the same for the blank 0.001 M NaCl solution. The results presented in Figure 6.1 also show that the membrane support material also required less volume of acid to lower the pH from pH 10 to pH 3. This result showed that there was significantly less surface activity on the neutral polysulfone support layer than the sulfonated polyethersulfone active layer. To further investigate the surface chemistry of the thin film permselective skin "active" layer, the data was re-plotted as shown in Figure 6.2. Figure 6.2 presented the 1$^{st}$ differential calculation for the active layer titration data plotted in the same fashion as that used by Bowen and Hughes (1991) (*x*-axis; pH, *y*-axis; d(V)/d(pH)). Traditionally these types of graphs are plotted the other way around, but the format used by Bowen and Hughes allows for clear identification of inflection points. Bowen and Hughes preformed acid titrations of capillary pore inorganic microfiltration membranes. They found that sharp inflection points on titration and differential titration curves correlated with the surface chemistry of a membrane.

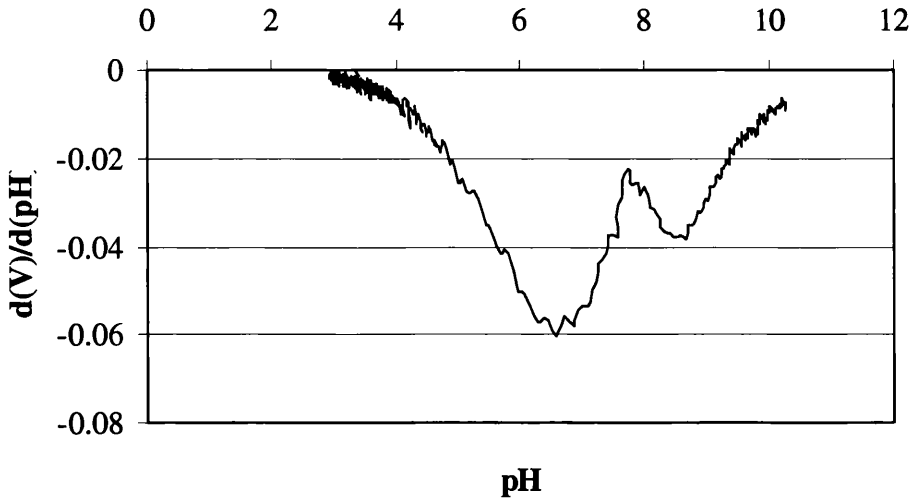


**Figure 6.2 Differentiation of acid titration data for the active layer of a NTR 7450 membrane**

The experimental results presented in Figure 6.2 showed sharp inflection points in the regions of pH 6.5 -7 and pH 8.5. The NTR 7450 nanofiltration membrane active layer was manufactured from sulfonated polyethyersulfone. Schaep and Vandercasteele (2001) stated that sulfonic acid groups ($-SO_3^-$), which were present on the NTR 7450 membrane, were strongly acidic and are completely dissociated over a wide pH range. Sulfonic acid is a hypothetical tautomer of sulphurous acid, but less stable, and would likely convert to that very quickly if it were formed. Sulfurous acid has two ionisable protons with $pK_1 = 1.85$ and $pK_2 = 7.2$ (Lide, 2000). On that basis, it was possible to provide identification for the NTR 7450 membrane, suggesting that the inflection point at approximately pH 7 (Figure 6.2) was primarily due to sulfonic acid groups dissociated from the membrane matrix. The inflection point at pH 8.5 was not explained by this method, but careful examination of the results presented in Figure 6.1 revealed that the inflection point was present for all three titrated materials (active layer, support material and blank electrolyte solution). Therefore, the inflection point observed at pH 8.5 was considered to be an artefact of the system, possibly due to the titration of the glass walls of the reaction vessel. To allow for this, and other system effects, the curve plotted in Figure 6.3 was corrected by subtraction of the acid required for the titration of the blank electrolyte solution.

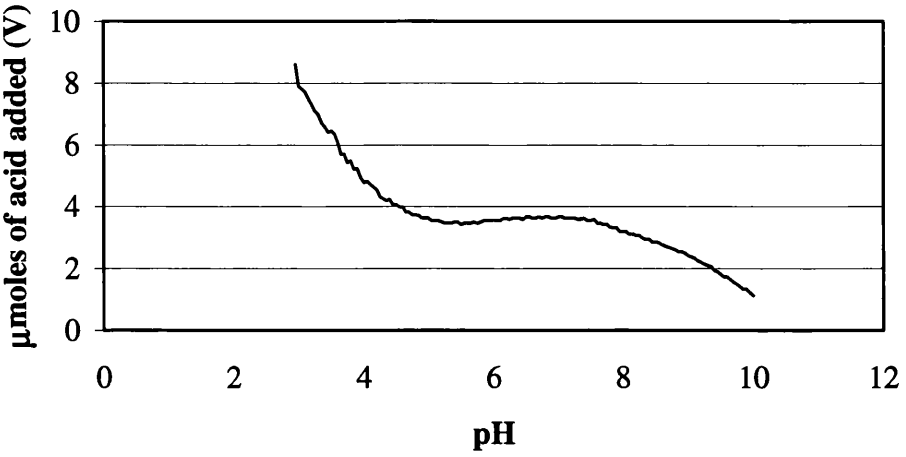


**Figure 6.3 Acid titration of NTR 7450 active layer corrected for electrolyte solution**

The curve shown in Figure 6.3 was then differentiated using the numerical method of Savitzky and Golay (1964), to give the resulting curve shown in Figure 6.4. The gradient of the curve in Figure 6.3 pass through an inflection point and becomes positive at approximately pH 6.5. This result was due to accumulation of error in the subtraction calculation.

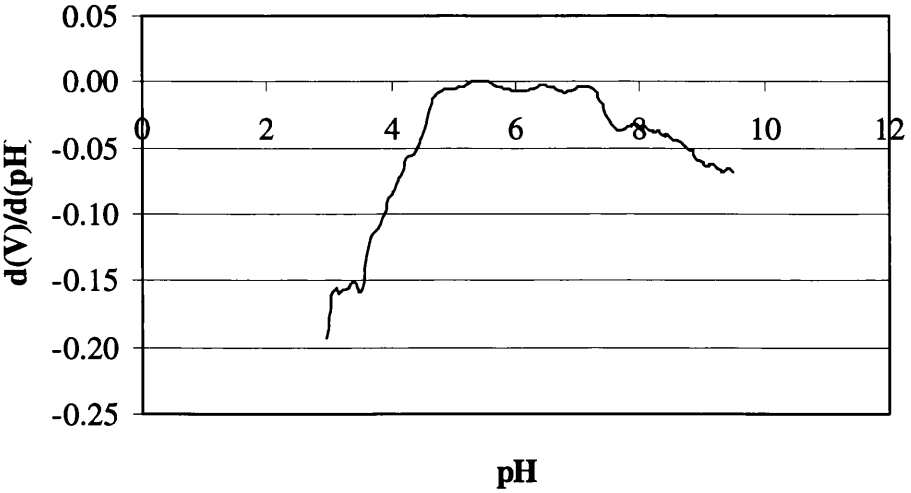


**Figure 6.4 Differentiation of acid titration data for the active layer of a NTR 7450 membrane corrected for electrolyte solution**

The calculated data plotted in Figure 6.4 has lost all of the sharp inflection points exhibited in Figure 6.2. Subsequently, Figure 6.4 cannot be used to make predictions of the density of charged groups present on the membrane surface. Bowen and Hughes (1991), who had been very successful in using this technique, were

themselves surprised at the striking inflection points observed for capillary pore inorganic microfiltration membranes. Sharp inflection points are unusual for solid surfaces. Schaep and Vandercasteele (2001) remarked that for their initial acid-base titrations, the limitation was situated at determining the equivalence point, resulting in a less sensitive method compared to the adsorption-desorption method. The charge of the membrane was further investigated by streaming potential measurements.

## 6.2 Membrane charge

When a membrane is brought into contact with an aqueous electrolyte solution, the membrane acquires an electric charge through several possible mechanisms. These mechanisms may include dissociation of functional groups, adsorption of ions from solution, and adsorption of polyelectrolytes, ionic surfactants and charged macromolecules. These charging mechanisms occur on the exterior as well as the interior pore surface. These charges influence the distribution of ions in solution, which leads to the formation of an electrical double layer.

The relationship between the measurable streaming potential and the zeta potential is given by the Helmholts-Smoluchowski equation (equation (2.44)). However, this equation is only valid when the Debye length of the solution is much smaller than the pore radius. Therefore this equation is used for the calculation of the external membrane charge and it cannot be used for the determination of the zeta potential within the membrane pores.

Membrane charge can be measured and plotted as a function of both pH or electrolyte concentration. The result is a charge variation profile that provides an impression of the properties of the membrane. Figure 6.5 shows the zeta potential variation, according to pH, for a NTR 7450 membrane at different concentrations of electrolyte solution.

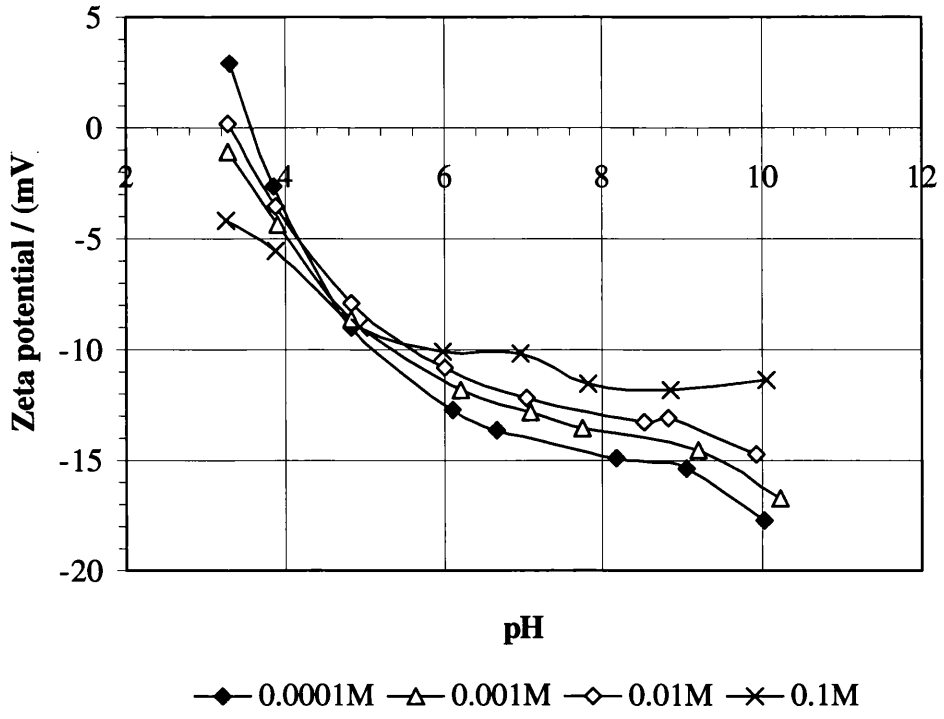


**Figure 6.5 NTR 7450 membrane surface charge variation with pH and electrolyte concentration**

Figure 6.5 shows that as the concentration of electrolyte is increased, the overall change in zeta potential is decreased. For a 0.1 M KCl solution, the zeta potential reduces from -4.3 mV at pH 3.2 to -11.4 mV at pH 10.1. Where as, for a 0.0001 M KCl solution, the zeta potential reduces from -2.9 mV at pH 3.3 to -17.7 mV at pH 10.1. Figure 6.5 showed the NTR 7450 membrane retained a negative charge for almost all of the pH range investigated. This result was in agreement with expectations knowing the kind of material the membrane was composed of. Sulfonic acid groups ($-SO_2^-$) which are present on the NTR 7450 membrane are strongly acidic and are completely dissociated over the entire pH range investigated. Scheap and Vandecasteele (2001) found that other membranes composed of carboxylic groups ($-COO^-$), which may be present in polyamide and cellulose acetate membranes, are weakly acidic and will not be dissociated at a low pH. Therefore, these types of membranes usually exhibit a positive zeta potential for some of the pH range.

The point at which the plot of zeta potential versus pH passes through zero is known as the isoelectric point. The pH at isoelectric point was 3.6 for 0.0001 M KCl and pH 3.3 for 0.01 M KCl solutions (Figure 6.5). A much lower pH (pH < 2) would have been required to reach the isoelectric point of 0.1 M KCl solution. Inorganic ions

interact with charged surfaces in one of two distinct ways, (i) non-specific adsorption, where the inorganic ions have no effect on the isoelectric point, or (ii) specific ion adsorption, that leads to a change in the value of the isoelectric point, such as in this case. The specific adsorption of ions onto a particle surface, even at low concentrations, could have an effect on the zeta potential. In some cases, specific ion adsorption can lead to charge reversal of the surface[1].

The value of the zeta potentials at pH 7 were used to calculate the membrane surface charge density at the shear plane, $\sigma_s$, using equation 6.1.

$$\sigma_s = \frac{\varepsilon_0 \varepsilon \xi}{\lambda_{Deb}} \tag{6.1}$$

The Debye length $\lambda_{Deb}$ was calculated according to:

$$\lambda_{Deb} = \sqrt{\frac{\varepsilon_0 \varepsilon RT}{2F^2 I}} \tag{6.2}$$

where the ionic strength, I, was given by:

$$I = \frac{1}{2}\sum_i z_1^2 c_i \tag{6.3}$$

The number of charged groups per membrane surface area was then calculated by:

$$N = \frac{\sigma_s}{F} \tag{6.4}$$

All of the symbols are in the nomenclature list. The results are given in Table 6.1.

| Concentration of electrolyte (M) | Zeta Potential, $\zeta$ (mV) | Debye length, $\lambda_{Deb}$ (m) | Surface charge density at shear plane, $\sigma_s$ (C m$^{-2}$) | No. of charged groups per membrane surface area, N (eq m$^{-2}$) |
|---|---|---|---|---|
| 0.0001 | -15.3 | $3.05 \times 10^{-8}$ | $-3.5 \times 10^{-4}$ | $-3.6 \times 10^{-9}$ |
| 0.001 | -14.3 | $9.64 \times 10^{-9}$ | $-1.0 \times 10^{-3}$ | $-1.1 \times 10^{-8}$ |
| 0.01 | -13.2 | $3.05 \times 10^{-9}$ | $-3.0 \times 10^{-3}$ | $-3.1 \times 10^{-8}$ |
| 0.1 | -11.8 | $9.64 \times 10^{-10}$ | $-8.5 \times 10^{-3}$ | $-8.8 \times 10^{-8}$ |

**Table 6.1 Zeta potential, surface charge density and number of charged groups for NTR 7450 nanofiltration membrane at different electrolyte concentrations and pH 7**

[1] Zeta Potential, Zetasizer Nano series technical note, MAK654-01 Malvern Instruments Ltd.

Table 6.1 shows that as the concentration of electrolyte is increased from 0.0001 M to 0.1 M the Debye length is reduced from 30.5 nm to 0.96 nm. This implied that the thickness of the double layer was dependant upon the concentration of ions in solution. As the Debye length is reduced, this in turn caused the membrane surface charge density, $\sigma_s$, (equation 6.1) to increase. The increases in $\sigma_s$ caused the calculated number of charged groups per surface area, $N$, to increase. Therefore the overall effect of raising the electrolyte concentration was an increase in the number of charged groups per unit area of the membrane (Table 6.1).

Now that the membrane charge has been quantified, the amount of adsorption occurring on this membrane charge was investigated

## 6.3 Direct adsorption and desorption measurements

Adsorption and desorption of a small number of organic compounds on NTR 7450 and NF 200 nanofiltration membranes were determined by batch experiments. The results for adsorption and desorption were compared to one another to close the mass balance and check the reliability of the results.

The partition coefficient between the membrane and the bulk phase was used as a measure of adsorption (Van der Bruggen *et al.*, 2002, Kiso *et al.*, 2000). The partition coefficient is defined as:

$$k = \frac{Q}{C} \tag{6.5}$$

where $k$ is the partition coefficient ($1/m^2$)

$Q$ is the adsorbed quantity ($mmol/m^2$)

and $C$ is the concentration in solution at equilibrium (mmol/l)

The results of the adsorption and desorption measurements are summarised in Table 6.2.

| System organic compound & membrane | Membrane surface area ($m^2$) | Amount adsorbed, $Q$ ($mmol/m^2$) | Amount desorbed ($mmol/m^2$) | Partition coefficient, $k$ ($1/m^2$) |
|---|---|---|---|---|
| Sucrose – NTR 7450 | 0.0187 | 0.013 | 0.011 | 0.015 |
| Sucrose – NF 200 | 0.1639 | 0.021 | 0.003 | 0.021 |
| Benzylalcohol – NTR 7450 | 0.0194 | 1.530 | 2.131 | 2.256 |
| Glycine – NTR 7450 | 0.0158 | 0.092 | 0.009 | 0.105 |

**Table 6.2 Adsorption and desorption results for NTR 7450 and NF 200 membranes**

The partition coefficients were calculated after subtraction of the blank solution. No major adsorption was found with any of the compounds. The results presented in Table 6.2 show that the highest measured adsorption was for benzylalcohol (1.530 $mmol/m^2$). The lowest measured adsorption was 0.013 $mmol/m^2$ for a sucrose-NTR 7450 membrane system. The partition coefficients were comparable and low for sucrose with both membranes. The largest partition coefficient was for benzylalcohol. Van der Bruggen *et al.* (2002) found that benzylalcohol produced a high partition coefficient for a NF 70 membrane. They also found that the partition coefficient for saccharides was low. In the current study, the support layer was investigated separately to the active layer. No reduction in concentration was observed for the support layer. However, after 24h contact with benzylalcohol, the solution containing the support material appeared cloudy, implying that benzylalcohol had dissolved some of the support material. If after long exposure to benzylalcohol the support material became damaged, then it was quite possible that the active layer could become damaged as well as they are constructed from similar material (active layer: sulfonated polyethersulfone, support layer: neutral polysulfone (Nyström *et al.*, 1995)). If the membrane structure was damaged then this may affect adsorption and could be a possible explanation for a larger observed adsorption for benzylalcohol in Table 6.2.

A NF 200 membrane was investigated in this study as it had been previously noted that sulfonated polyethersulfone membranes (NTR 7450) exhibit a greater adsorption capacity than that for a polyamide membrane (NF 200) (Kiso *et al.*, 2000). This was not observed in this study as both the NTR 7450 and NF 200 membrane's had a similar adsorption capacity (Table 6.2). Table 6.2 presented the results for the desorption experiments. It was found that the amount adsorbed was comparable for

the amount desorbed for sucrose-NTR7450 and benzylalcohol-NTR 7450 indicating a good reliable result. However, the other adsorption-desorption results are quite different, indicating problems with this method.

### 6.3.1 Limitations of the adsorption desorption experiment

The results in Table 6.2 show that there was not a conservation of material throughout the adsorption and desorption experiments. This may have resulted from inaccuracies in the analysis due to either measuring a very small difference or a very small quantity. These inaccuracies may have been due to the experimental technique. As described in the materials and methods section, the membrane was rinsed with deionised water in between the adsorption and desorption experiments (as outlined by Schaep and Vandecasteele (2001)). The problem with rinsing was that only the bulk solution was changed causing a hold-up volume of the organic compound. This may explain why the amount desorbed was greater than the amount adsorbed for the benzylalcohol-NTR 7450 system. A major flaw with type of experiment was that material measured during the desorption stage may not be due to adsorption. Because of the limitations of this direct adsorption investigation, the effect of adsorption was characterised by an indirect method, namely flux decline and the modelling of rejection with adsorption isotherms.

## *6.4 Flux decline*

The purpose of this section was to consider the mechanisms involved in flux decline during nanofiltrations. Different phenomena have been attributed to causing flux decline. They are; adsorption at the membrane surface or inside the pore, pore blocking, osmotic pressure, concentration polarisation, formation of a gel layer, and deposition of suspended solids on the membrane. The two latter effects are specific for solutions containing high concentrations of macromolecules or suspended solids. In the experimental data presented here, only solutions of organic components in deionised water were used. Therefore, these two effects are less applicable. In this case, it was found that pore blocking and adsorption on the membrane surface were important mechanisms for flux decline.

### 6.4.1 Mechanisms of flux decline

Flux decline was evaluated from filtration measurements. The mass of permeate was measured using a balance and was recorded with respect to time (g/min). This was converted to take into account the surface area of membrane, and was expressed in units of $m^3/m^2s$. The flux decline was calculated by comparison of the solute flux to the initial deionised water flux. One membrane was used per set of solute experiments. A disadvantage of this approach was that preceding components could have influenced the result of the following experiments. Van der Bruggen and Vandecasteele (2001) used this method and stated that when the largest fraction of the flux decline was reversible, the results were reliable. This approach had the advantage that solute fluxes could be compared because the same membrane sheet was used. Use of different membrane sheets made it impossible to compare data within a specific solute set as the flux decline was a relative value. The maximum measured flux for the NTR 7450 nanofiltration membrane was $2.8 \times 10^{-5}$ $m^3/m^2s$, when the average flux was $1.6 \times 10^{-5}$ $m^3/m^2s$ (for a pressure of 1693 kPa). Different membrane permeate fluxes were due to slight changes in the membrane structure/properties.

The general membrane model used to describe membrane flux was given by Equation 6.6

$$J = \frac{\Delta P}{R_{tot}\eta} \tag{6.6}$$

Equation (6.6) represented the maximum value of membrane flux that could be expected from any process. Determination of the total resistance to filtration $R_{tot}$, was strongly dependent on the filtration parameters. $R_{tot}$ was expressed in equation (6.7):

$$R_{tot} = R_p + R_a + R_m + R_g + R_{cp} + R_i + R_d \tag{6.7}$$

where $R_p$ is the resistance due to pore blocking

$R_a$ is the resistance due to adsorption inside the pore

$R_m$ is the intrinsic membrane resistance

$R_g$ is the resistance caused by the formation of a gel layer

$R_{cp}$ is the concentration polarisation resistance

$R_i$ is the resistance caused by specific interactions

$R_d$ is the resistance from deposits on the membranes

For the filtration of pure water, the membrane was considered as an ideal case and the only resistance to flux is the membrane resistance ($R_m$). This is an intrinsic membrane characteristic that corresponds to the resistance calculated from the Hagen-Poiseuille equation:

$$J = \frac{\varepsilon r^2}{8\eta\tau}\frac{\Delta P}{\Delta x} \qquad (6.8)$$

Equation (6.8) showed that the membrane resistance is dependent on the porosity ($\varepsilon$), the tortuosity ($\tau$), the membrane radius ($r$) and the membrane thickness ($\Delta x$). The membrane resistance, $R_m$, does not change during filtration or by changing the feed solution. It reflects the minimum resistance of the membrane against mass transport and determines the maximum water flux for a given pressure driving force (Van der Bruggen and Vandecasteele, 2001). The other resistances shown in equation (6.7) have the effect of reducing the trans-membrane flux. They do this by reducing the effective pore size (adsorption) or increasing the effective membrane thickness (double layer effects).

The resistance to flux $R_{cp}$, is caused by concentration polarisation, resulting in an increased concentration of solutes at the membrane surface. This acts as an extra barrier to mass transfer. If the concentration at the surface of the membrane is large enough, then a gel layer is formed that prevents mass transfer. The concentration polarisation resistance is dependent on the experimental conditions. In this study, it was minimised by applying a high cross-flow velocity in all experiments (stirrer speed was 200 rpm, which equates to a cross flow velocity of 0.46 m/s). The Reynolds Number that was obtained from this operating condition was over 25 000 (Appendix A.6). Van der Bruggen and Vandecasteele (2001) stated that a Reynolds Number of over 25 000 justified neglecting concentration polarization for filtration experiments. Bowen *et al.* (2004) also used a stirred filtration cell and found that concentration polarization effects were negligible. Therefore, the resistance due to concentration polarisation $R_{cp}$ was neglected. The resistance due to the formation of a gel layer ($R_g$) was dependent on the formation of a gel layer and on the type of feed solution used.

The formation of a gel layer is related to the presence of macromolecules, which were not used in this case.

The only remaining resistances to trans-membrane flux are membrane resistance ($R_m$), pore blocking ($R_p$) and adsorption inside the pores ($R_a$). The pore surface was believed to have a certain adsorptive capacity (Elford, 1933). This caused the effective pore radius to become narrowed when the molecules have a similar size as the pores.

As the concentration increases, the osmotic pressure would also increase. Thus, the osmotic pressure caused flux decline, but this was due to a decrease of the pressure driving force instead of an increase of the resistance against mass transport. The effect of osmotic pressure on trans-membrane flux is given by equation (6.9) (Spiegler and Kedem, 1966):

$$J = L_p(\Delta P - \sigma \Delta \pi) \qquad (6.9)$$

where $\sigma$ is the reflection coefficient that represents the maximal retention of a component at infinite pressure. Equation (6.9) showed that as the osmotic pressure ($\pi$) was increased, then the applied pressure would be required to be increased to maintain a constant trans-membrane pressure. Van der Bruggen and Vandecasteele (2001) concluded that the influence of osmotic pressure on flux decline was only minor. They stated that the calculated flux decline due to osmotic pressure for benzonitrile was less than 5% of that found experimentally. Therefore the remaining flux decline was explained by adsorption on the membrane pores that may be enhance by pore blocking.

### 6.4.2 Flux decline results

Flux decline was observed for each solute investigated. Flux decline was plotted as a function of concentration. The results for nine solutes are presented in Figure 6.6.

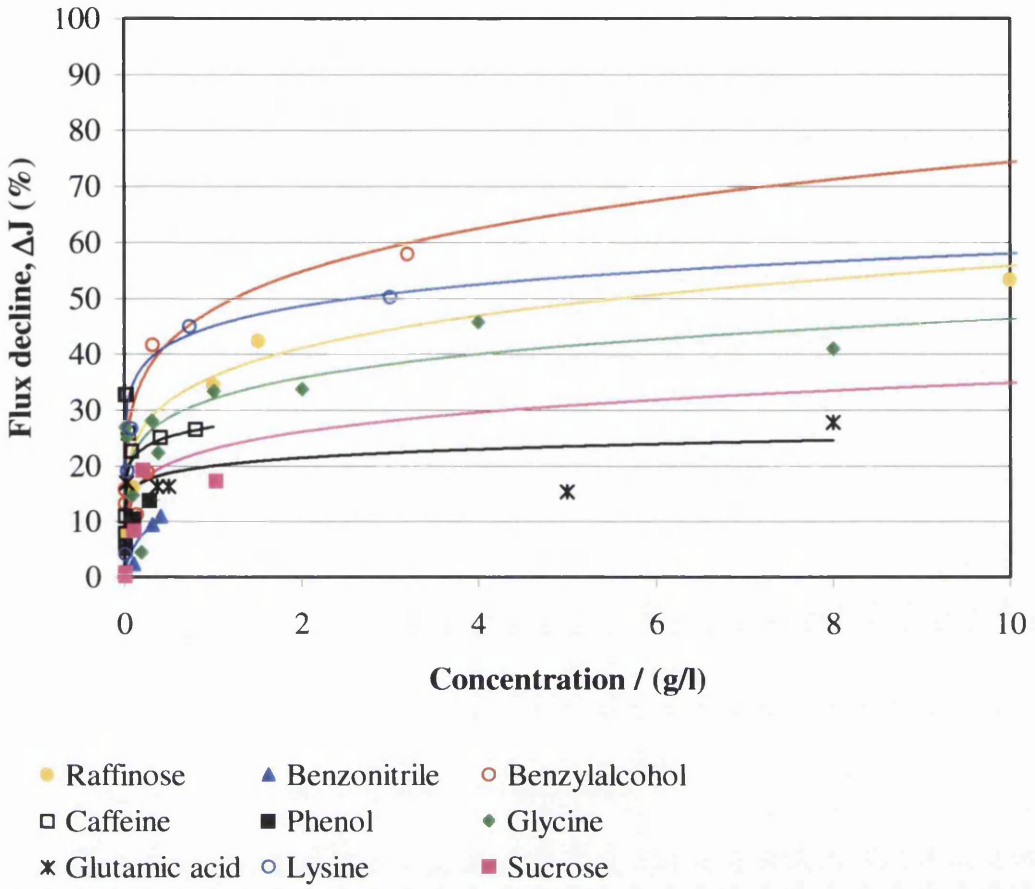


**Figure 6.6 Flux decline as a function of concentration (concentration scale reduced for clarity)**

The data shown in Figure 6.6 was fitted with an adapted form of the Freundlich adsorption isotherm. The Freundlich isotherm is a commonly used model for adsorption. The equation is:

$$q = K c^m \qquad (6.10)$$

where $q$ was the amount of a component adsorbed onto the material, $K$ and $m$ are empirical constants. Van der Bruggen and Vandecasteele (2001) assumed that adsorption was proportional to flux decline, then:

$$\Delta J = K_f c^n \qquad (6.11)$$

where $\Delta J$ was the flux decline, $K_f$ and n are another set of empirical constants. The $K_f$ parameter set the asymptotic maximum value of the curve and the n parameter dictated the sharpness of the curve. The values of both parameters used to fit the curves in Figure 6.6 are shown in Table 6.3. It shows that the Freundlich constant $K_f$

ranged from 16 for phenol, to 48 for benzylalcohol. The empirical constant $n$ was mostly in the range 0.1 – 0.2 (Table 6.3)

| Molecule | $K_f$ | $n$ |
|---|---|---|
| Raffinose | 36 | 0.19 |
| Benzonitrile | 17 | 0.5 |
| Benzylalcihol | 48 | 0.19 |
| Caffeine | 27 | 0.1 |
| Phenol | 16 | 0.15 |
| Glycine | 32 | 0.16 |
| Glutamic acid | 20 | 0.1 |
| Lysine | 45 | 0.11 |
| Sucrose | 23 | 0.18 |

**Table 6.3 Modelling of flux decline with the Freundlich equation**

The data presented in Figure 6.6 showed that the maximum flux decline observed was 58% for benzylalcohol at 3.2 g/l. The Freundlich parameters used to fit the isotherm to this data was $K_f$ = 48 and $n$ = 0.19 (Table 6.3). This was a similar result to that observed by Van der Bruggen and Vandecasteele (2001) for a NF 70 membrane. Out of the eight compounds investigated by Van der Bruggen and Vandecasteele (2001), benzylalcohol exhibited the largest flux decline. They attributed this flux decline to adsorption on the inside of the pore walls and pore blocking.

Membrane pores can become blocked when molecules with a similar size to the pore enters the pore and prevents further permeation of solute or solvent. Membranes have a pore size distribution, therefore only the pores within a specified size range would be affected for the filtration of a pure solute. Once all the pores were blocked within this size range, the flux decline would reach a maximal value. Adsorption occurred as soon as the surface of the membrane was brought into contact with the solution. The molecules would also adsorb on the pore walls when pressure-driving force was applied across the membrane. The extent of adsorption occurring at the membrane surface was attributed to physiochemical interactions such as; dispersion forces, polar interactions, and charge transfer (hydrogen bonding).

Polar interactions refer to dipole-dipole and dipole-induced-dipole interactions. Because the electric field induced by the charge of the membrane was small (Section

6.2), the induced dipole moment was neglected. Therefore, the permanent dipole moment of the uncharged molecules was considered. Benzylalcohol had the smallest dipole moment ($\mu^0$ = 1.7 Debye) out of all of the molecules shown in Figure 6.6, yet benzylalcohol exhibited the largest measured flux decline. This result was surprising. As benzylalcohol had such a low dipole moment, the flux decline caused by adsorption, as proposed by Van der Bruggen and Vandecasteele (2001) was unlikely. Figure 6.6 showed that the flux decline for molecules with larger dipole moments, such as sucrose ($\mu^0$ = 12.4 – 14.3 Debye), was less than that measured for benzylalcohol. The second highest flux decline measured was 51% for lysine (Figure 6.6). Lysine was filtered at its isoelectric point (pH 9.74), at this pH the lysine molecule carried no net charge. This flux decline was higher than that measured for other amino acids in Figure 6.6, namely glycine and glutamic acid. Glutamic acid had the highest average molecular charge (-0.34 electrons per molecule) out of the three amino acids. However, glutamic acid had the lowest flux decline measured for the amino acids (Figure 6.6). The average charge for all the glycine molecules was found to be –0.001 electrons per molecule and the maximum flux decline measured for glycine was 46%. Therefore the experimental data presented in Figure 6.6 showed that for amino acids, the closer the average charge of the molecules is to zero, then the larger the measured flux decline.

The current theory states that the flux decline observed during filtration of uncharged organic molecules was due to adsorption, which in turn was related to polar interactions such as the dipole moment of a molecule. The experimental data presented in Figure 6.6 do not support this theory. Hence, pore blocking was the only remaining explanation for benzylalcohol exhibiting the largest flux decline. The effect of adsorption and pore blocking on the selectivity of the membrane was examined further by examining the relationship between rejection and concentration.

## 6.5 Membrane adsorption

The flux decline observed during the filtration of organic molecules was attributed to adsorption occurring on the membrane surface (Van der Bruggen and Vandecasteele, 2001). They stated that this adsorption was governed by the dipole moment of the

molecule. However, the previous section showed that proposed mechanism was not as simple as that suggested by Van der Bruggen and Vandecasteele (2001).

Hong and Bruening (2006) investigated the use of a new class of polyelectrolyte multilayer nanofiltration membrane for the separation of amino acids. They found that larger concentrations of amino acids resulted in a greater rejection. A similar increase in rejection with concentration was observed during the nanofiltration of sugars (Hong and Bruening, 2006). They speculated that increased rejections with higher concentration of amino acids or sugars resulted from adsorption on the membrane, which decreased the effective pore size and molecular weight cut-off.

Elford (1933) proposed an ideal membrane that had uniform pores, which were circular in cross-section. This membrane was considered in the filtration of a suspension of uniform dispersion, and the particles were non-deformable spheres. Elford (1933) described the case when adsorption occurred on this membrane. The pore surface was assumed to have a certain adsorptive capacity that was satisfied when a layer, one particle thick, covered the surface. This caused the pore to become narrowed. Hence the membrane could now reject smaller particles. Should the conditions be such that the adsorption was not confined to a monolayer, a layer several molecules thick (a diffuse double layer) may be formed (Elford, 1933). Therefore, the pores could retain particles much smaller than the original pore diameter.

The effect of adsorption on the rejection of molecules has yet to be investigated and reported in the literature. In this section, the effect of concentration on the rejection of the membrane was investigated. This combined with the flux decline results provided knowledge of the mass transport phenomena occurring during nanofiltration.

## 6.6 Adsorption isotherm

The previous flux decline section outlined the use of the Freundlich adsorption isotherm for fitting flux decline experimental data, as proposed by Van der Bruggen and Vandecasteele (2001). If the amount of adsorbed material, $q$ (equation 6.10) could be assumed to be proportional to the flux decline, $\Delta J$ (equation 6.11), then the next

logical step was to assume that $q$ was proportional to rejection ($R$), as shown by equation (6.12):

$$R = K_R C^Q \tag{6.12}$$

where $K_R$ and $Q$ are empirical constants.

### 6.6.1 Model performance

The Freundlich adsorption model, now modified to fit rejection data was tested for all experimental data in which rejection increased with concentration. The results of this modelling are shown in Figures 6.7 to 6.12. The quality of agreement between the model and the experimental data was assessed according to the shape of the resulting curve in comparison with the experimental data.

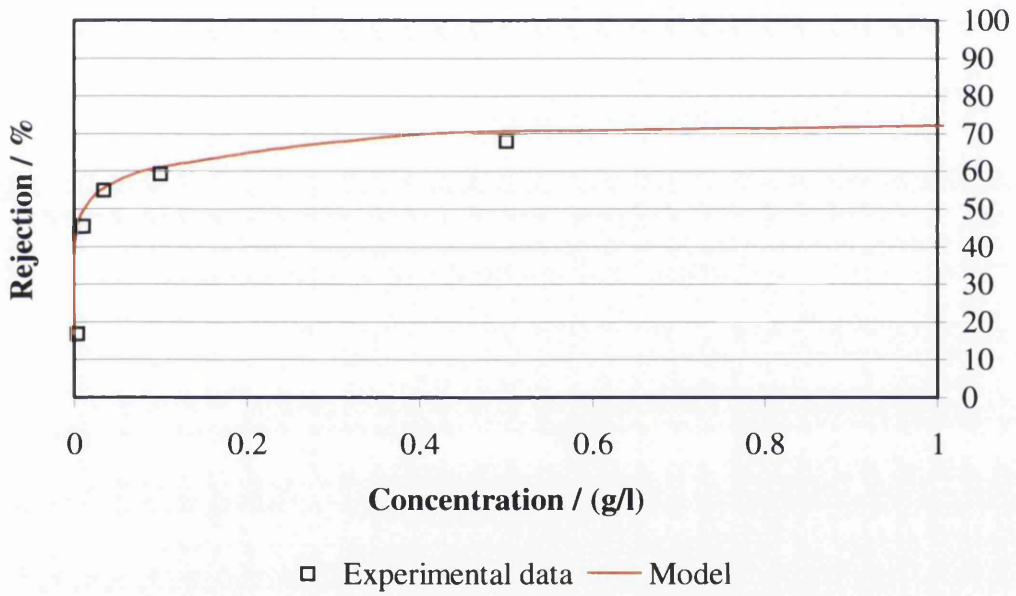


**Figure 6.7 Rejection of glucose as a function of concentration, experimental data and fitted model**

The graph shown in Figure 6.7 indicated that that rejection of glucose was a function of its concentration. The Freundlich model (equation 6.12) provides a very good fit of the curve presented by the individual experimental data points. This suggested that adsorption was governing rejection.

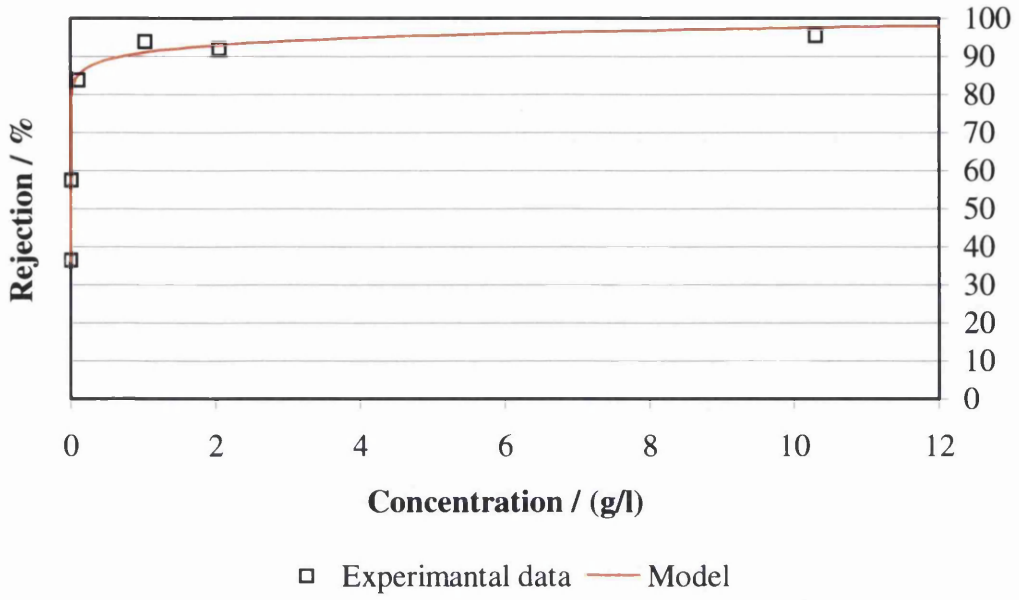


**Figure 6.8 Rejection of sucrose as a function of concentration, experimental data and fitted model**

Figures 6.7, 6.8 and 6.9 all demonstrated rejection increasing with concentration for glucose, sucrose and raffinose respectively. In all three cases, the quality of the model fit was good.

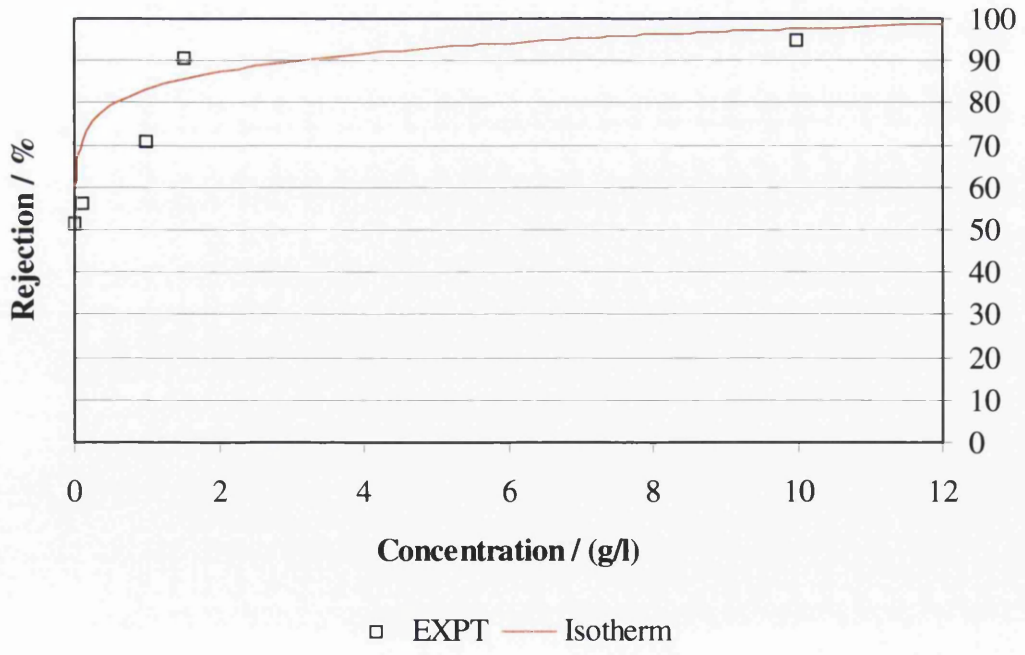


**Figure 6.9 Rejection of raffinose as a function of concentration, experimental data and fitted model**

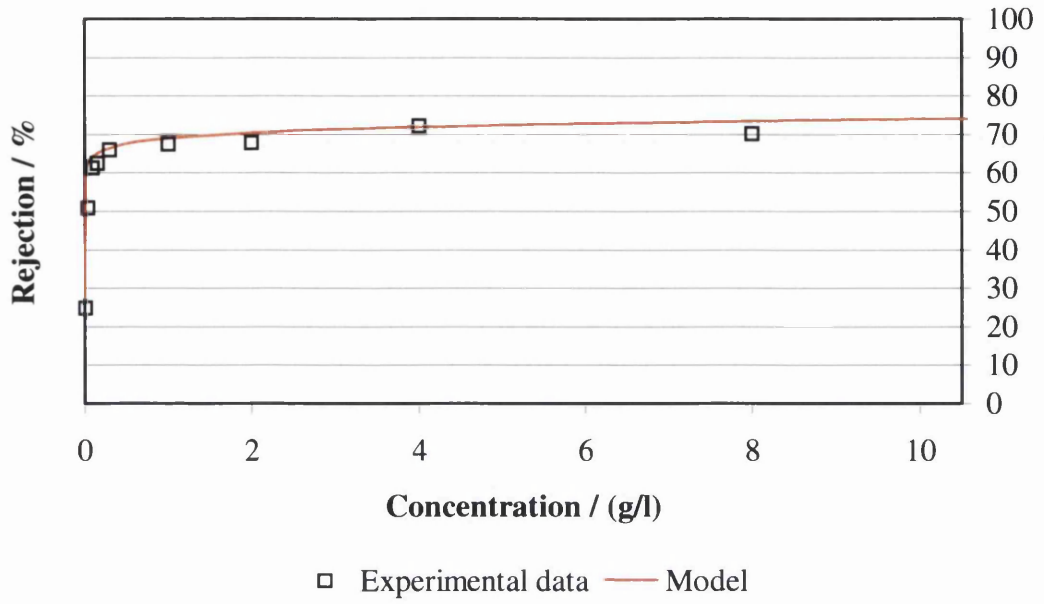


**Figure 6.10 Rejection of glycine as a function of concentration, experimental data and fitted model**

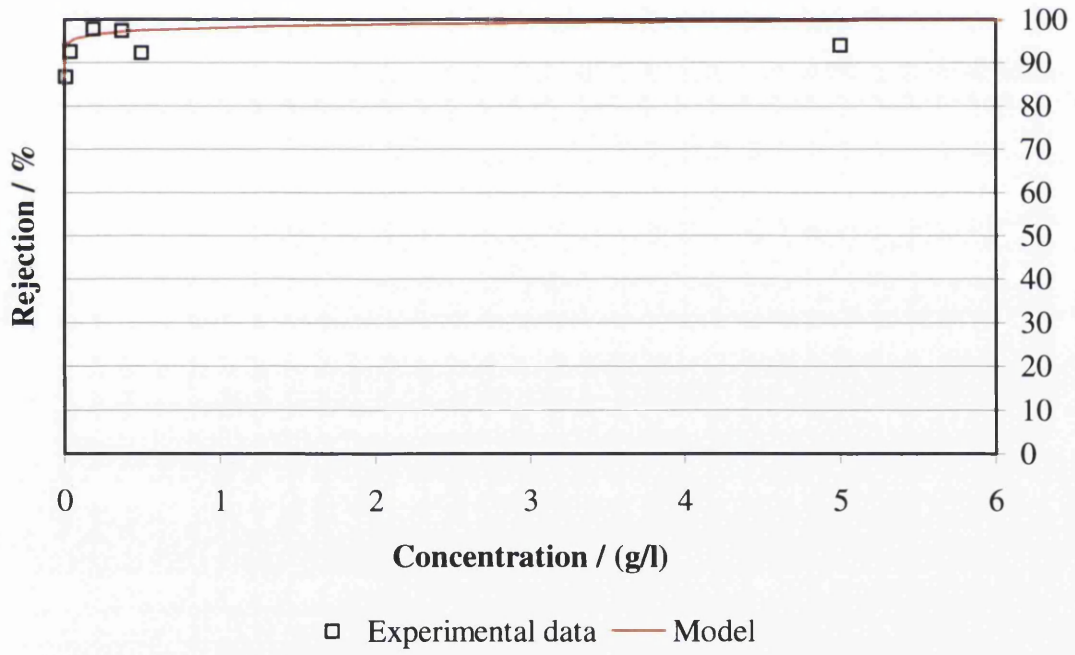


**Figure 6.11 Rejection of glutamic acid as a function of concentration, experimental data and fitted model**

Figures 6.10, 6.11 and 6.12 demonstrate the rejection increasing with concentration for glycine, glutamic acid and glutamine. As with the plots for the three saccharides, the trend for the rejection behaviour was well presented by the model. Overall the best

standard of fit was observed for glucose, sucrose and glycine. The poorest fit of the model to experimental data was for raffinose, glutamic acid and glutamine.

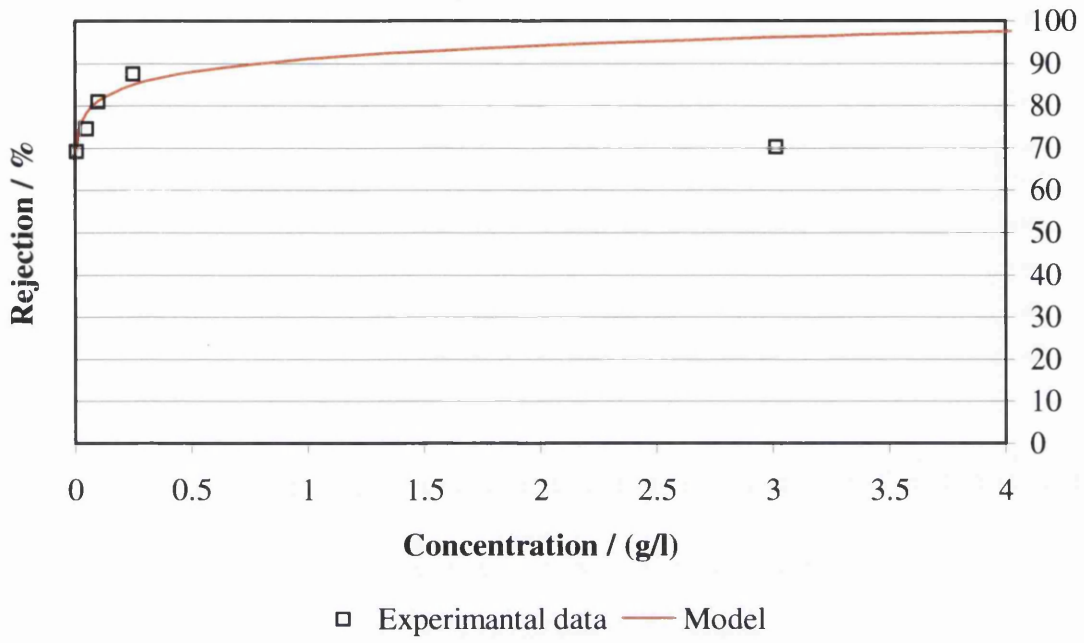


**Figure 6.12 Rejection of glutamine as a function of concentration, experimental data and fitted model**

## 6.6.2 Model parameters

The empirical constants used to fit the Freundlich model (equation (6.12)) to Figures 6.7 to 6.12 are shown in Table 6.4.

| Molecule | $K_R$ | Q | Dipole moment / Average charge |
|---|---|---|---|
| Glucose | 75 | 0.09 | 14.1 Debye |
| Sucrose | 91 | 0.03 | 14.3 Debye |
| Raffinose | 83 | 0.07 | Assume ~ 14 Debye |
| Glycine | 69 | 0.03 | -0.001 e/mol |
| Glutamic acid | 98 | 0.01 | -0.34 e/mol |
| Glutamine | 91 | 0.05 | -0.002 e/mol |

(Where e/mol represents electrons per molecule)

**Table 6.4 Modelling of rejection with adapted Freundlich model**

Table 6.4 shows that $K_R$ used in the Freundlich model (equation (6.12)) ranged from 98 to 69, and $Q$ ranged from 0.09 to 0.01. It is apparent from the data presented in

Table 6.4, that the phenomena of rejection increasing with concentration only occurred for molecules with either a high dipole moment (approximately 14 Debye) or amino acids with small negative average charges. Therefore it was possible to conclude that Figures 6.7 to 6.12 supported the assumption that the dipole moment acted as small charges influencing the rejection by controlling adsorption on the surface of the membrane.

## 6.7 Reversible and irreversible adsorption

Fouling is caused by deposition of material, such as organic compounds, on the surface of the membrane. Fouling was defined as that which causes an irreversible flux decline that can only be removed by chemical cleaning (Van der Bruggen *et al.*, 2002). When the flux can be restored to the original level by simply changing the feed solution to pure water, the phenomenon is reversible, and is not referred to as fouling.

Flux permeate decline and rejection was evaluated in this work by using the same piece of membrane for a complete solute set of filtrations. A disadvantage of this approach was that preceding components might have influenced the results of the following experiments. The effect was quantified by conducting a set of glucose filtrations out of sequence. Figure 6.13 shows the experimental data for the filtration of glucose through a NTR 7450 nanofiltration membrane. The numbers shown on Figure 6.13 represent the order in which the filtrations were conducted.

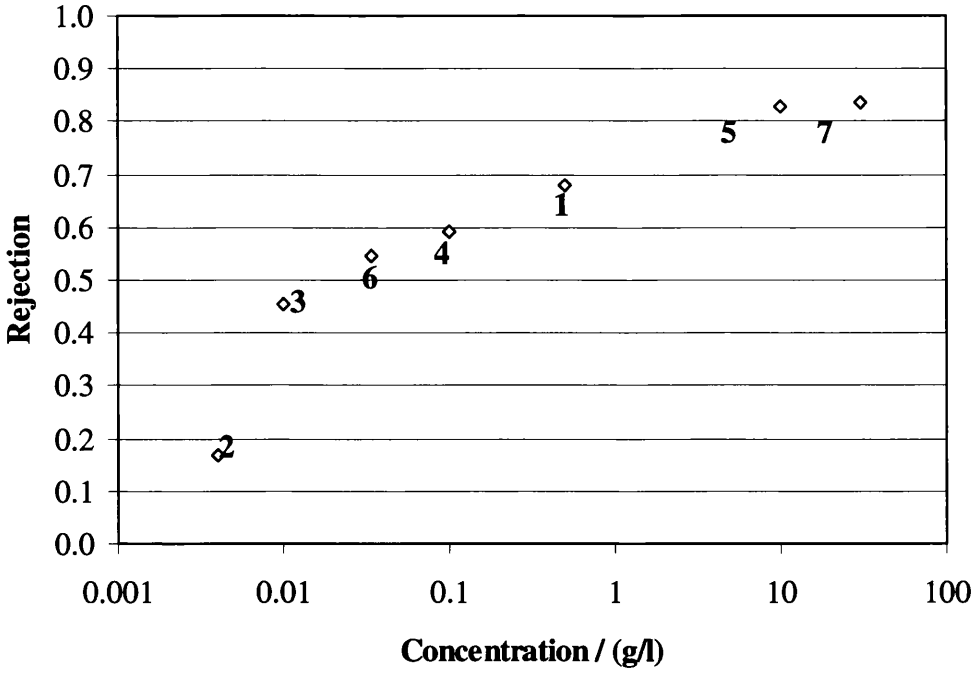


**Figure 6.13 Rejection of glucose and filtration sequence**

The data presented in Figure 6.13 show that the sequence in which the filtrations were conducted had no obvious effect on the resulting rejection and therefore most of adsorption occurring was reversible. Some permanent flux decline was observed throughout the filtrations, indicating some irreversible adsorption, but this did not appear to affect the experimental results.

## *6.8 Electrical double layer*

This study has provided a fuller investigation than that presented by Van der Bruggen and Vandecasteele (2001) as it considered rejection along with flux decline. Combining rejection and flux decline data allowed an indirect assessment of the resistance to membrane transport. This method was more reliable than the direct adsorption experimental data due to the problems highlighted in the earlier section.

### 6.8.1 Diffuse part of the double layer

It has been shown that the molecule's dipole moment had an effect on its rejection by a NTR 7450 membrane. Van der Bruggen *et al.* 1999 acknowledged that a molecule with a large dipole moment became orientated towards the membrane charge in such

a way that the side of the dipole with the opposite charge to the inherent membrane charge was towards the membrane surface. If a molecule experienced a force at some distance from the membrane surface that resulted in the molecule having a specified orientation, then an electrical double layer would have to be present. A characteristic of the diffuse part of the double layer is that its thickness diminishes with increasing electrolyte concentration, so that the electrostatic potential falls off more quickly with distance. This effect was observed during the steaming potential experiments. As the concentration of electrolyte was increased from 0.0001 M to 0.1 M the Debye length was reduced from 30.5 nm to 0.96 nm

The rejection of amino acids was observed to decrease at high concentrations (Chapter 4). At high concentrations the Freundlich model (equation (6.12)) exhibited a poor fit for glutamic acid and glutamine (Figures 6.11 and 6.12). Figure 6.14 shows the rejection of glycine, glutamic acid and glutamine at high concentrations.

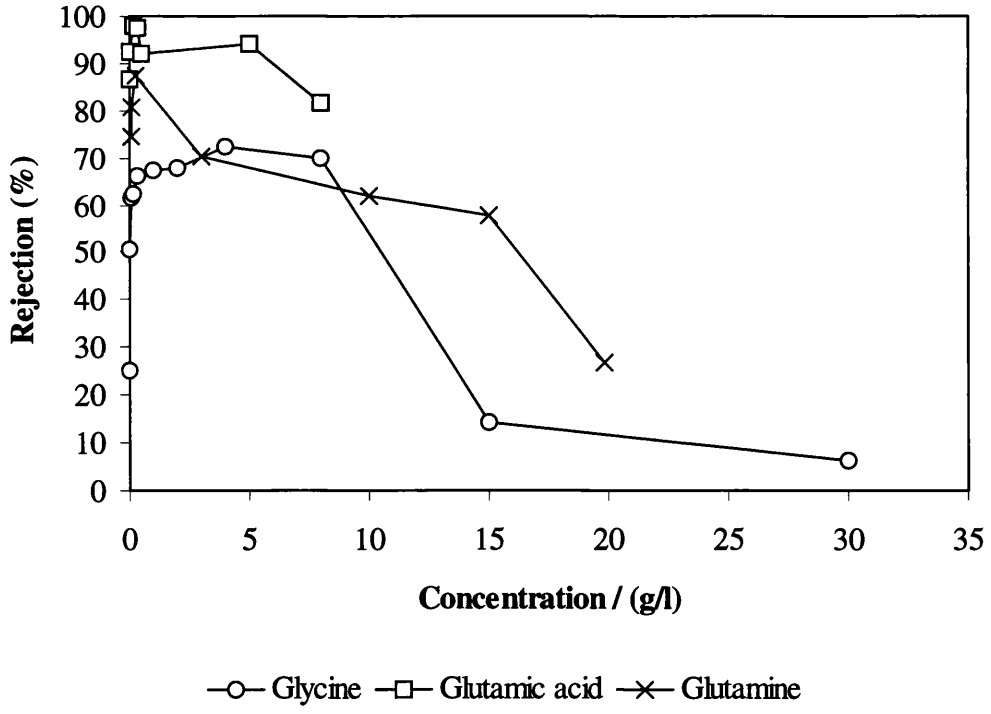


**Figure 6.14 Rejection of glycine, glutamic acid and glutamine at high concentrations**

The experimental data presented in Figure 6.14 shows that the rejection initially increased for a small amino acid concentration (< 1 g/l), then as the concentration was increased, the rejection fell sharply. For glycine, the rejection increased from 25% to 61% for a concentration of 0.004 g/l and 0.09 g/l respectively (Figure 6.14). Once the

concentration was in the range 1-8 g/l, the rejection of glycine remained approximately constant at 70%. However, when the concentration was increased further (> 10 g/l), the rejection fell to 6% for a concentration of 30 g/l. This rejection was influenced by the double layer effect. At low concentrations, the rejection was governed by adsorption occurring on the inside of the pores, reducing the effective pore diameter. Whilst this caused the rejection to increase, when the concentration increased further, a double layer was formed. This had the effect of increasing the effective thickness of the membrane, which in turn shielded solutes from entering the pore, thus increasing the rejection still further. However, when a high concentration was reached (~ 10 g/l), the double layer was compressed and brought closer to the membrane surface. This reduced the amount of pore shielding and subsequently, the rejection dropped.

### 6.8.2 Rejection mechanisms of organic molecules

With consideration of the results presented for flux decline (Figure 6.6), rejection as a function of concentration (Figures 6.7 – 6.12) and the rejection at high concentration (Figure 6.14), the mechanisms governing membrane resistance are as follows:

**(i) Uncharged organic molecule with a low dipole moment**

These molecules caused an unusually large permeate flux decline (Figure 6.6). However, the experimental rejection data presented in Chapter 5 showed that the rejection of these molecules was unaffected by increasing concentration. Therefore the membrane selectivity was unchanged. The governing membrane resistance mechanism in this case was pore blocking. Pore blocking had the effect of reducing the number of pores available for permeation of solute *and* solvent. Thus, the flux was reduced but the selectivity of the membrane remained constant.

**(ii) Uncharged organic molecules with a high dipole moment**

These molecules were associated with a permeate flux decline (Figure 6.6) and their rejection was a function of concentration (Figures 6.7, 6.8 and 6.9). In this case, as the flux declined, the rejection (and the selectivity) of the membrane also changed. Initially, at low concentrations adsorption was occurring on the membrane surface. The, adsorbed molecules built up on the membrane surface reducing the effective pore diameter, thus increasing the rejection of the solute. The rejection was well

described by a Freundlich model (equation 6.12). As the concentration was further increased, the amount of adsorption reached a maximum when the adsorption capacity of the membrane was satisfied, thus causing the rejection to reach a constant maximum value (Figures 6.7, 6.8 and 6.9).

**(iii) Charged organic molecules**

In this study, amino acids at pH values that caused them to have a small negative overall average charge were used. These molecules exhibited a flux decline during filtration, and their rejection was seen to be a function of concentration. The results presented in Figures 6.10, 6.11 and 6.12 showed a good fit for the Freundlich model (equation 6.12) at low concentrations, which indicated that adsorption was occurring. The selectivity of the membrane changed with concentration, and the rejection increased. At high concentrations, a double layer formed that shielded the pore and resisted permeation of the solute but solvent was still able to permeate the membrane. At this high concentration (Figure 6.14), the rejection reduced for these amino acids.

# 7 Conclusions and Recommendations

## 7.1 Conclusions

Nanofiltration is the most recent advance in the development of synthetic membrane technology and is of significant interest in membrane research since its characteristics fall between those of Reverse Osmosis and Ultrafiltration membranes where *MWCO* and rejection ratios become more important.

The aim of this thesis was to investigate nanofiltration as a separation tool at various concentrations of amino acids and neutral organic molecules. Current nanofiltration theory states that the rejection of solutes decreases with increasing solute concentration. This is a typical phenomenon if electrostatic interactions are involved in the rejection mechanism but some workers had observed the opposite occurring where rejection increases with concentration.

Nanofiltrations of five different amino acids were conducted. The acids were specifically selected to cover a range of sizes and charges. Their rejections characteristics were observed for a NTR 7450 nanofiltration membrane. Phenylalanine and lysine both showed rejection decreasing with increasing concentration. The rejection of phenylalanine decreased more rapidly than that for lysine as it had a net positive charge (at the working pH of 4.0) and Donnan attraction forces predominate. Lysine at a working pH of 9.74 carried no net charge and therefore behaved as a neutral molecule and concentration had little effect on rejection. At their working pH's, glutamic acid, glutamine and glycine all carry a mean overall net negative charge and exhibited an unusual rejection mechanism that caused the rejection to increase.

To ensure that the phenomenon observed in the experimental data was true, the error associated with results was analysed to assess whether the results could be attributed to more than just experimental error. For example, the rejection and associated error for glycine at 1.0 g/l was 67 ± 3%, when the measured increase in rejection was from 25% to 72%. Therefore, the observed increase in rejection was not attributed to experimental error.

The claim that the observed molecular weight of an amino acid increases with concentration due to dimerisation (Li *et al.*, 2003) has been investigated. Work conducted with the HPPS instrument showed that molecules with a diameter of 0.5 nm could be measured and although the HPPS instrument was at the limit of operation at this particle size, the results suggested that no dimerisation was occurring. Osmotic pressure analysis was found to support the HPPS findings and no nonlinear solute-solute interactions were observed over the nanofiltration range. These two results lead to the conclusion that no significant dimmerisation occurred for the amino acid system.

The experimental results for the amino acids were compared to the predictions of a steric and charge rejection model. It was found that the steric rejection model could describe the experimental rejection of lysine at its isoelectric point, as the lysine molecule would behave as a neutral species. The charge rejection amino acid model was compared to the experimental data for phenylalanine at pH 4 (net charge equivalent to 0.007 electrons per molecule) and good agreement between the model and the experimental data was observed. This was due to the fact that phenylalanine exhibited classic Donnan attraction effects. However, poor agreement was obtained for the charge model when compared to amino acids with a net negative charge, in which rejection increased with concentration. This result indicated that another mechanism, other than electrostatic rejection was occurring.

The *MWCO* is an important membrane parameter that is used for the selection of a membrane for a specific filtration. It was found that under certain circumstances the published *MWCO* for the NTR 7450 membrane was over estimated and therefore this was investigated. The *MWCO* of a NTR 7450 membrane was dependent on solute concentration. The experimental data was fitted by using the Log Normal Model. The *MWCO* decreased from 870 Da to 210 Da for solute concentrations of 0.02 mmol/l and 3 mmol/l respectively. The Log Normal Model was then compared to the experimental rejection data for uncharged organic molecules. It was found that the Log Normal Model could be used to describe the rejection of molecules with a low dipole moment (<4 Debye) and amino acids at their isoelectric point as they exhibited little or no change in rejection for increasing concentration. However, a poor fit was exhibited by the Log Normal Model for uncharged organic molecules with high

dipole moments (~ 14 Debye). For these molecules, the rejection increased with increasing concentration. This result and the *MWCO* data suggested that *effective* pores size was a function of concentration. This was further investigated by means of determining the surface characteristics of the NTR 7450 membrane and the solute-membrane interactions.

Titrimetric measurements were conducted for the membrane material. It was found that acidic groups were present on the surface of the NTR 7450 membrane. The charge of the acid groups was determined by streaming potential experiments, which showed that the surface of the membrane had a strong negative charge (zeta potential at pH 7.0 was –14.3 mV for an electrolyte concentration of 0.001 M). The effect of this strong negative charge was investigated by direct and indirect adsorption measurements and in both cases the results indicated that adsorption was occurring at the membrane surface. The results for both flux decline and rejection as a function of concentration were fitted with an adapted form of the Freundlich adsorption isotherm. The good quality of fit between the experimental data and the isotherm supported the proposition that solute adsorption was occurring and that this influenced the rejection of the solute.

In summary, rejection was shown to increase with concentration for charged amino acids and uncharged molecules with high dipole moments. The *MWCO* of the membrane decreased with respect to increasing concentration. Therefore the effective pore size was changing. This was attributed to the build up of adsorbed molecules on the inside of the pore with the effect that the rejection capacity of the membrane increased.

## 7.2 Recommendations

Further work related to the content of this thesis should be concerned with assessing the possibilities of exploiting the information to either expedite or enhance the process. This may be achieved by the use of chemical additives to promote or hinder the formation of adsorbed layers on the membrane surface.

The results presented in Section 5.3 show that a rejection of over 90% was achieved for sugars by controlling the feed concentration (> 1 g/l for sucrose and raffinose). Further optimisation of the process may lead to nanofiltration technology that offers energy saving benefits over traditional reverse osmosis methods for concentrating sugar solutions.

Ultimately a modification or addition would be made to contemporary transport theories that would successfully account for the behaviour of such systems. The Log Normal model has been shown to be lacking in the case of charged species and those with high dipole moments. Development of the Log Normal model could incorporate a factor that accounts for concentration and dipole moments.

A method for the direct measurement of adsorption on the surface of the membrane was used in this thesis that exhibited some limitations (Section 6.3.1). Further development of this technique is needed. The first issue to be addressed would be to improve the rinsing method, with the aim of removing the unabsorbed lamina layer which would help to close the mass balance. Another area of improvement would be to maximise the wetted surface area with minimum solution, this would allow for an increased change in the solutions concentration and hence a larger measurable difference in concentration between the two solutions. An alternative method of direct adsorption measurement may be the determination of surface roughness by Atomic Force Microscope (AFM). This technique may give some indication to the level of adsorption on the top layer of the membrane surface. Reliable direct measurement results would be required to validate any predictive theoretical results.

# Nomenclature

| | | |
|---|---|---|
| $A_k$ | Fraction of membrane area occupied by pores | [-] |
| $a_r$ | hydrodynamic (Stokes) radius of solute or ion | [m] |
| $a_s$ | solute activity | [mol $m^{-3}$] |
| $C$ | capacitance | [C $V^{-1}$] |
| $c$ | electrolyte concentration | [mol $m^{-3}$] |
| $C$ | concentration in solution at equilibrium | [mmol $l^{-1}$] |
| $C_r$ | concentration of amino acid | [mol $l^{-1}$] |
| $c_s$ | concentration of solute in feed | [mol $m^{-3}$] |
| $D_{i,p}$ | pore diffusion coefficient of ion $i$ | [$m^2$ $s^{-1}$] |
| $d_s$ | solute diameter | [m] |
| $e$ | electronic charge, 1.602177 x $10^{-19}$ | [C] |
| $F$ | Faraday constant, 96496 | [C $mol^{-1}$] |
| $F$ | flow parameter, defined by equation (5.4) | [$m^2$ $s^{-1}$] |
| $I$ | ionic strength | [mol] |
| $J$ or $J_v$ | membrane permeate flux | [$m^3$ $m^{-2}$ s] |
| $j_i$ | flux of ion $i$ | [mol $m^{-2}$ $s^{-1}$] |
| $J_s$ | solute flux | [$m^3$ $m^{-2}$ s] |
| $k$ | Boltzmann constant, 1.38066 x $10^{-23}$ | [J $K^{-1}$] |
| $k$ | adsorption partition coefficient | [$m^{-2}$] |
| $K$ | adsorption partition coefficient used in equation (6.10) | [$m^{-2}$] |
| $K_c$ | hindrance factor for convection used in equation (2.17) | [-] |
| $K_f$ | adsorption partition coefficient used in equation (6.11) | [$m^{-2}$] |
| $L_p$ | hydraulic permeability | [$m^3$ $m^{-2}$] |
| $m$ | empirical constant used in equation (6.10) | [-] |
| $M$ | membrane charge density | [eq $m^{-2}$] |
| $N$ | number of charged groups per membrane surface area | [eq $m^{-2}$] |
| $n$ | empirical constant used in equation (6.11) | [-] |
| $n$ | number of positive and negative ions per unit volume | [$m^{-3}$] |

| | | |
|---|---|---|
| $n_+$, $n_-$ | ionic volume densities of cations and anions | [$m^{-3}$] |
| $N_A$ | Avagadro's number, 6.023 x $10^{23}$ | [g mol] |
| $P$ | applied pressure | [Pa] |
| $P_1$ or $P_2$ | local solute permeability | [$m^2$ $s^{-1}$] |
| $P_{max}$ | maximum osmotic pressure | [kPa] |
| $P_s$ | solute permeability | [$m^2$ $s^{-1}$] |
| $Q$ | adsorbed quantity | [mmol $m^{-2}$] |
| $q$ | amount of a component adsorbed used in equation (6.10) | [mmol $m^{-2}$] |
| $R$ | gas constant, 8.314 | [J $K^{-1}mol^{-1}$] |
| $r$ | membrane radius | [m] |
| $R$ | rejection coefficient | [-] |
| $R_a$ | resistance due to adsorption inside the pore | [$m^{-1}$] |
| $R_c$ | rejection due to charge effects | [-] |
| $R_{cp}$ | concentration polarisation resistance | [$m^{-1}$] |
| Re | Reynolds number | [-] |
| $R_{el}$ | electrical resistance | [Ω] |
| $R_{el,s}$ | standard electrical resistance | [Ω] |
| $R_g$ | resistance caused by the formation of a gel layer | [$m^{-1}$] |
| $R_i$ | resistance caused by specific interactions | [$m^{-1}$] |
| $R_m$ | intrinsic membrane resistance | [$m^{-1}$] |
| $r_p$ | effective pore radius | [m] |
| $R_p$ | resistance due to pore blocking | [$m^{-1}$] |
| $r_p$ | radius of membrane pore | [m] |
| $r_s$ | radius of solute | [m] |
| $R_s$ | rejection due to steric effects | [-] |
| $R_{tot}$ | total resistance to rejection | [$m^{-1}$] |
| $S_{MW}$ | standard deviation for molecular weight | [-] |
| $S_p$ | standard deviation for effective solute diameter | [-] |
| $T$ | absolute temperature | [K] |
| $t_{max}$ | time when maximum osmotic pressure was achived | [h] |

| | | |
|---|---|---|
| $Tr$ | transmission of a solute through the membrane | [-] |
| $Tr_c$ | charge dependent transmission of a solute through the membrane | [-] |
| $Tr_s$ | size dependent transmission of a solute through the membrane | [-] |
| $V$ | solvent velocity used in equation (2.17) | [m $s^{-1}$] |
| $V_m$ | molar volume of solvent | [$m^{-3}$] |
| $V_w$ | partial molar volume of the solvent | [$m^3$ $mol^{-1}$] |
| $Y_i$ | dimensionless group equation (2.22) | [-] |
| $z$ | solute charge | [-] |
| z | charge of amino acid | [e $mol^{-1}$] |
| $z_{ct}$ | charge of counter-ion | [e $mol^{-1}$] |
| $z_i$ | ion valence | [-] |

**Greek symbols**

| | | |
|---|---|---|
| $\Delta E_{str}$ | streaming potential | [V] |
| $\delta$ | Stern layer thickness | [m] |
| $\Delta P$ | applied pressure difference | [N $m^{-2}$] |
| $\Delta P$ | differential pressure across the membrane | [Pa] |
| $\Delta P_e$ | effective pressure driving force | [Pa] |
| $\Delta W_i$ | Born solvation energy barrier | [J] |
| $\Delta x$ | membrane thickness | [m] |
| $\varepsilon$ | permittivity | [-] |
| $\varepsilon_0$ | permittivity of free space, 8.85419 x $10^{-12}$ | [$J^{-1}C^2m^{-1}$] |
| $\varepsilon_b$ | bulk dielectric constant | [-] |
| $\varepsilon_p$ | pore dielectric constant | [-] |
| $\phi$ | van der Waals term | [-] |
| $\Phi$ | steric partition coefficient | [-] |
| $\gamma$ | activity coefficient | [-] |
| $\eta$ | solvent viscosity | [N $m^{-2}$] |
| $\kappa$ | Debye-Hückel parameter | [$m^{-1}$] |
| $\kappa_s$ | standard specific conductivity | [S $m^{-1}$] |

| | | |
|---|---|---|
| $\lambda$ | solute-pore size ratio | [-] |
| $\lambda_{Deb}$ | Debye length | [m] |
| $\pi$ | osmotic pressure | [Pa] |
| $\rho$ | particle density | [kg $m^{-3}$] |
| $\rho$ | specific diffusion parameter, 2.07 x $10^{-15}$ | [$m^2$ $s^{-1}$] |
| $\sigma$ | reflection coefficient | [-] |
| $\sigma_0$ | surface charge density | [C $m^{-2}$] |
| $\sigma_d$ | net charge density | [C $m^{-2}$] |
| $\sigma_m$ | surface charge density (monolayer counter ions) | [C $m^{-2}$] |
| $\sigma_s$ | charge density at shear plane | [C $m^{-2}$] |
| $\tau$ | tortuosity | [-] |
| $\omega$ | solute mobility | [mol $s^{-1}$ $N^{-1}$] |
| $\psi$ | electrical potential at some distance | [V] |
| $\psi_0$ | electrical potential at surface | [V] |
| $\psi_d$ | Stern potential | [V] |
| $\zeta$ | zeta potential | [V] |
| $\upsilon_{AA}$ | membrane stoichiometric coefficient | [-] |
| $\upsilon_{ct}$ | membrane counter-ion stoichiometric coefficient | [-] |
| $\Psi_D$ | Donnan potential | [V] |
| $\mu^0$ | Molecules permanent dipole moment | [Debye] |
| $\mu^{ind}$ | Molecules induced permanent dipole moment | [Debye] |

**Abbreviations**

| | |
|---|---|
| AFM | atomic force microscopy |
| MF | microfiltration |
| *MW* | molecular weight |
| *MWCO* | molecular weight cut off |
| NF | nanofiltration |
| RO | reverse osmosis |
| UF | ultrafiltration |

# Bibliography


Aguilella, V., Aguilella-Arzo , M. and Ramirez, P., 1996. Electrokinetic Phenomena in Microporous Membranes with a Fixed Transverse Charge Distribution. Journal of membrane science, 113: 191-204.

Alvarez, V., Alvarez, S., Riera, E.A. and Alvarez, R., 1997. Permeate flux prediction in apple juice concentration by Reverse Osmosis. Journal of membrane science, 127: 25-34.

Atra, R., Vatai, G., Bekassy-Molnar, E. and Balint, A., 2004. Investigation of ultra- and nanofiltration for utilization of whey protein and lactose. Journal of Food Engineering, 67(3): 325-332.

Balannec, B., Vourch, M., Rabiller-Baudry, M. and Chaufer, B., 2004. Comparative study of different nanofiltration and reverse osmosis membranes for dairy effluent treatment by dead-end filtration. Separation and Purification Technology.

Bandini, S. and Vezzani, D., 2003. Nanofiltration modelling: the role of dielectric exclusion in membrane characterization. Chemical Engineering Science, 58: 3303-3326.

Bardot, C., Gaubert, E. and E., Y.A., 1995. Unusual mutual influence of electrolytes during pressure-driven transport of their mixtures across charged porous membranes. Journal of Membrane Science, 103(1-2): 11-17.

Bes-Pía, A., Iborra-Clar, A., Mendoza-Roca, J.A., Iborra-Clar, M.I. and Alcaina-Miranda, M.I., 2004. Nanofiltration of biologically treated textile effluents using ozone as a pre-treatment. Desalination, 167: 387-392.

Bessarabov, D. and Twardowski, Z., 2002. Industrial application of nanofiltration - new perspectives. Membrane Technology, 9: 6.

Bobreshova, O., Novikova, L., Kulintsov, P. and Balavadze, E., 2002. Amino acids and water electrotransport through cation-exchange membranes. Desalination, 149: 363-368.

Born, M., 1920. Volumen and hydratationswarme der ioen. Z. Physik. Chem., 1: 45-48.

Boussu, K., Van der Bruggen, B., Volodin, A., Van Haesendonck, C., Delcour, J.A., 2006. Characterization of commercial nanofiltration membranes and

comparison with self-made polyethersulfone membranes. Desalination, 191: 245-253.

Bowen, J.H., 2001a. Adsorption. In: J.M. Coulson and J.F. Richardson (Editors), Chemical Engineering. Butterworth-Heinemann.

Bowen, W.R., 2001b. Membrane Separation Processes. In: J.M. Coulson and J.F. Richardson (Editors), Chemical Engineering. Butterworth-Heinemann.

Bowen, W.R., Cassey, B., Jones, P. and Oatley, D.L., 2004. Modelling the performance of membrane nanofiltration—application to an industrially relevant separation. Journal of Membrane Science, 242(1-2): 211-220.

Bowen, W.R., Hilal, N., Jain, M., Lovitt, R.W, Sharif, A.O and Wright, C.J., 1999. The effects of electrostatic interactions on the rejection of colloids by membrane pores—visualisation and quantification. Chemical Engineering Science, 54(3): 369-375.

Bowen, W.R., Hilal, N., Lovitt, R.W., O. Sharif, A. and Williams, P.M., 1997a. Atomic force microscope studies of membranes: force measurement and imaging in electrolyte solutions. Journal of Membrane Science, 126(1): 77-89.

Bowen, W.R. and Hughes, D.T., 1991. Properties of Microfiltration Membranes; The Surface Electrochemistry of Anodic Film Membranes. Journal of Colloid and Interface Science, 143(1): 252-256.

Bowen, W.R. and Jenner, F., 1995. Electroviscous Effects in Charged Capillaries. Journal of Colloid and Interface Science, 173: 388-395.

Bowen, W.R. and Mohammad, A.W., 1998. Diafiltration by Nanofiltration: Prediction and Optimisation. AICheE J, 44: 1799.

Bowen, W.R., Mohammad, A.W. and Hilal, N., 1997b. Characterisation of nanofiltration membranes for predictive purposes - use of salts, uncharged soluted and atomic force microscopy. Journal of Membrane Science, 126: 91-105.

Bowen, W.R. and Mukhtar, H., 1996. Characterisation and prediction of separation performance of nanofiltration membranes. Journal of Membrane Science, 112: 263-274.

Bowen, W.R. and Welfoot, J.S., 2002a. Modelling of membrane nanofiltration - pore size distribution effects. Chemical Engineering Science, 57: 1393-1407.

Bowen, W.R. and Welfoot, J.S., 2002b. Modelling the performance of membrane nanofiltration—critical assessment and model development. Chemical Engineering Science, 57: 1121-1137.

Cadotte, J., Forester, R., Kim, M., Petersen, R. and Stocker, T., 1988. Nanofiltration membranes broaden the use of membrane separation technology. Desalination, 70(1-3): 77-88.

Cao, X., 1999. Colloid and Interface Aspects of Ultrafiltration. Ph.D. Thesis, University of Wales Swansea.

Chapman, D.L. 1913. A contribution to the theory of electrocapillarity. Philosophical Magazine 25:475.

Childress, A.E. and Elimelech, M., 1996. Effect of solution chemistry on the surface charge of polymeric reverse osmosis and nanofiltration membranes. Journal of Membrane Science, 119: 253-268.

Coulson, J.M. and Richardson, J.F., 2001. Chemical Engineering, 1-6. Butterworth Heinemann.

Deen, W.M., 1987. Hindered transport of large molecules in liquid filled pores. AIChE Journal, 33.

Derjaguin, B.V. and Abrikossova, I.I., 1954. Investigations of the forces of interactions of surfaces in different media and their application to the problem of colloid stability. Discussions of the Faraday Society., 18: 24-41.

Derjaguin, B.V., Abrikossova, I.I. and Lifshitz, E.M., 1956. Direct measurement of molecular attraction between solids separated by a narrow gap. Quarterly reviews Chemical Society, 10: 295-329.

Ding, Y., Yu, H. and Shifen, M., 2002. Direct determination of free amino acids and sugars in green tea by anion-exchange chromatography with integrated pulsed amperometric detection. Journal of Chromatography A, 982: 237-244.

Donnan, F.G., 1911. Theory of membrane equilibria and membrane potentials in the presence of non-dialysing electrolytes. A contribution to physical-chemical physiology. Zeitschrift fur Elektrochemie und angewandte Physilakische Chemie, 17: 572-581.

Dubois, M., Gilles, K., Hamilton, J., Rebers, P. and Smith, F., 1956. Colourimetric method for determination of sugars and related substances. Analytical Chemistry, 28: 350-356.

Elford, W.J., 1933. The principles of ultrafiltration as applied in biological studies. Proceedings of the Royal Society of London. Series B., 112: 384-406.

Elimelech, M., Chen, W.H. and Wapya, J.J., 1994. Measuring the Zeta (electrokinetic) Potential of Reverse osmosis Membranes by Streaming Potential Analyser. Desalination, 95: 269-286.

Elimelech, M. and O'Melia, C.R., 1990. Effect of Electrlyte Type on the Electrophoretic Mobility of Polystrene Latex Colloids. Colloids and Surfaces, 44: 165-178.

Elisseva, T.V., Shaposhnik, V.A. and Luschik, I.G., 2002. Demineralisation and separation of amino acids by electrodialysis with ion-exchange membranes. Desalination, 149: 405-409.

Ferry, J.D., 1936. Ultrafilter membranes and ultrafiltration. Chemical Reviews, 18: 373-455.

Flory, P.J., 1943. Molecular Weights amd Intrinsic Viscosities of Polyisobutylenes. Journal of American Chemical Society, 65: 372-382.

Garba, Y., Taha, S., Cabon, J. and Dorange, G., 2003. Modeling of cadmium salts rejection through a nanofiltration membrane: relationships between solute concentration and transport parameters. Journal of Membrane Science, 211: 51-58.

Garem, A., Daufin, G., Maubois, J.L. and Leonil, J., 1997. Selective Separation of Amino Acids with a Charged Inorganic Nanofiltration Membrane: Effect of Physicochemical Parameters on Selectivity. Biotechnology and Bioengineering, 54: 291-302.

Garner, W.E., 1929. Osmotic Pressure, International Critical Tables. McGraw-Hill, New York.

Gotoh, T., Iguchi, H. and Kikuchi, K.-I., 2004. Separation of glutathione and its related amino acids by nanofiltration. Biochemical Engineering Journal, 19: 165-170.

Gouy, G. 1910. Sur la constitution de la charge électrique a la surface d'un électrolyte. Journal de Physique Théorique et Appliquée 9:455-468.

Grib, H. et al., 2000. Amino acid retention with alumina (gamma) nanofiltration membrane. Journal of Membrane Science, 172: 9-17.

Hagmeyer, G. and Gimbel, R., 1998. Modelling the salt rejection of nanofiltration membranes for ternary ion mixtures and for single salts at different pH values. Desalination, 117: 247-256.

Hong, S.U. and Bruening, M.L., 2006. Separation of amino acid mixtures using multilayer polyelectrolyte nanofiltration membranes. Journal of Membrane Science, 280: 1-5.

Horie, H. and Kohata, K., 2000. Review: Analysis of tea components by high-performance liquid chromatography and high-performance capillary electrophesis. Journal of Chromatography A, 881: 425-438.

Hunter, R.J., 1986. Foundations of Colloid Science. Oxford University Press, Oxford.

Israelachvili, J.N., 1986. Measurement of the viscosity of liquids in very thin layers. Journal of Colloid and Interface Science, 110(1): 263-271.

Israelachvili, J.N., 1991. Intermolecular and surface forces. Academic Press, London.

Israelachvili, J.N. and Pashley, R.M., 1983. Molecular layering of water at surfaces and origin of repulsive hydration forces. Nature, 306: 249-250.

Jacobasch, H.J. and Schurz, J., 1988. Characterization of Polymer Surfaces by Means of Electrokinetic Measurements. Progress in Colloid and Polymer Science, 77: 40-48.

Kim, T., Park, C. and Kim, S., 2004. Water recycling from desalination and purification process of reactive dye manufacturing industry by combined membrane filtration. Journal of Cleaner Production.

Kimura, S. and Tamano, A., 1984. Separation of amino acids by charged ultrafiltration membranes. Membranes and membrane processes. Plenum Press, New York.

Kiso, Y., Nishimura, Y., Kitao, T. and Nishimura, K., 2000. Rejection properties of non-phenylic pesticides with nanofiltration membranes. Journal of Membrane Science, 171: 229-237.

Lastra, A., Gómez, D., Romero, J., Francisco, J.L., Luque, S. and Álvarez, J.R., 2004. Removal of metal complexes by nanofiltration in a TCF pulp mill: technical and economic feasibility. Journal of Membrane Science, 242(1-2): 97-105.

Levenstein, R., Hasson, D. and Semiat, R., 1996. Utilization of the Donnan effect for improving electroylte separation with nanofiltration membranes. Journal of Membrane Science, 116: 77-92.

Levine, 1988. Physical chemistry, 3rd Edition, McGraw-Hill.

Li, S., Li, C., Liu, Y., Wang, X. and Cao, Z., 2003. Separation of L-glutamine from fermentation broth by nanofiltration. Journal of Membrane Science, 222: 191-201.

Li, S., Shen, Y.L. and Chi, L.L., 2000. The stability of L-glutamine on strong acidic ion-exchange resins. Industrial Microbiology, 30: 1-4.

Lide, D.R., 2000. CRC handbook of chemistry and physics : a ready-reference book of chemical and physical data. Boca Raton, Fla. ; CRC., London.

Loeb, S. and Sourirajan, S., 1960. Seawater demineralisation by means of a semi-permeable membrane, University of California at Los Angeles Engineering Report No. 60-60.

Mandale, S., 2005. Nanofiltration of Multi-Solute Systems: Solute Interactions and Theory, University of Wales Swansea.

Martin-Orue, C., Bouhallab, S. and Garem, A., 1998. Nanofiltration of amino acid and peptide solutions: mechanisms of separation. Journal of Membrane Science, 142: 225-233.

McClellan, A.L., 1974. Tables of experimental dipole moments, 2. Rahara Enterprises, El Cerrito, California, 999 pp.

McMurry, J., 2000. Organic Chemistry. Brooks/Cole, New York.

Merry, A., 2001. The right membrane for the job. Filtration & Separation, 38(1): 16-18.

Minagawa, M., Tanioka, A., Ramirez, P. and Mafe, S., 1997. Amino acid transport through cation exchange membranes: effects of pH on interfacial transport. Journal of colloid and interface science, 188: 176-182.

Minhalma, M. and Norberta de Pinho, M., 2004. Integration of nanofiltration/steam stripping for the treatment of coke plant ammoniacal wastewaters. Journal of Membrane Science, 242(1-2): 87-95.

Mohammad, A.W., Othaman, R. and Hilal, N., 2004. Potential use of nanofiltration membranes in treatment of industrial wastewater from Ni-P electroless plating. Desalination, 168: 241-252.

Mohammad, A.W. and Takiiff, M.S., 2003. Predicting flux and rejection of multicomponent salts mixture in nanofiltration membranes. Desalination, 157: 105-111.

Moore, S., 1968. Amino acid analysis: Aqueous dimethyl sulfoxide as solvent for the ninhydrin reaction. The Journal of Biological Chemistry, 243(23): 6281-6283.

Moss, S., 2001. The Adsorption of Lipase onto Prepared Surfaces, University of Wales Swansea.

Nabetani, H. Nakajima, M., Watanabe, A., 1992. Development of a New Type of Membranes Osmometer. Journal of Chemical Engineering of Japan, 25(3): 269-274.

Nabetani, H., Nakajima, M., Watanabe, A., Nakao, S. and Kimura, S., 1990. Effect of Osmotic Pressure and Absorption on Ultrafiltration of Ovalbumin. AIChE Journal, 36(6): 907-915.

Nghiem, L.D., Manis, A., Soldenhoff, K. and Schäfer, A.I., 2004. Estrogenic hormone removal from wastewater using NF/RO membranes. Journal of Membrane Science, 242(1-2): 37-45.

Nguyen, M., Reynolds, N. and Vigneswaran, S., 2003. By-product recovery from cottage cheese production by nanofiltration. Journal of Cleaner Production, 11(7): 803-807.

Nyström, M., Kaipia, L. and Luque, S., 1995. Fouling and retention of nanofiltration membranes. Journal of Membrane Science, 98(3): 249-262.

Nyström, M., Pihlajamaki, A. and Ehsani, N., 1994. Characterisation of Ultrafiltration Membranes by Simultaneous Streaming Potential and Flux Measurements. Journal of Membrane Science, 87: 245-256.

Oatley, D.L., 2004. Characterisation and prediction of membrane separation performance: an industrial assessment. Ph.D Thesis University of Wales Swansea.

Oatley, D.L., Cassey, B., Jones, P. and Bowen, W.R., 2005. Modelling the performance of membrane nanofiltration—recovery of a high-value product from a process waste stream. Chemical Engineering Science, 60: 1953 – 1964.

Peeters, J.M.M., 1997. Characterization of nanofiltration membranes,. Ph.D Thesis, University of Twente, Enschede (NL).

Peeters, J.M.M., Boom, J.P., Mulder, M.H.V. and Strathmann, H., 1998. Retention measurements of nanofiltration membranes with electrolyte solutions. Journal of Membrane Science, 145: 199-209.

Pentz, M. and Shott, M., 1988. Handling experimental data. Open University Press, Milton Keynes.

Platt, S., Nyström, M., Bottino, A. and Capannelli, G., 2004. Stability of NF membranes under extreme acidic conditions. Journal of Membrane Science, 239: 91-103.

Rautenbach, R. and Gröschl, A., 1990. Separation potential of nanofiltration membranes. Desalination, 77: 73-84.

Sato, K., 2002. Effects of the feed solution concentration on the separation degree in Donnan dialysis for binary systems of amino acids. Journal of Membrane Science, 196: 211-220.

Savitzky, A. and Golay, M.J.E., 1964. Smoothing and differentiation of data by simplified least squares procedures. Analytical Chemistry, 36(8): 1627-1639.

Scarpello, J.P., Nair, D., Freitas dos Santos, L.M., White, L.S. and Livingston, A.G., 2002. The separation of homogeneous organometallic catalysts using solvent resistant nanofiltration. Journal of Membrane Science, 203(1-2): 71-85.

Schaep, J. and Vandecasteele, C., 2001. Evaluating the charge of nanofiltration membranes. Journal of Membrane Science, 188: 129-136.

Schaep, J., Vandecasteele, C., Mohammad, A.W. and Bowen, W.R., 2001. Modelling the retention of ionic components for different nanofiltration membranes. Separation and Purification Technology, 22-23: 169-179.

Schnabel, R., Langer, P. and RBreitenbach, S., 1988. Separation of protein mixtures by Bioran porous glass membranes. Journal of Membrane Science, 36: 55-66.

Senden, T.J., Drummond, C.J. and Kekicheff, P., 1994. Atomic force microscopy; imaging with electrical double layer interactions. Langmuir, 10: 358-362.

Shaw, D.J., 1980. Introduction to Colloid and Surface Chemistry. Butterworths, London.

Sourirajan, S., 1970. Reverse Osmosis. Logo Press Ltd., London.

Spiegler, K.S. and Kedem, O., 1966. Thermodynamics of Hyperfiltration (Reverse Osmosis): Criteria for Efficient Membranes. Desalination, 1: 311-326.

Stern, O., 1924. Zur Theorie der Elektrolytischen Doppelschicht. Z. Elektrochem 30: 508-516

Strathmann, H., 1981. Membrane separation processes (review). Journal of Membrane Science, 9: 121.

Tanford, C., 1961. Physical Chemistry of Macromolecules. Wiley, New York.

Timmer, J.M.K., Speelmans, M.P.J. and van der Horst, H.C., 1998. Separation of amino acids by nanofiltration and ultrafiltration membranes. Separation and Purification Technology, 14: 133-144.

Tsuru, T., Shutou, T., Kakao, S. and Kimura, S., 1994. Peptide and amino acid separation with nanofiltration membranes. Separation Science and Technology, 29: 971.

Tsuru, T., Urairi, M., Nakao, S. and Kimura, S., 1991. Reverse osmosis of single and mixed electrolytes with charged membranes: experiment and analysis. Journal of Chemical Engineering of Japan, 24: 518.

Van der Bruggen, B., Braeken, L. and Vandecasteele, C., 2002. Flux decline in nanofiltration due to adsorption of organic compounds. Separation and Purification Technology, 29: 23-31.

Van der Bruggen, B., Daems, B., Wilms, D. and Vandecasteele, C., 2001. Mechanisms of retention and flux decline for the nanofiltration of dye baths from the textile industry. Separation and Purification Technology, 22-23: 519-528.

Van der Bruggen, B., Schaep, J., Wilms, D. and Vandecasteele, C., 1999. Influence of molecular size, polarity and charge on the retention of organic molecules by nanofiltration. Journal of Membrane Science, 156: 29-41.

Van der Bruggen, B., Schaep, J., Wilms, D. and Vandecasteele, C., 2000. A Comparison of Models to Describe the Maximal Retention of Organic Molecules in Nanofiltration. Separation Science and Technology, 35(2): 169-182.

Van der Bruggen, B. and Vandecasteele, C., 2001. Flux Decline during Nanofiltration of Organic Components in Aqueous Solutions. Environmental Science and Technology, 35: 3535-3540.

Van der Bruggen, B. and Vandecasteele, C., 2002. Modelling of the retention of uncharged molecules with nanofiltration. Water Research, 36(5): 1360-1368.

Vilker, V.L., Colton, C.K. and Smith, K.A., 1981. The Osmotic Pressure of Concentrated Protein Solutions: Effect of Concentration and pH in Saline Solutions of Bovine Serum Albmin. Journal of Colloid and Interface Science, 79(2): 548-566.

Villaluenga, J.P.G. and Tabe-Mohammadi, A., 2000. A review on the separation of benzene/cyclohexane mixtures by pervaporation processes. Journal of Membrane Science, 169(2): 159-174.

Wang, X.-L., Ying, A.-L. and Wang, W.-N., 2002. Nanofiltration of L-phenylalanine and L-aspartic acid aqueous solutions. Journal of Membrane Science, 196: 59-67.

Welfoot, J. S., 2001: Predictive modelling of membrane nanofiltration. *PhD Thesis* University of Wales Swansea

Yaroshchuk, A. and Staude, E., 1992. Charged membranes for low pressure reverse osmosis properties and applications. Desalination, 86: 115-134.

Yaroshchuk, A.E., 1998. Rejection mechanisms of NF membranes. Membrane Technology, 100: 9-12.

Yousef, M.A., Datta, R. and Rodgers, V.G.J., 1998. Understanding Nonidealities of the Osmotic Pressure of Concentrated Bovine Serum Albumin. Journal of Colloid and Interface Science, 207: 273-282.

Yousef, M.A., Datta, R. and Rodgers, V.G.J., 2002. Monolayer Hydration Governs Nonideality in Osmotic Pressure of Protein Solutions. AIChE Journal, 48(6): 1301-1308.

Zeman, L. and Wales, M., 1981. Steric rejection of polymeric solutes by membrane with uniform pore size distribution. Separation Science and Technology, 16: 275-290.

Zhu, A., Zhu, W., Wu, Z. and Jing, Y., 2003. Recovery of clindamycin from fermentation wastewater with nanofiltration membranes. Water Research, 37(15): 3718-3732.

# Appendix

## *A.1 Error in glutamic acid analysis*

Table A.1.1 contains the error margins attributed to the equipment used for the Ninhydrin Reagent method for amino acid analysis.

| Source of error | Maximum condition | Absolute error ± | Units |
|---|---|---|---|
| Variable pipette | 1 | 0.006 | ml |
| Variable pipette | 5 | 0.03 | ml |
| Volumetric flask | 25 | 0.04 | ml |
| Volumetric flask | 500 | 0.25 | ml |
| Spectrophotometer | 2 | 0.005 | - |
| Balance | 200 | 0.00005 | g |

**Table A.1.1 Error sources and magnitudes for amino acid analysis using Ninhydrin Reagent method**

A feed concentration of 5 g/l of glutamic acid was chosen for this example calculation as the sample required a large dilution to get the sample into the measurable range, and the observed rejection was high (94%) resulting in a higher error margin.

### A.1.1 Accumulated error

The 5 g/l sample was diluted so that the sample concentration fell in between 0.0005 – 0.0015 g/l. An out of tube dilution was conducted by adding 1 ml of sample (5 g/l) to a 25 ml volumetric flask. This reduced the sample concentration to 0.2 g/l. Further dilution was achieved by repeating the process. The resulting sample concentration was 0.008 g/l. Further dilution of the sample was achieved adding 2 ml of the diluted sample to a test tube, into which 1 ml of Ninhydrin Reagent and 5 ml of ethanol was added. The error in the dilution step was represented by the standard error equations presented by Penz and Shott (1988):

$$\frac{\Delta X}{X}=\sqrt{\left(\frac{\Delta A}{A}\right)^2+\left(\frac{\Delta A}{A}\right)^2+\left(\frac{\Delta B}{B}\right)^2+\left(\frac{\Delta B}{B}\right)^2+\left(\frac{\Delta C}{C}\right)^2+\left(\frac{\Delta A}{A}\right)^2+\left(\frac{\Delta D}{D}\right)^2} \quad \text{(A.1.1)}$$

Where $A$ is the measured volume of the 1 ml pipette and $\Delta A$ is the associated error in the measurement (± 0.006 ml). The volume of the 25 ml volumetric flask is $B$, and the error associated with that measurement is $\Delta B$ (0.04 ml). The terms $\Delta C$ and $\Delta D$ are the errors associated with the addition of 2 ml of sample and 5 ml of ethanol respectively.

Use of equation (A.1.1) established an accumulated error value of $2.0 \times 10^{-3} \pm 3.86 \times 10^{-5}$ g/l for the two dilutions.

The final step that contributes error is the colour measurement by the spectrophotometer. The calibration curve for glutamic acid shows that there was the following relationship between concentration and absorbance

$$Abs = C \times 190.87$$

A spectrophotometer reading of ± 0.005 equates to a concentration error of $\pm 2.65 \times 10^{-5}$ g/l. Which is 0.3% of the measured value. Therefore the total accumulated error in the measurement of a 5 g/l glutamic acid sample was ± 2.0% of the measured value.

## A.1.2 Statistical error analysis

The four data sets used to construct the glutamic acid calibration chart are shown in Table A.1.2. The last two columns in Table A.1.2 represent the mean average absorbance and the calculated best fit of the data. A statistical calculation of the error based on the mean absorbance is given in Table A.1.3. Table A.1.4 presents the results of the same error calculations based on the best-fit values.

| | Adsorption | | | | | |
|---|---|---|---|---|---|---|
| Concentration (mg/l) | Data set 1 | Data set 2 | Data set 3 | Data set 4 | Mean | Best-fit |
| 0.46 | 0.074 | 0.071 | 0.089 | 0.088 | 0.0805 | 0.0878 |
| 0.92 | 0.161 | 0.157 | 0.177 | 0.175 | 0.1675 | 0.1756 |
| 1.38 | 0.264 | 0.262 | 0.28 | 0.277 | 0.27075 | 0.2634 |
| 1.84 | 0.347 | 0.343 | 0.36 | 0.355 | 0.35125 | 0.3512 |

**Table A.1.2 Glutamic acid adsorption calibration data**

| Concentration (mg/l) | Standard deviation | % Standard deviation | Standard error on the mean | % Standard error on the mean |
|---|---|---|---|---|
| 0.46 | 0.00808 | 10.03 | 0.0047 | 5.793 |
| 0.92 | 0.00865 | 5.16 | 0.0050 | 2.980 |
| 1.38 | 0.00785 | 2.90 | 0.0045 | 1.675 |
| 1.84 | 0.00665 | 1.89 | 0.0038 | 1.093 |

**Table A.1.3 Statistical error evaluation based on the mean**

| Concentration (mg/l) | Standard deviation | % Standard deviation | Standard error on the best fit value | % Standard error on the best fit value |
|---|---|---|---|---|
| 0.46 | 0.0109 | 12.40 | 0.00629 | 7.16 |
| 0.92 | 0.0118 | 6.75 | 0.00684 | 3.90 |
| 1.38 | 0.0108 | 4.08 | 0.00621 | 2.36 |
| 1.84 | 0.0066 | 1.89 | 0.00384 | 1.09 |

**Table A.1.4 Statistical error evaluation based on the best-fit value**

The standard error on the mean is defined as

$$S_m = \frac{s}{\sqrt{n-1}} \qquad \text{(A.1.2)}$$

Where $s$ is the standard deviation and $n$ is the number of absorbance measurements.

The average error was 2.9% for the deviation from the mean, or 3.6% when based on the deviation from the best-fit calculations. The largest error was used for the rest of the error calculation.

For a feed concentration of 5 g/l glutamic acid, the permeate concentration was 0.3 g/l and subsequently, the rejection was 94%. An error of 3.6% in absorbance measurement of the feed equated to an error of ± 0.18 g/l. A 3.6 % error in the absorbance measurement of the product equated to an error of ± 0.011 g/l. Thus the error in the rejection was found to be:

$$\Delta X = 0.94 \times \sqrt{\left(\frac{0.18}{5}\right)^2 + \left(\frac{0.011}{0.3}\right)^2}$$

$$\Delta X = 0.048$$

Therefore the error margin is 94 ± 5%. The associated error for the other amino acids was smaller as the measured rejection value was less than that for glutamic acid.

## *A.2 Instrument Calibration Curves*

### A.2.1 Pressure Transducers

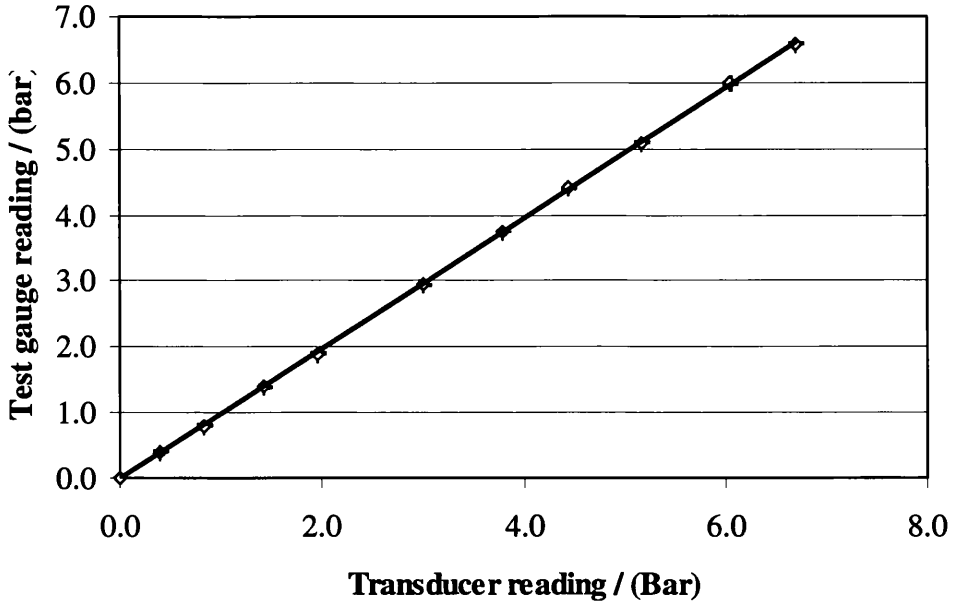


**Figure A.2.1 Osmometer 0-700 kPa transducer calibration**

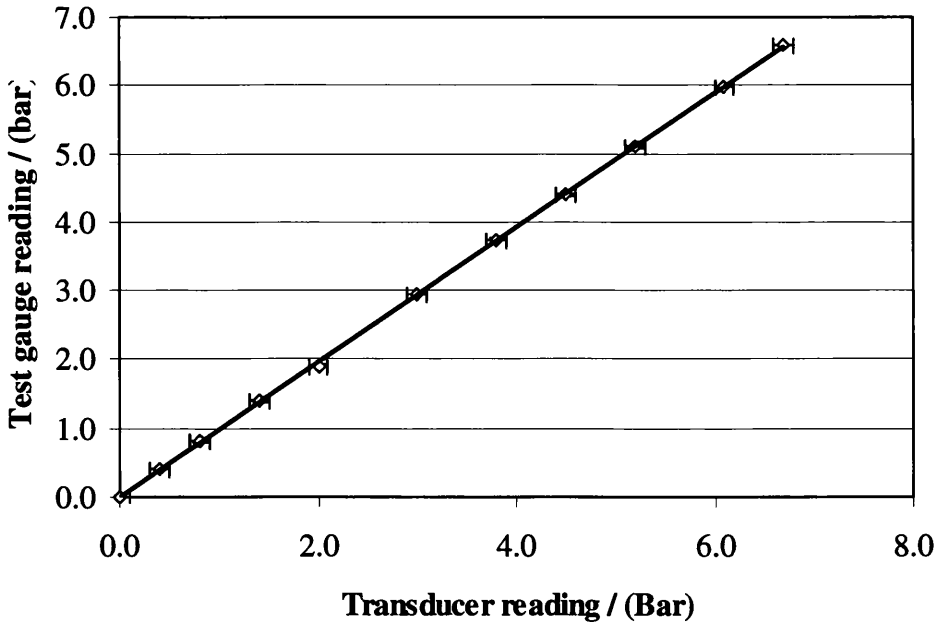


**Figure A.2.2 Filtration cell 0-100 bar transducer calibration**

## A.3 Chemical analysis curves

### A.3.1 Visible absorption

#### Phenol – sulphuric acid method

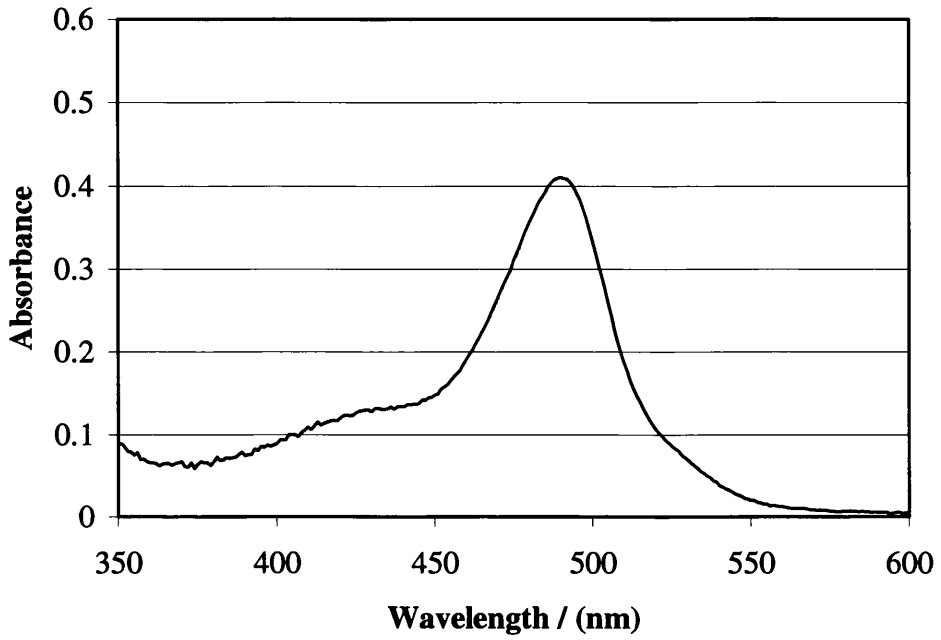


**Figure A.3.1 Absorption scan peak for glucose prepared using the phenol-sulphuric acid method**

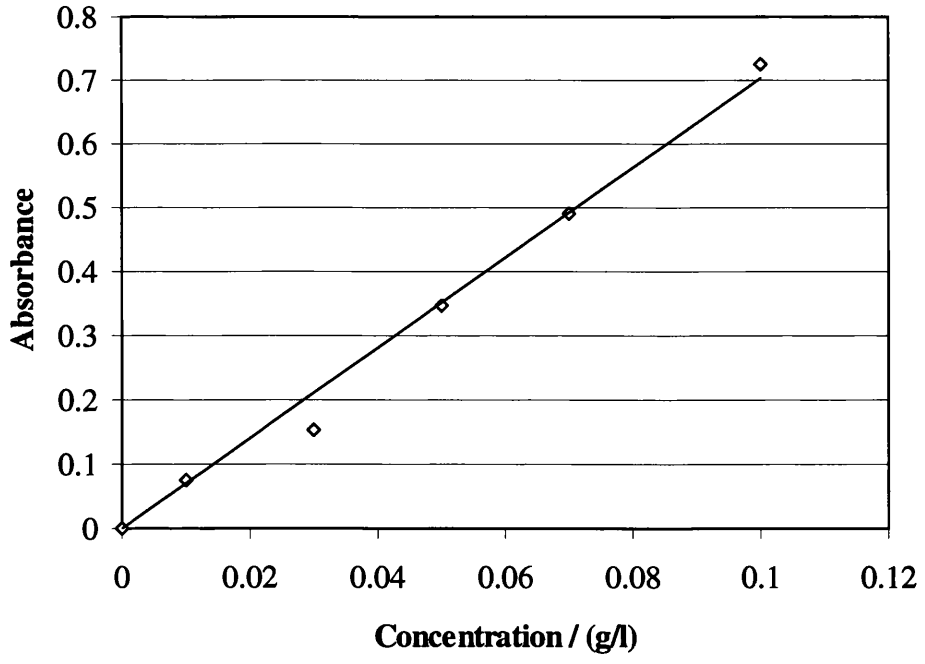


**Figure A.3.2 Calibration plot for glucose prepared using the phenol-sulphuric acid analysis technique at 490 nm (1 cm curvetted)**

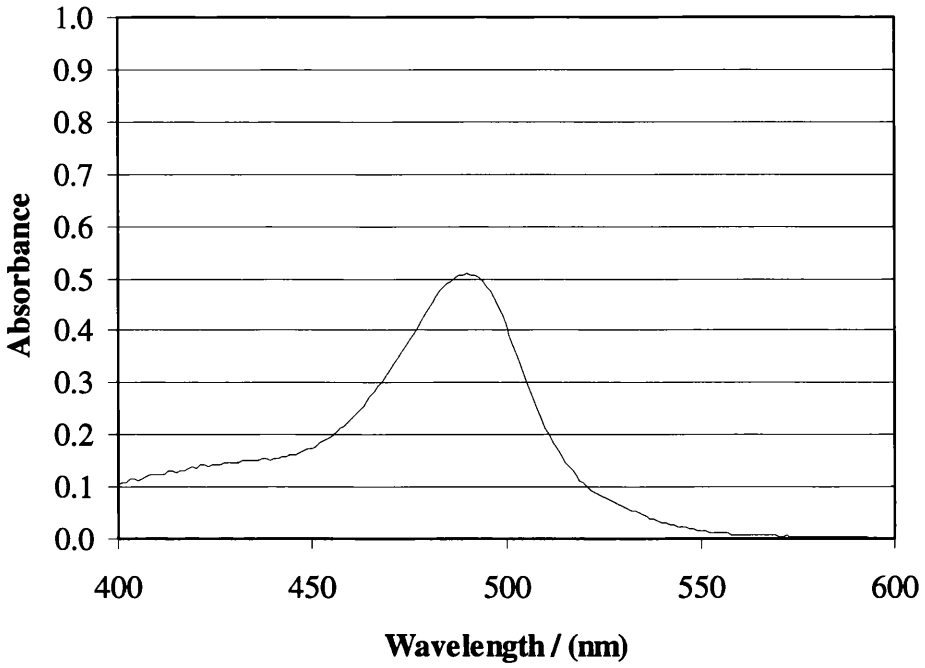


**Figure A.3.3 Absorption scan peak for sucrose prepared using the phenol-sulphuric acid method**

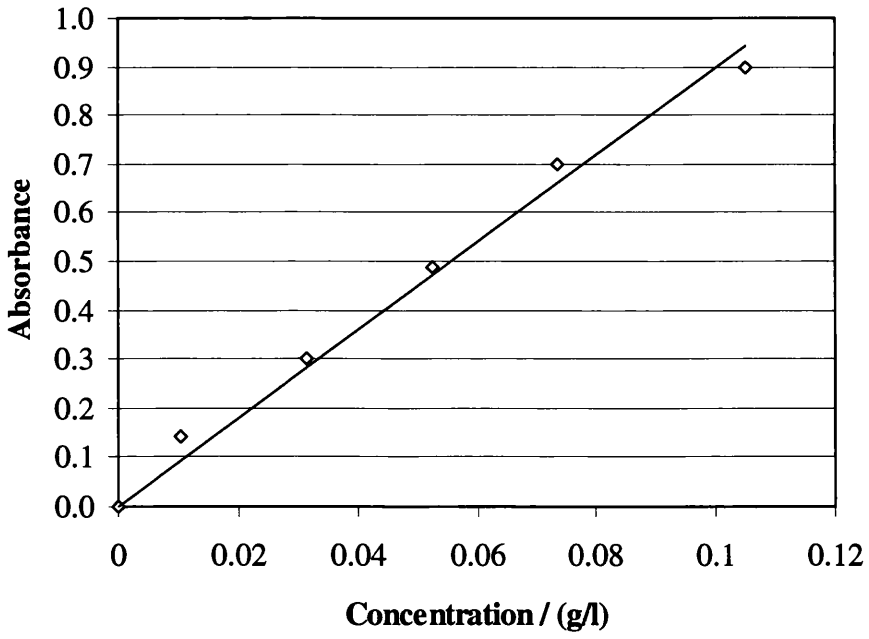


**Figure A.3.4 Calibration plot for sucrose prepared using the phenol-sulphuric acid analysis technique at 490 nm (1 cm curvetted)**

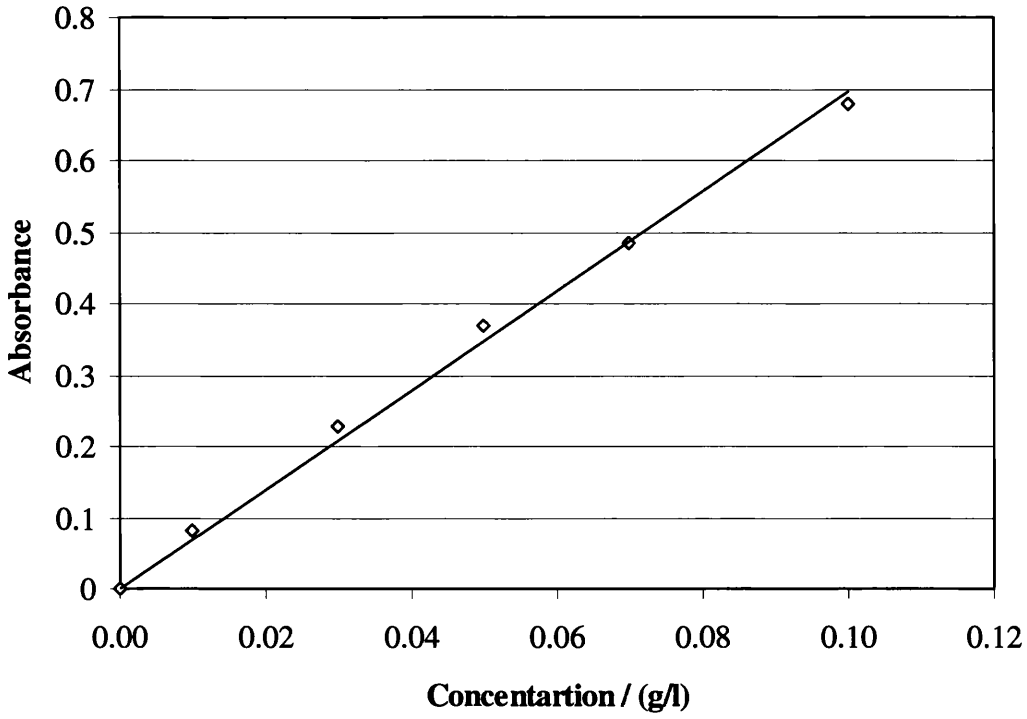


**Figure A.3.5 Calibration plot for raffinose prepared using the phenol-sulphuric acid analysis technique at 490 nm (1 cm curvetted)**

## Ninhydrin reagent method

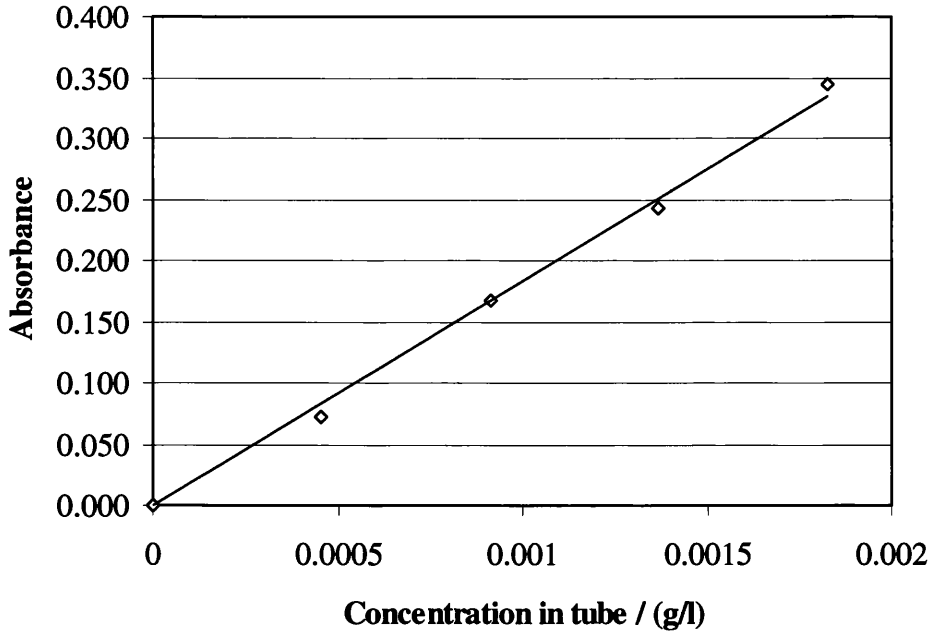


**Figure A.3.6 Calibration plot for glutamine prepared using Ninhydrin reagent analysis technique at 570 nm (1 cm curvetted)**

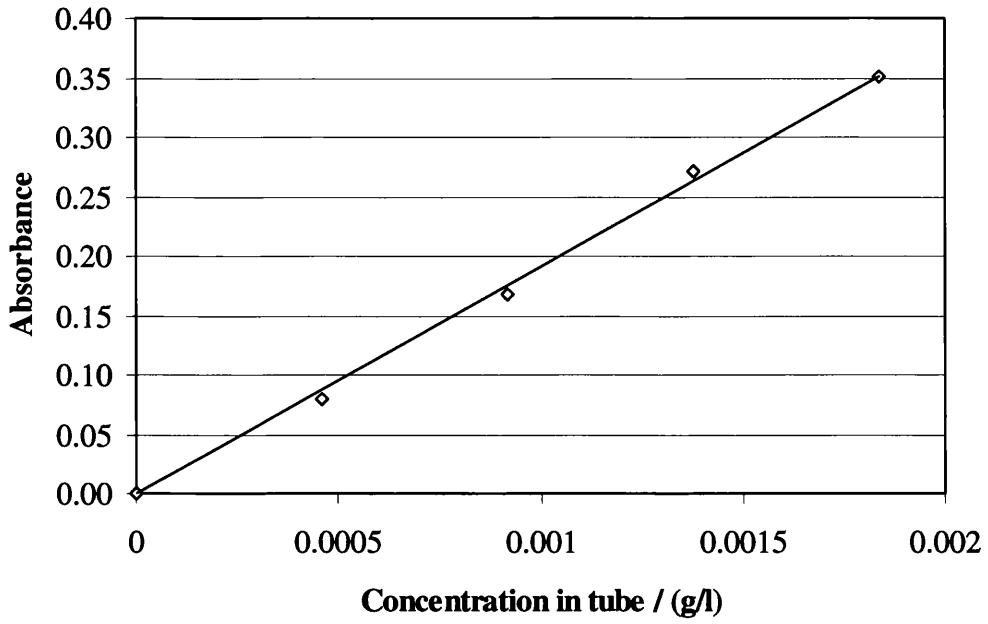


**Figure A.3.7 Calibration plot for glutamic acid prepared using Ninhydrin reagent analysis technique at 570 nm (1 cm curvetted)**

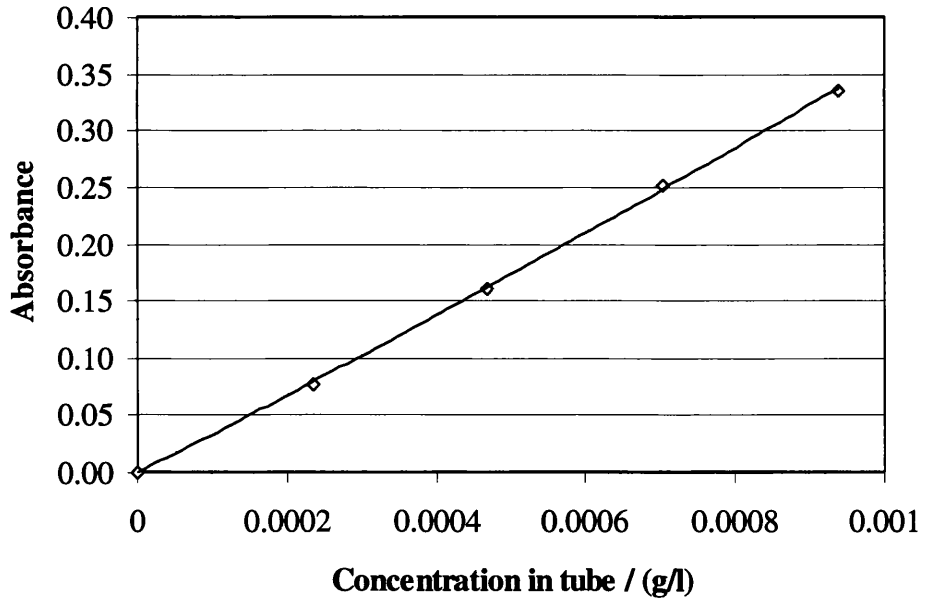


**Figure A.3.8 Calibration plot for glycine prepared using Ninhydrin reagent analysis technique at 570 nm (1 cm curvetted)**

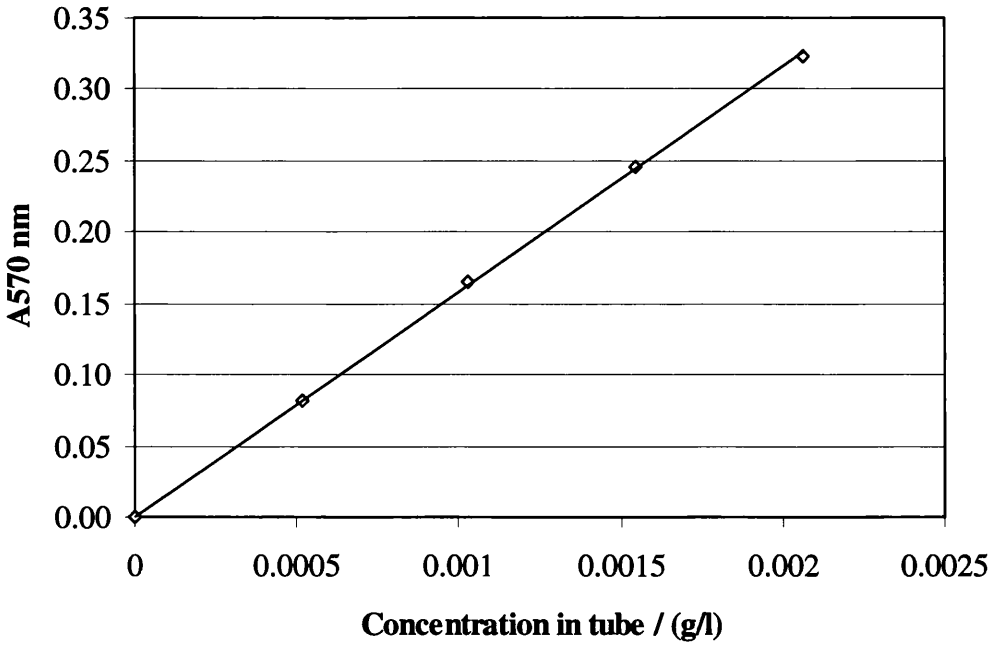


**A.3.9 Calibration plot for phenylalanine prepared using Ninhydrin reagent analysis technique at 570 nm (1 cm curvetted)**

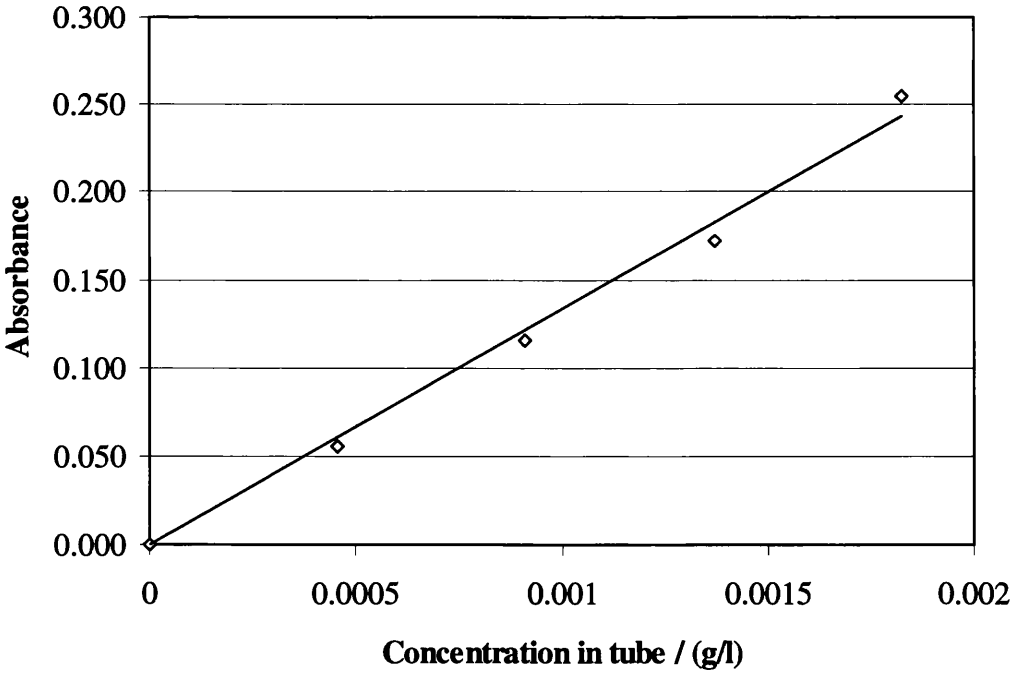


**A.3.10 Calibration plot for lysine prepared using Ninhydrin reagent analysis technique at 570 nm (1 cm curvetted)**

## UV absorption

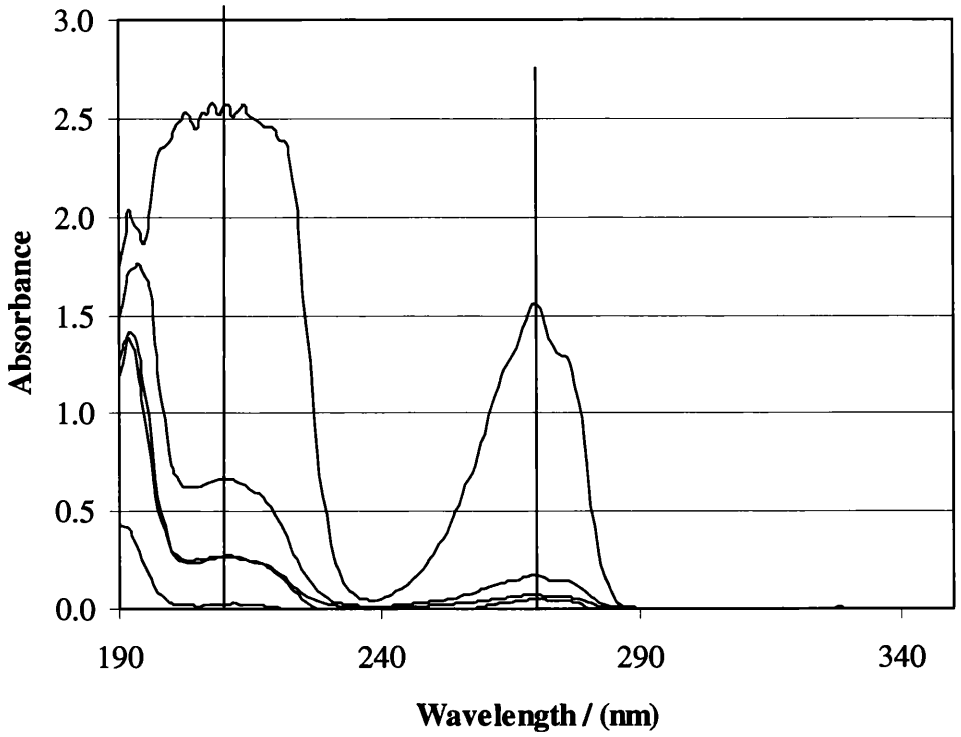


**Figure A.3.11 UV absorption scans showing multiple peaks for phenol**

Two peaks present in the scan (210 and 270 nm). 270 nm was used for experimental phenol concentration analysis, as the peak at 210 nm is actually a multiple peak at high concentrations.

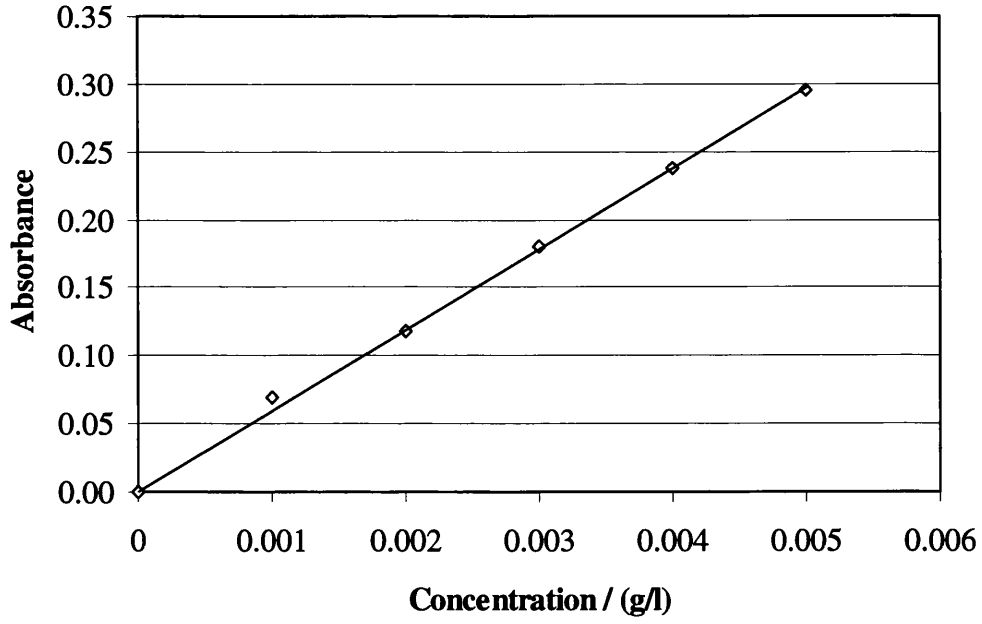


**Figure A.3.12 Calibration plot for phenol using UV absorbance at 270 nm (4 cm curvetted)**

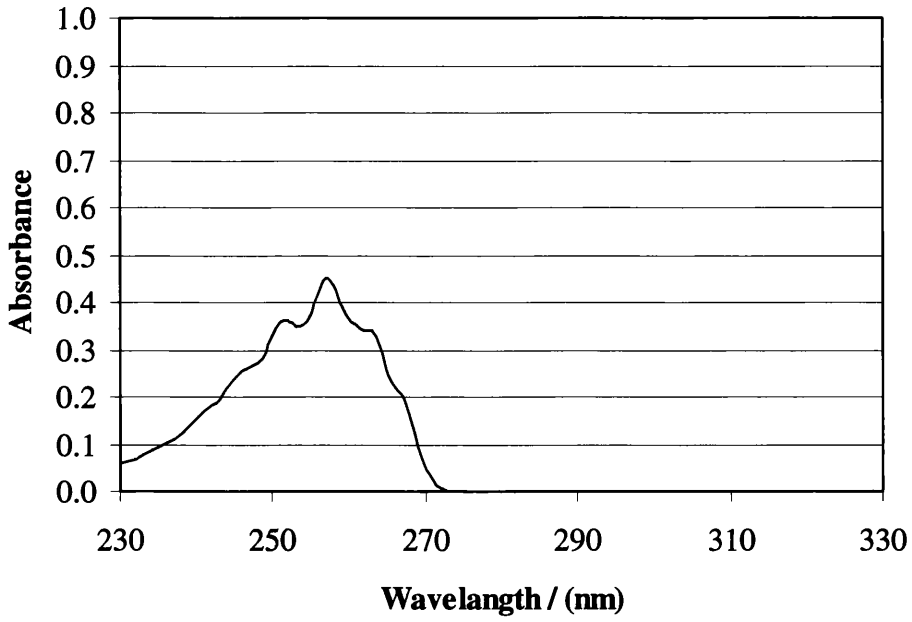


**A.3.13 UV absorption scans showing multiple peaks for benzylalcohol**

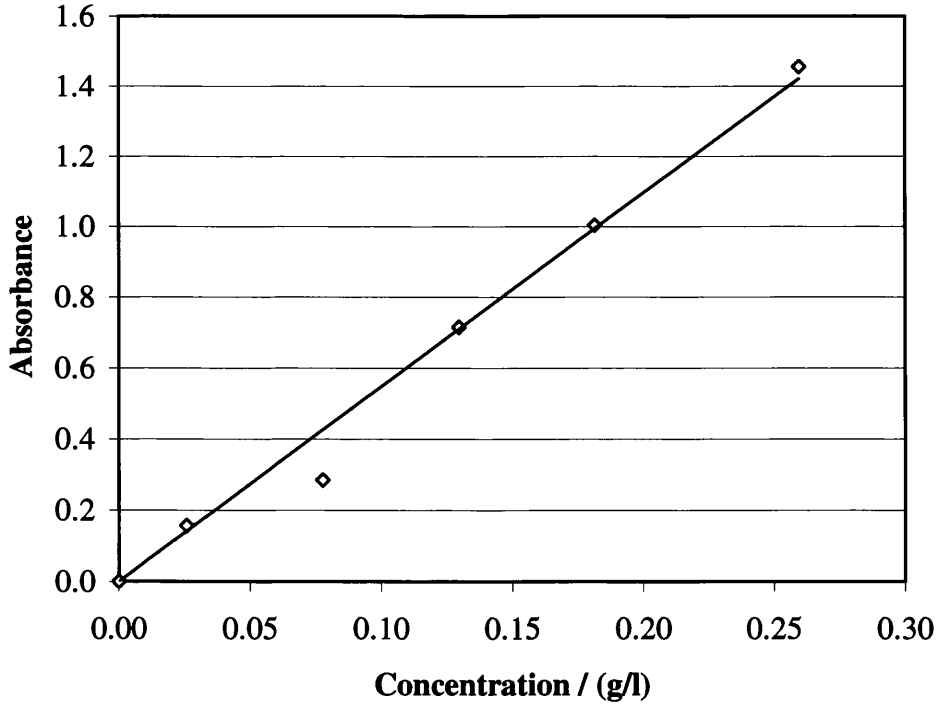


**A.3.14 Calibration plot for benzylalcohol using UV absorbance at 257 nm (4 cm curvetted)**

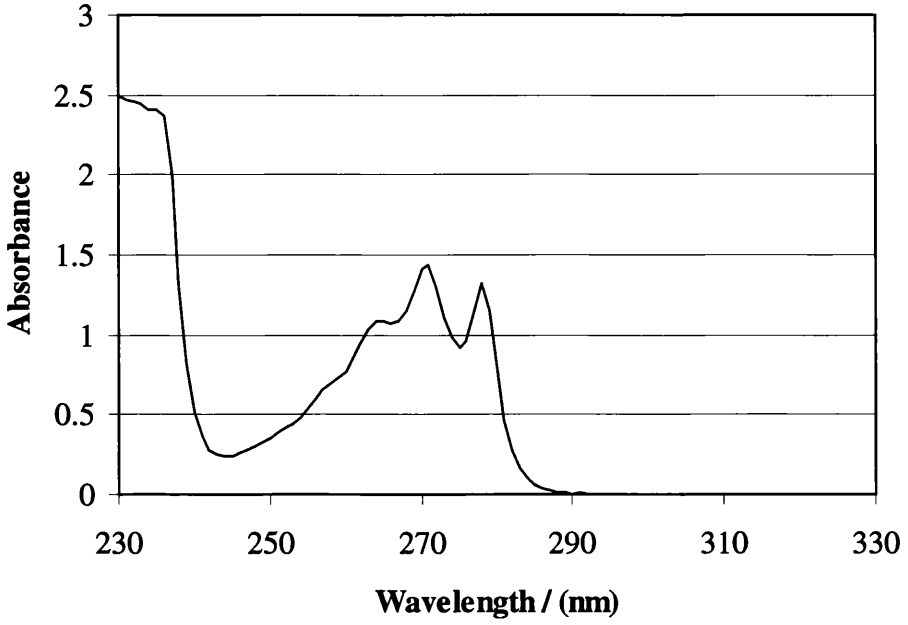


**Figure A.3.15 UV absorption scans showing multiple peaks for benzonitrile**

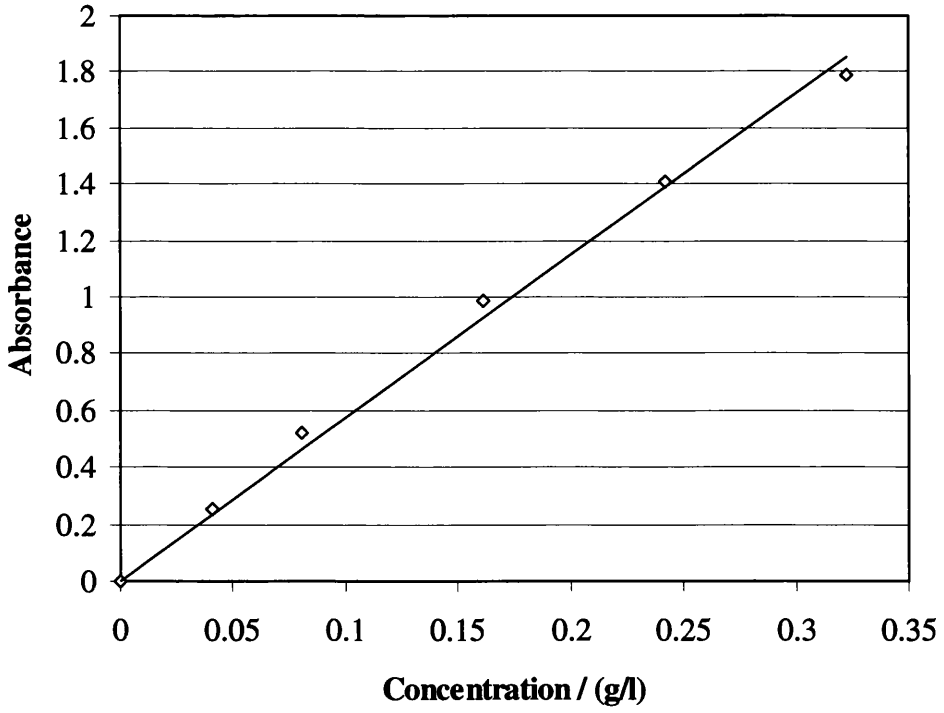


**Figure A.3.16 Calibration plot for benzonitrile using UV absorbance at 271 nm (1 cm curvetted)**

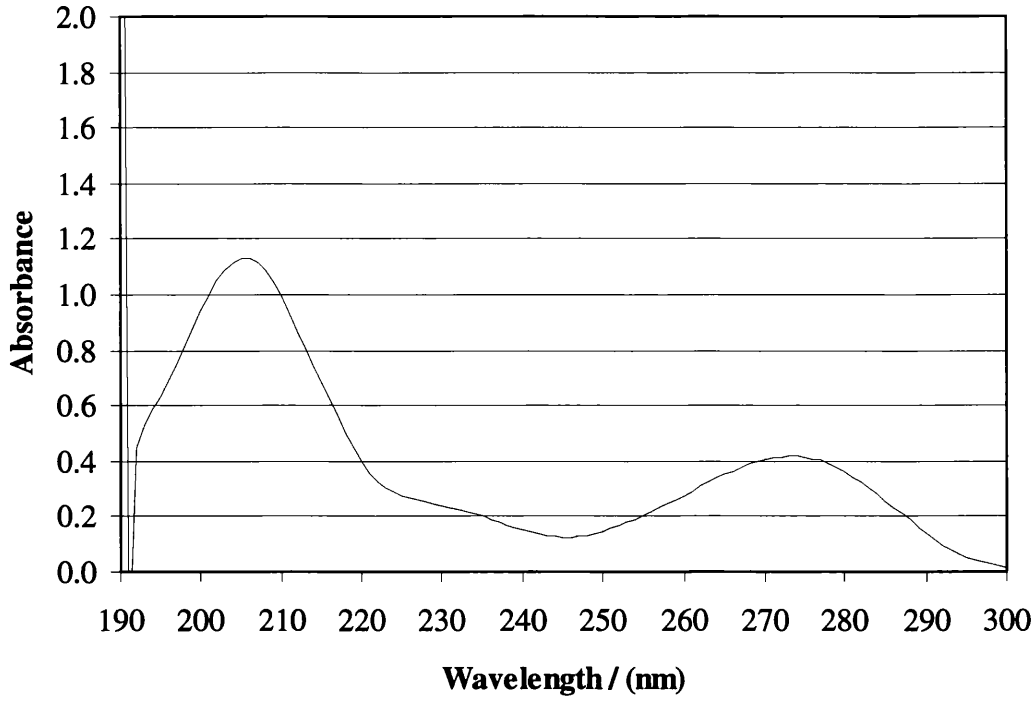


**FigureA.3.17 UV absorption scans showing multiple peaks for Caffeine**

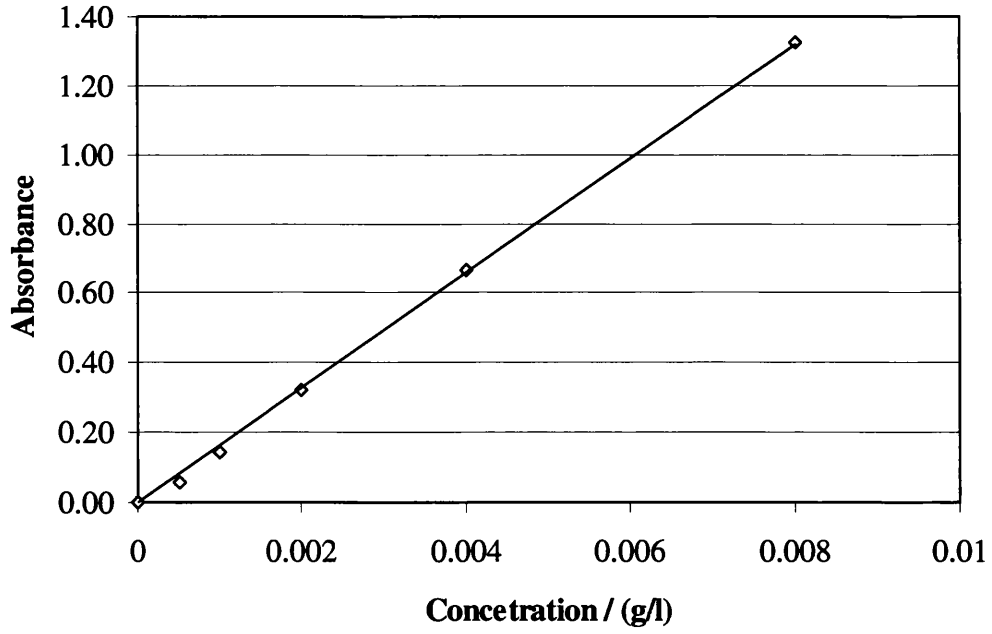


**Figure A.3.18 Calibration plot for caffeine using UV absorbance at 275 nm (4 cm curvetted)**

## *A.4 High Performance Particle Sizing (HPPS)*

The particle radius is an extremely important factor for membrane processes. This property is difficult to obtain with reliable accuracy from either predictive models or experimental measurements, even more so for very small solutes. Malvern Instruments (Malvern, Worces., U.K.) has developed the Malvern HPPS 3.1, which claims to have the ability to measure the solute radius of particles as small as 0.3 nm (HPPS Operators Guide, MAN0314, Issue 1.0, Dec 2001).

### A.4.1 Sample preparation

Samples were prepared using deionised water and were filtered with 0.22 μm Millex syringe driven filter unit (Millipore U.K. Ltd.) into a 4.5 ml capacity UV range 1 cm cuvette (Merck Ltd). For a particle size of less than 10 nm, a concentration greater than 0.5 g/l is recommended with no upper limit (HPPS Operators Guide Guide).

### A.4.2 Results and discussion

Oately (2004) obtained results for particle size measurements for several solutes (concentration 80 g/l) using the Malvern HPPS, the results are shown in Table A.4.1.

| Particle | MW (Da) . | Measured particle diameter (nm) | Particle radius (nm) | Published radius (nm) | Difference (%) |
|---|---|---|---|---|---|
| Glucose | 180 | 0.81 | 0.41 | 0.36 | 11.1 |
| Sucrose | 342 | 0.99 | 0.50 | 0.47 | 5.1 |
| Raffinose | 504 | 1.28 | 0.64 | 0.58 | 9.4 |
| PEG 3400 | 3406 | 3.49 | 1.75 | 1.61 | 7.6 |
| PEG 4600 | 4594 | 3.69 | 1.85 | 1.84 | 0.3 |

**Table A.4.1 Particle size measurements using the Malvern HPPS**

The results provided in Table A.4.1 show that the maximum deviation between the literature value and the experimental findings occur for glucose. This represents the smallest molecule, with an available literature size value, and indicates the machine may be at the limit of operation for this molecule. The deviation is approximately 11% and becomes less as the particle size is increased. Therefore, the equipment is capable of providing a reasonable estimate of particle radius for very small solutes.

## A.5 Calculation of the average net charge on an amino acid

Worked example for glycine at pH 6.5. Known information is shown in Table A.5.1.

| R-group | COOH (charged negative)[1] |
|---|---|
| $pK_{\alpha\text{-}COOH}$ | 2.34 |
| $pK_R$ | - |
| $pK_{\alpha\text{-}NH2}$ | 9.60 |
| Working pH | 6.5 |

1 McMurry, 2000

**Table A.5.1 Glycine properties**

1) Charge contribution from *α-COOH*:

$$\log\frac{[-COO^-]}{[-COOH]} = 6.5-2.34=4.16$$

$$\frac{[-COO^-]}{[-COOH]} = 10^{4.16} = 14454.4$$

Fraction of *α-COOH* group in charged state at pH 6.5

$$f(-COO^-) = \frac{14454.4}{1+14454.4} = 1$$

Therefore, the charge contribution = $f$ (*-COO⁻*) x –1 = 1 x –1 = **-1**

2) Charge contribution from *α-NH₂*:

$$\log\frac{[-NH_2]}{[-NH_3^+]} = 6.5-9.6=-3.1$$

$$\frac{[-NH_2]}{[-NH_3^+]} = 10^{-3.1} = 0.001$$

Fraction of *α-NH₂* in charged state at pH 6.5

$$f(-NH_3^+) = \frac{1}{1+0.001} = 1$$

Therefore, the charge contribution = $f$ (*-NH₃⁺*) x 1 = 1 x 1 = **1**

3) The charge contribution from R-group is zero

Therefore, the overall average net charge on glycine at pH 6.5 is:

$$(-1) + 1 + 0 = \mathbf{0}$$

## A.6 Calculation of Reynolds Number

Worked example of Reynolds number for the SEPA® ST cell, for the operating conditions shown in Table A.6.1.

| Properties | Value |
|---|---|
| Density of water at 35°C, $\rho$ | 994 kg/m$^3$ |
| Membrane diameter, $d$ | 0.049 m |
| Stirrer velocity, $u$ | 0.46 m/s |
| Viscosity of water at 35°C, $\mu$ | 8.9 x 10$^{-4}$ Ns/m$^2$ |

**Table A.6.1 SEPA® ST cell operating conditions for Reynolds Number calculation**

Reynolds Number is given by:

$$\mathrm{Re} = \frac{\rho d u}{\mu} \qquad \text{(A.6.1)}$$

Inserting the information form Table A.6.1 into equation A.6.1:

$$\mathrm{Re} = \frac{994 \times 0.049 \times 0.46}{8.9 \times 10^{-4}} = 25174$$

This Reynolds number is high enough to justify neglecting concentration polarisation for the filtration experiments.